Spring 2020

# Microgrid design, control, and performance evaluation for sustainable energy management in manufacturing

Md. Monirul Islam

# MICROGRID DESIGN, CONTROL, AND PERFORMANCE EVALUATION FOR SUSTAINABLE ENERGY MANAGEMENT IN MANUFACTURING

by

MD. MONIRUL ISLAM

A DISSERTATION

Presented to the Graduate Faculty of the

MISSOURI UNIVERSITY OF SCIENCE AND TECHNOLOGY

In Partial Fulfillment of the Requirements for the Degree

DOCTOR OF PHILOSOPHY

in

SYSTEMS ENGINEERING

2020

Approved by:

Dr. Cihan H. Dagli, Advisor
Dr. Zeyi Sun
Dr. Ruwen Qin
Dr. Steven Corns
Dr. Rui Bo

# ABSTRACT

This research studies the capacity sizing, control strategies, and performance evaluation of the microgrids with hybrid renewable sources for manufacturing end use customers towards a distributed sustainable energy system paradigm. Microgrid technology has been widely investigated and applied in commercial and residential sector, while for manufacturers, it has been less explored and utilized. To fill the gap, the dissertation first proposes a cost-effective sizing model to identify the capacities as well as control strategies of the components in microgrids considering a commonly used energy tariff, i.e., Time of Use (TOU). Then, the sizing model is extended by integrating control strategies for both microgrid components and manufacturing systems considering a typical demand response program, i.e., Critical Peak Pricing (CPP), where customer side load adjustment is highly encouraged. After that, the control strategy of the manufacturers in an overgeneration mitigation-oriented demand response program is further investigated based on the identified optimal size of onsite microgrid to minimize the energy cost. Later, the system is analyzed from its higher level of abstraction where a prosumer community is developed by aggregating such manufacturers with onsite microgrid system. To enhance the reliable energy operation in the community, the performance of the microgrid is investigated through the estimation of the lifetime of Battery Energy Storage System (BESS), a critical design parameter the architecture. Finally, conclusions are presented and future research on real-time joint control strategy for both microgrids and manufacturing systems and identification as well as optimal energy management of the controllable loads in manufacturing system are discussed.

# ACKNOWLEDGMENTS

First and foremost, I would like to thank Allah S.W.T for giving me the strength, ability, and patience to finish the research and complete my PhD satisfactorily. Without his grace and blessings, this achievement would not have been possible.

I am ineffably indebted to Dr. Zeyi Sun for encouraging and allowing me to grow as a researcher. Your indispensable advice on both research and my career have been invaluable. Thank you from the bottom of my heart. I would also like to express my special appreciation and thanks to my committee chair, Dr. Cihan H. Dagli, for providing me exceptional insight, personal experience, and support throughout the journey of the program. To the rest of my advisory committee, Dr. Ruwen Qin, Dr. Steven Corns, and Dr. Rui Bo, I am extremely grateful to you for reviewing my work and providing lots of helpful insight and encouragement to significantly improve the quality of the work.

I would like to extend my deepest appreciation to all my friends and well-wishers for their support, encouragement, and wishes throughout the endeavor.

A special thanks to my family. Words cannot express how grateful I am to my father, mother, brother, father in law, and mother in law that you've made on my behalf. Your prayer for me was what sustained me thus far. Most importantly, I wish to thank my loving and supportive wife, Ishrat Jahan, and my wonderful son, Yaeesh Bin Monir. Without their love and sacrifices, I would not have been able to pursue my dreams. Therefore, I dedicate this dissertation to my family as a token of my appreciation.

# TABLE OF CONTENTS

Page

# LIST OF ILLUSTRATIONS

Page

# LIST OF TABLES

Page

# 1. INTRODUCTION

## 1.1. BACKGROUND MOTIVATION AND OBJECTIVE

The need to satisfy the increasing energy demand in a sustainable way leads to the recent innovations of small-scale distributed power systems, and technological advancement of power electronics which have brought the concept of future distributed energy system paradigm known as microgrids. The concept of microgrid was first proposed by Consortium for Electric Reliability Technology Solutions (CERTS) in America. It is considered as a recent novel concept in part of the development of smart grid. Microgrids are the localized grids which are formed by the interconnection of small and modular generation (solar PV, micro-turbines, fuel cells etc.) along with storage devices (batteries, flywheels, and energy capacitors) and controllable loads. The microgrids can be operated either grid-connected mode or islanded (autonomous) mode in a controlled and coordinated way.

In recent years, the microgrids have been considered a reliable solution to satisfy the growing demand of electricity through strengthening the resilience and mitigating the disturbances of electricity grids. As the system can work in a decentralized manner, it can relieve the ramified and complex central coordination/planning mechanism in traditional centralized grid operation by utilizing the distributed sources to serve the loads locally. The efficiency of the delivery system can be significantly improved by minimizing the transmission and distribution losses. In addition, the microgrid system can enable a flexible and efficient electricity grid through the integration of growing deployment of distributed renewable energy resources. Therefore, it has been widely recognized that two

major challenges of sustainable energy development strategies, i.e., efficiency improvement in energy production and replacement for fossil fuels by various sources of renewable energy can be addressed by successfully implementing the microgrid systems.

The research on microgrid system can roughly be categorized into two groups, i.e., operational control and strategic design. On one hand, many existing studies of microgrid system focus on the optimal management and control schemes for the components such as solar PV, wind turbine, and BESS. On the other hand, many studies focusing on the microgrid system sizing and design on various scopes ranging from community-wide, city-wide, state-wide, to country-wide have been implemented considering techno-economic concerns. The target end-use customers typically include residential customers, commercial customers, agricultural customers, and critical facilities such as medical centers, financial corporations, military bases, jails etc.

Previous research on the microgrid design and control has been mainly focused on residential and commercial buildings while largely neglected industrial manufacturing systems. However, according to the statistics of International Energy Agency (IEA), the industrial sector accounted for more than one-third of the total electricity use in 2018 and about 90% of the consumed electricity is contributed by manufacturing sector. Based on the report of IEA, the demand is expected to keep growing at an average rate of 1.5% per year. Besides, the manufacturing system is considered a complex system where there exist complicated interrelations between component-level characteristics (e.g., cycle time, machining reliabilities, and buffer capacities) and system-level characteristics (e.g., total demand, production rate, and electricity consumption). Therefore, it is challenging and essential to develop a sustainable energy infrastructure for the customers of this largest

and fastest growing sector to alleviate the negative impacts of carbon emissions, decrease the cost of the electricity, and enjoy the benefits from various schemes of government tariff.

The next step in this research is to promote such a sustainable energy infrastructure among the manufacturers and extend the boundary of the research to the next higher level of abstraction where the manufacturers with OGS will form a community-based network. In this network, each of the participants will be considered as the prosumer who will not only consume the energy but also generate the energy and share with the utility grid or other manufacturers to achieve a mutual goal of sustainable and less grid-dependent power system. To ensure the energy infrastructure for the community, it is required to monitor the performance of each component existed in the network to ensure the reliable operation of the network. Therefore, there is an urgent need to develop a framework to design the microgrid system cost-effectively, control both manufacturing and microgrid system optimally, and evaluate the performance of the design parameters for energy infrastructure considering the growing demand of the manufacturing, environmental concerns, and sustainability of the manufacturing and microgrid system.

The dissertation begins with a mathematical model to optimally design an onsite microgrid system for manufacturing plant considering the variation of energy load and the control of the components with the designed capacity. The variations of the energy demand from manufacturing plants including both manufacturing and HVAC systems are captured and used as the input for sizing and controlling the microgrid in a most commonly used energy tariff (or demand response program), TOU. The design model is

further extended considering another typical demand response program, CPP, to identify the optimal size of the microgrid as well as operational strategies for both microgrid and manufacturing system. After designing the onsite microgrid, the control strategy of manufacturers in an overgeneration mitigation-oriented demand response program is investigated based on the identified optimal size of the microgrid to minimize the overall energy related cost. Finally, the performance of the OGS is evaluated through investigating a critical characteristic of the design parameter, the lifetime of the BESS, when such manufacturers will participate in a community-based network and are considered as prosumers to build a future smart energy community.

The objective of this dissertation is to present a framework towards a cost-effective and environmentally sustainable onsite microgrid system for manufacturing practitioners. To build the energy infrastructure, both microgrid system design and supply-demand control under various energy tariffs or demand response programs are investigated. Finally, a higher level of abstraction of the system is considered where the manufacturers with OGS will develop a community-based network to meet the goal of sustainable, resilient, and less grid-dependent energy sharing network. To ensure reliable operation of the network, the performance of the microgrid is investigated though the evaluation of the critical characteristics of the designed parameters. The dissertation is expected to serve the decision makers such as manufacturing industry and other similar sectors with microgrid energy system to optimally design the capacities of system components, control both the microgrids and the corresponding load sides, and evaluate the performance of the microgrid structure for advancing the future sustainable multi-microgrid network.

## 1.2. DISSERTATION SYNOPSIS

This dissertation is organized as follows:

Section 1, Introduction. It briefly introduces the background, motivation, and objective of this dissertation research.

Section 2, Literature review. It reviews the concept of microgrids, design and control of the microgrids, control strategy for different demand response programs, performance evaluation of the onsite microgrid system through battery life estimation, and research opportunities.

Section 3, Optimal sizing and controlling of microgrid system for manufacturing in TOU based demand response program. It formulates a mathematical model for optimally sizing the capacity of microgrid system with hybrid renewable sources and BESS as well as planning it operational strategies for the manufacturers considering the energy loads from both manufacturing system and HVAC system in a typical manufacturing plant. Both linearization and meta-heuristic solution strategies are discussed for the mixed integer non-linear programming optimization model and compared the solution startegy based on the solution quality and computational time. A case study employing the relevant data of a real auto component manufacturing plant and renewable sources in the Chicago area is implemented to illustrate the effectiveness of the proposed model.

Section 4, Optimal sizing and controlling of microgrid system for manufacturing in CPP based demand response program. A mathematical model is proposed to identify the optimal size and utilization strategy of the microgrids, as well as the corresponding production plan of the manufacturing system to minimize the overall energy related cost.

Linearization strategy and metaheuristic algorithm are discussed for solving the proposed mixed integer non-linear programming optimization model with a reasonable computational cost and a good solution quality. A case study based on a real auto component manufacturing system and an existing CPP program is implemented to examine the effects of the proposed model.

Section 5, Optimal scheduling of manufacturing and microgrid system in over-generation mitigation-oriented electricity demand response. A mathematical model is proposed to identify the optimal participation strategy for manufacturing end use customers with onsite microgrid generation system in the demand response program designed for mitigating electricity over-generation. Particle swarm optimization is used to find a near optimal solution for the MINLP problem. A numerical case study with sensitivity analysis is then conducted to demonstrate the effectiveness and robustness of the proposed model.

Section 6, Battery life estimation for performance evaluation of the onsite microgrid system in a prosumer-based community network. A lifetime estimation model is proposed for the BESS of the OGS while participating in such a network using an integrated approach of cellular automata and system dynamic (SD). The framework is developed to prevent any sudden power outage and build a reliable energy management framework for the community. The major factors such as energy demand of the manufacturing plant, intermittent generation from the OGS, energy sharing capability of the prosumers etc. are considered to simulate the model and determine the amount of battery degradation. Based on the estimated lifetime of the battery, the manufacturers

further can control the energy management plan (charging/discharging scheme) to prolong the battery lifetime and ensure a reliable operation for the community.

Section 7, Study limitation and opportunities for future work, lists contributions, and provides the insights for future work to address limitations as well as to challenges of this research.

# 2. LITERATURE REVIEW

## 2.1. CONCEPT OF MICROGRID

Due to the potential benefits of providing reliable, economic, environmentally friendly electricity from the renewable energy sources, the concept of "microgrid" has been researched and implemented intensively worldwide in last few years (Lasseter, 2001; Lasseter and Piagi, 2004; Lasseter, 2007). The microgrid is an interconnection of the distributed energy sources, such as solar PV, wind turbines, fuel cells etc. integrated with the storage devices, such as batteries, flywheels and power capacitors on low voltage distribution systems (Hatziargyriou et al., 2006). As the microgrid system works in a decentralized manner, it provides the opportunity of dispersed generation and meeting the demand of the loads with the maximum decision autonomy. In addition, the efficiency of the system is significantly improved by minimizing the transmission and distribution losses. Therefore, the system has been considered a reliable solution to satisfy the growing demand of electric power through strengthening the resilience and mitigating the disturbances of electricity grid (Olivares et al., 2014; Dohn, 2011; Shahidehpour and Clair, 2012).

Before the concept of microgrid, the distributed generation (DG) system (usually built by a single source: solar or wind) was adopted for flexible generation in terms of its operation, size, and expandability. Generally, the system was operated along with a diesel generator so that the intermittency of the energy supply from the renewable source can be overcome (Wichert, 1997). In other words, the DG source worked as a secondary/backup source under the architecture for improving the grid reliability and reducing the

greenhouse gas emission (Rehman and Al-Hadhrami, 2010; Yamegueu et al., 2011; Usman et al., 2018; Luickx and D'haeseleer, 2007). However, the DG system with single renewable source is associated with high system cost and low reliability (Deshmukh and Deshmukh, 2008). Therefore, the concept of DG system with hybrid renewable sources has emerged to address the limitations. The rapid advancement of the research focusing on environment-friendly and mutually complementary nature between different renewable sources (Boyle, 2004; Sinha and Chandel, 2015; Prasad et al., 2017; Ma et al., 2014; dos Anjos et al., 2015), as well as the technological development of integrating various renewable sources into the microgrid system (Connolly, 2012; Farret and Simoes, 2006; Johnstone et al., 2010; Elhadidy and Shaahid, 2000) have brought a sea change in the outlook of the grid system. Currently, the DG system with hybrid renewable sources along with the BESS and controllable loads are known as the microgrid system. One typical microgrid generation system consists of solar PV, wind turbine, and BESS. The BESS is used to provide power quickly to minimize the interruptions due to the inherent intermittency of solar PV and wind turbine systems (Hill et al., 2012, Suberu et al., 2014, Nazaripouya et al., 2017). Such a microgrid system can be operated either completely separate from, or connected to, the existing utility power grid (Mahieux C, 2015; U.S. DOE, 2014; Lawrence Berkeley National Laboratory, 2016), and address the limitations in terms of intermittency, fuel flexibility, efficiency, reliability, emissions, and economics (Ma et al., 2014; Singh et al., 2016; Bahmani-Firouzi and Azizipanah-Abarghooee, 2014).

## 2.2. DESIGN AND CONTROL OF THE MICROGRID

Sizing, operation, and control of the microgrid system are very essential for its techno-economic feasibility and sustainability (Zhao et al., 2013; Deshmukh and Deshmukh, 2008). The research on microgrid system can be roughly categorized into two groups, i.e., operational control and strategic design. On one hand, many existing studies on microgrid system focus on the optimal management and control schemes for the components such as solar PV, wind turbine, and BESS (Guerrero et al., 2008; Hill and Chen, 2011; Parker and Garche, 2004; Logesh, 2017; Li et al., 2004; Pourmousavi et al., 2010; Fazli and Wang, 2018). For example, the control strategy for a flexible microgrid is presented in (Guerrero et al., 2008). Real-time analysis of the control structure and management functions of a solar-wind hybrid microgrid system has been reported in (Logesh, 2017; Li et al., 2004; Pourmousavi et al., 2010; Fazli Khalaf and Wang, 2018). The optimal control schemes of microgrid system for providing distributed energy to meet the local manufacturing loads was investigated in (Fazli and Wang, 2018).

On the other hand, many studies focusing on the microgrid system sizing and design on various scopes ranging from community-wide (Herrando and Markides, 2016), city-wide (Chong et al., 2011), state-wide (Kanase-Patil et al., 2011), to country-wide (Jung and Villaran, 2017) have been implemented considering techno-economic concerns. The target end-use customers typically include residential customers (Truong et al., 2016; Su et al., 2010; Georges et. al., 2017; Ahourai and Al Faruque, 2013; Roggia et al., 2011; Hawkes and Leach, 2007), commercial customers (Marnay et al.,2008; Eichholtz et al., 2010), agricultural customers (Carroquino et al., 2015), and critical facilities such as medical centers, financial corporations, military bases, and jails

(Buonomano et al., 2014; Arcuri et al., 2007; NYDHSES, 2014; Stadler, 2014) . More comprehensive reviews in this area can be found in a few survey papers (Siddaiah and Saini, 2016; Al Busaidi et al., 2016; Fadae and Radzi, 2012).

## 2.3. MICROGRID CONTROL STRATEGY DURING DEMAND RESPONSE PROGRAM

Electricity demand response has been considered as a critical and cost-effective methodology to balance the resources in power system. According to the US Department of Energy, DR is "a tariff or program established to motivate changes in electric usage by end-use customers, in response to the changes in the price of electricity over time, or to give incentive payments designed to induce lower electricity usage at times of high market prices or when grid reliability is jeopardized" (Qdr, 2006). The impacts of the demand response programs are enormous. The average energy saving ratio by adopting the demand response programs was reported to be 65 kWh per kW of peak demand reduction (Siddiqui et al., 2008). Federal Energy Regulatory Commission (FERC) has estimated that the existing demand response resources are about 41,000 MW, representing 5.8% of 2008 summer peak demand (FERC, 2008). It is projected an increase to 138,000 MW, representing 14% of peak demand by 2019 (FERC, 2009).

The existing demand response programs can be categorized into two categories: price-driven and event-driven (Goldman et al., 2010). For the price-based program, the electricity rates fluctuate along the time horizon to encourage the customers to shift their demand from peak-hours to off-peak hours, resulting in a more level demand curve. The most prevalently used price-based program is TOU tariff mechanism (Federal Energy Regulatory Commission, 2012). Unit electricity consumption rate varies depending on

the time periods. Some TOU tariffs also include the demand charge based on the maximum power drawn from the grid throughout the billing cycle, typically, a month, in addition to electricity consumption charge (Zhang et al., 2018). In event-driven program, the customers can be rewarded under specific contracts like reducing their power consumption in response to specific conditions, e.g., extreme local weather, regional transmission congestion, and generation equipment failures. The aim of this type of demand response program is to reduce the load on a short-term basis upon the occurrence of such events. CPP is a typical event-based demand response program. An extremely high rate of energy consumption is applied for the periods when "critical peaks" occur during which the electricity demand is extremely high, while a discounted price for the time periods of the remaining time is also offered to the customers (Chino Valley Unified School D., 2012). In comparison to traditional TOU that has already been widely used in many areas of the United States as a base electricity tariff system, CPP is comparatively new, but it has obtained more and more attention. Many utility companies, for example, Pacific Gas & Electric (PGE), Southern California Edison (SCE), and San Diego Gas & Electric (SDGE) (California Public Utilities Commission, 2014; Wang and Li, 2016), have started to implement the program by providing critical peak price as an optional electric service to complement the existing TOU systems.

The onsite microgrid has an economic advantage due to avoiding energy purchases during the demand response program and creation of carbon benefits through low-carbon/low-pollutant generation (Zhang et al., 2013, Amrollahi and Bathaee, 2017). It also provides secure and reliable energy supply during serious blackout period as a back-up energy supplying system. Therefore, the microgrid can significantly help to

decrease the energy cost for energy-intensive utility customers as well as ensure reliable energy management for the customers.

Significant number of researches can be reported while microgrid is used to lower the electricity cost during demand response program and enhance the energy security (Thompson et al., 2016; Wu et al., 2015; Pascual et al., 2014; Zhang et al., 2013; Al-Saedi et al., 2013; Mizani and Yazdani, 2009). For example, Optimal scheduling of a smart homes with microgrid system is studied to minimize the energy consumption cost considering the demand response program in (Zhang et al., 2013). To reduce the electricity cost, microgrid lifetime cost, and emission, optimally design the renewable power sources of the microgrid system and developing strategic control plan of the devices in grid-connected mode is investigated in (Mizani and Yazdani, 2009).

In addition to the demand response programs, another category of demand response program known as the overgeneration oriented demand response program is also implemented by the grid when the electricity generation from the grid exceeds the load. Due to the high penetration of renewable sources in the grid, it can occur during the period when the solar energy ramps so fast or the wind speed is very high. At the period, the electricity grid offers lower price to consumers the excess electricity by increasing the load of the customers to maintain the reliability of the grid. Very few studies focusing on the strategy dealing with overgeneration mitigation-oriented demand response program that encourages higher consumption during the given periods have been reported. Among the studies, Joo et al. illustrated the feasibility and benefits of such over-generation mitigation-oriented demand response programs from the perspective of grid operator (Joo et al., 2016). Islam et al. (2017a, 2017b) quantified the incentive and penalty mechanism

as well as desired energy consumption level for over-generation periods in such over-generation mitigation-oriented demand response programs considering the interests from both utility and customer sides. Later, Islam et al. (2017a, 2017b) also proposed a simulation-in-the-loop model to examine the potential benefits regarding cost reduction for the manufacturers with onsite microgrid systems when participating in such overgeneration mitigation-oriented demand response programs using some intuitive participation strategies, e.g., keeping the load as high as possible by running all the production equipment and consuming less energy from the microgrid system during over-generation periods.

## 2.4. PERFORMANCE EVALUATION OF THE ONSITE MICROGRID THROUGH BATTERY LIFE ESTIMATION

Due to the technological advancement, the smart grid has taken the grid technology to the next level where an individual customer not only consumes the energy but also generate the green energy and has the facility to share the surplus with the main utility grid or other energy consumers. The individual having the capability is known as the “prosumer” in the energy value network (Rathnayaka et al., 2014). The sustainability and efficiency of the infrastructure can be enriched by aggregating such prosumers to develop a community-based network. To ensure a resilient, long-term, and sustainable energy-sharing process in the network, effective energy management of prosumers is crucial.

Most promising OGS built by the prosumers (especially manufacturer) consists of solar PV, wind turbine, and BESS (Deshmukh and Deshmukh, 2008; Islam et al., 2019; Zhang et al., 2018). The BESS is used as the backup resources for the OGS to address the

intermittency of the renewable sources (Bahramirad et al., 2012; Koohi-Kamali et al., 2013). A significant number of researches can be reported to estimate and improve the lifetime of BESS for reliable operation in hybrid OGS (Drouilhet et al., 1997; Kaiser, 2017; Layadi et al., 2017). For example, Drouilhet et al. proposed a battery life prediction method to investigate the effects of varying depths of discharge and rates of discharge in hybrid power applications (Drouilhet et al., 1997). Layadi et al. developed a battery aging model using rain flow method to estimate the lifetime of lead–acid batteries for hybrid power sources design (Layadi et al., 2017).

## 2.5. GAPS IN THE LITERATURE

The industrial sector is a main contributor to this increasing trend of electricity demand. Approximately, over one-quarter of electricity is consumed by the industrial sector in the United States (EIA, 2011) where the manufacturing activities dominate industrial energy consumption (Duflou et al., 2012). It is reported that about 90% of industry energy consumption and 84% of energy-related industry carbon dioxide emissions are contributed by manufacturing sector (Schipper, 2006).

While a great number of researches can be mentioned for the design and operational management for the residential, commercial, and critical facilities, a small number of studies focusing on the industrial sector regarding the sizing of the renewable sources and optimal energy management plan have been reported (Thornton et al., 2018; Ruangpattana et al., 2011; Suazo-Martínez et al., 2014; Pamparana et al., 2017). For example, the size of the microgrid system for a construction & demolition waste processing facility was investigated in (Thornton et al., 2018). As for the manufacturing

end-use customers, a few studies resorting to some simplification assumptions to analyze the design and sizing of microgrid system have been reported. For example, a time series model was proposed to predict the available renewable energy and energy demand of a manufacturing system based on which scenario analysis was further implemented to analyze the cost-effectiveness performance of the microgrid system considering different load & supply scenarios (Zhong et al., 2017). It can offer some insights in terms of microgrid system size; however, it cannot derive the optimal size of the system. In addition, this research ignored the demand from the HVAC system, which is typically considered the second top energy consumer in a manufacturing plant (U.S. Energy Information Administration, 2002), and thus, the energy demand used for sizing the microgrid is underestimated. It can be seen that there exists a research gap in terms of a sufficient investigation and modeling of microgrid generation system sizing and operational planning for the manufacturing end use customers considering the energy demand from both manufacturing system and HVAC system.

The process of microgrid design will be more practical when different demand response program will be integrated into the model. Generally, two different types of demand response program are adopted by the grid: TOU and CPP. In comparison to the traditional TOU that has already been widely used in many areas of the United States as a base electricity tariff system (He and David, 1997; Kamyab and Bahrami, 2016), CPP has obtained more and more attention (California Public Utilities Commission, 2014; Wang and Li, 2016) to maintain grid reliability during the emergency. A limited number of studies focused on the microgrid planning considering the demand response programs. For example, Nikmehr et al. investigated the impact of demand response programs on

optimal day-ahead scheduling in grid of microgrids under TOU demand response program. (Nikmehr et al. 2017). Shen et al. proposed a microgrid energy management strategy with demand response to provide peak shaving for the grid using the peak-time rebate scheme (Shen et al. 2016). However, optimally designing and developing operational strategy for the microgrid system for manufacturing considering the energy demand of both manufacturing system and HVAC system under different demand response programs (TOU and CPP) is still underexplored.

In addition to optimally sizing and controlling the microgrid, very few studies focusing on the strategy dealing with over-generation mitigation-oriented demand response program have been reported. It is crucial for grid reliability and effectively reduction of overall electricity cost for manufacturing. The quantitative metrics in the manufacturing such as production throughput, microgrid system utilization cost, electricity billing cost, etc., need to be carefully examined when participating in such demand response programs. However, the participation strategy of the manufacturers in such a demand response program, corresponding energy consumption profile depending on the production schedule of manufacturing system, and utilization schedule of microgrid system considering quantitative metrics of the manufacturing has not yet been well studied.

After designing the onsite microgrid and developing the optimal control strategies considering different demand response programs, the next leap for future energy infrastructure is to build a community-based network where each individual will generate energy and share the surplus energy with their neighbors and main utility grid. To ensure the sustainability of the network, it is required to evaluate and monitor the performance

of the components existed in the network for the reliable operations for the network. One of the critical as well as costly components used in the OGS to enhance the reliability of the network is the BESS. Typically, the users of the BESS determine the lifetime of the BESS based on the standard operating conditions (constant temperature, current, and depth of discharge) provided (quoted) by manufacturers of the BESS and develop the optimal energy management plan (Agarwal et al., 2010; Ecker et al., 2012; Kaiser, 2007). However, the environment becomes more dynamic and stochastic due to the additional uncertainty in the network: demand variability of the participants and their energy sharing capability. Therefore, the actual operating conditions are quite different from the standard ones. In such a situation, optimally designing the energy management plan using the standard condition can lead to gross errors and may result in a higher system cost due to the early failure of the BESS. Therefore, it is required to monitor the lifetime of the BESS and consider it as a critical performance evaluation metric for reliable operation of the OGS in the network. While the existing literature mostly focused on estimating the lifetime of BESS in residential and commercial sectors (Alramlawi and Li, 2020; Farinet et al., 2019; Soto et al., 2019; Stroe and Schaltz, 2019; Zhang et al., 2019), the estimation of the lifetime in a community-based network considering the additional stochasticity and dynamic behavior of the environment is still not appropriately addressed.

# 3. OPTIMAL SIZING AND PLANNING OF MICROGRID SYSTEM FOR MANUFACTURING IN TIME OF USE (TOU) DEMAND RESPONSE PROGRAM

## 3.1. STRATEGIC OVERVIEW

The goal of this section is to identify the size of the microgrid system including solar PV, wind turbine, and BESS, as well as the corresponding operational strategy of each component in the microgrid system to minimize the energy-related cost including electricity billing cost due to purchasing electricity from the grid, operational & maintenance cost of the microgrid system, and the income due to the energy sold back to the grid. An integrated simulation model is proposed to identify and capture the variations of the energy demand of a manufacturing plant including both manufacturing system and HVAC system without losing the mutual influence and interrelationship of the energy consumption between the two systems characterizing manufacturing plant parameters including productivity characteristics, energy consumption profile of the manufacturing machines on various operational states, manufacturing system layout, manufacturing building parameters, HVAC relevant parameters, etc. The energy demand data identified by the integrated simulation model is used along with the data series of solar irradiance and wind speed as the input to the Mixed Integer Nonlinear Programming (MINLP) optimization model. Linearization strategy is explored and compared to a meta-heuristic method, Particle Swarm Optimization (PSO), to solve the proposed MINLP model through examining the balance between computational cost and solution quality. A case study including sensitivity analysis based on a real auto component manufacturing plant is conducted to verify the effectiveness of the proposed model.

The major contributions of the section can be summarized as follows:

1. The sizing of the microgrid system is extended from traditional commercial customers, residential customers, critical facilities, etc. to manufacturing end-use customers.

2. The energy loads from both manufacturing system and HVAC system are modeled and quantified when sizing the microgrid system for manufacturing end-use customer through a joint simulation model.

The rest of the section is organized as follows. Section 3.2 introduces the integrated simulation model that can generate various energy demands of a manufacturing plant for the optimal sizing model. Section 3.3 presents the detailed formulation of the MINLP optimization model. Section 3.4 discusses the linearization techniques of the nonlinear equations and explores the solution strategies when solving the proposed MINLP model. Section 3.5 conducts a case study using relevant parameters from a real auto component manufacturing plant and the data of solar irradiance and wind speed in the Chicago area to illustrate the effectiveness of the proposed model. Section 3.6 concludes the section and discusses the future work.

## 3.2. AN INTEGRATED SIMULATION MODEL FOR MANUFACTURING LOAD ESTIMATION

In this section, an integrated simulation model consisting of two primary platforms as shown in Figure 3.1 is used to capture the variations of the energy demand of the manufacturing plant.

The first platform used is Plant Simulation (Crawley et al., 2000) where the simulation model of the manufacturing system is built using the parameters such as

system layout, logistic/flow relationship, equipment downtimes, and equipment energy consumption profile. By running the simulation model for a specified time horizon, the power consumption profile of the manufacturing system at different time intervals in the given horizon can be obtained.


Figure 3.1 Integrated simulation model.

The second platform used in the integrated simulation model is based on EnergyPlus, an energy analysis, and thermal load simulation program (SEIA, 2017). It combines the size and geometry of the facility, construction materials, internal heat loads, HVAC systems, and temperature to establish a proper thermal behaviors model for the manufacturing plant so that the energy consumption of the HVAC system can be dynamically recorded. The obtained power consumption profile of the manufacturing system using Plant Simulation for a specified period is modeled as an internal heat source when integrated into the building model in EnergyPlus to establish a combined manufacturing and HVAC system simulation model. With this integrated simulation model, we can examine the total energy demand of the entire manufacturing plant for the planning horizon.

## 3.3. PROPOSED MODEL

In this section, a mathematical model is proposed to optimally design the microgrid system and afterwards, effectively control the microgrid system for sustainable energy management in manufacturing. The notations used to develop the model in this section are listed as follows.

*Sizing Decision Variables*

| | |
|---|---|
| $a$ | area of solar PV system ($m^2$) |
| $e$ | capacity of the BESS (kW) |
| $h$ | number of wind turbines |

*Control Decision Variables*

| | |
|---|---|
| $bc_{t_m}$ | BESS charging rate at interval $t_m$ (kW) |
| $bd_{t_m}$ | BESS discharging rate at interval $t_m$ (kW) |
| $g_{t_m}$ | electricity purchased from the grid at interval $t_m$ (kW) |
| $s_{t_m}$ | electricity sold back to the grid at interval $t_m$ (kW) |

*Parameters* (Lower Case)

| | |
|---|---|
| $i$ | discount rate |
| $m$ | index of the months in a year |
| $n$ | number of the years in the lifetime of the microgrid system |
| $r$ | radius of the wind turbine blade |
| $s$ | index of the iterations in PSO |
| $t_m$ | index of the discretized intervals in month $m$ |
| $v_{avg}$ | average wind speed (m/s) |

$r_B$ percentage of operation & maintenance cost for BESS in terms of total investment

$r_S$ rate of yearly operation & maintenance cost of solar PV system ($/kW)

$r_W$ rate of yearly operation & maintenance cost of wind turbine system ($/kW)

*Parameters* (Upper Case)

$C_B$ investment per unit capacity of BESS ($/kW)

$C_S$ investment per unit capacity of solar PV ($/kW)

$C_W$ investment per unit capacity of wind turbine ($/kW)

$E^p_{t_m}$ electricity consumption charging rate ($/kWh) at interval $t_m$

$E^s_{t_m}$ electricity sold back price ($/kWh) at interval $t_m$

$I_{avg}$ average irradiance of solar energy (W/m$^2$)

$I_{t_m}$ irradiance of solar energy at interval $t_m$ (W/m$^2$)

$M$ number of months in a year

$N$ maximum number of charging-discharging cycles of the BESS

$P_m$ power demand charging rate ($/kW) in month $m$

$S$ maximum iteration number in PSO

$SOC_{t_m}$ state of charge of the BESS at the beginning of the interval $t_m$

$SOC_{\max}$ maximum state of charge of BESS (%)

$SOC_{\min}$ minimum state of charge of BESS (%)

$T_m$ number of intervals in month $m$

$W_S$ rated capacity of solar PV system

$W_W$ rated capacity of wind turbine system

$X$ minimum time required to fully charge or discharge the BESS

*Parameters* (Greek Letter)

$\Delta t$ constant duration of the discretized time interval

$\delta$ efficiency of solar system

$\eta_c$ charging efficiency of BESS

$\eta_d$ discharging efficiency of BESS

$\eta_g$ electrical generator efficiency of wind turbine

$\eta_t$ gearbox transmission efficiency of wind turbine

$\theta$ power coefficient of wind turbine

$\rho$ density of air

$\alpha_{\max}$ maximum inertia weight in PSO

$\alpha_{min}$ minimum inertia weight in PSO

$\alpha\ (s)$ inertia weight at iteration $s$ in PSO

The time horizon of each month m is discretized into a set of intervals with equal duration of $\Delta t$. Let $t_m$ be the index of such intervals in month $m$. An optimization model is proposed to identify the optimal size of solar PV, wind turbine, and BESS system as well as the corresponding control strategies in each interval to satisfy the energy demand of the manufacturing plant throughout a calendar year that can minimize the yearly energy-related cost including electricity billing cost due to the purchase of the electricity from the grid, the depreciation & operational & maintenance cost of the microgrid system, and the income due to selling electricity generated by the microgrid system back to the grid. The control strategies include the electricity purchased from or sold back to

the grid, and the BESS charging or discharging rate at interval $t_m$. The objective function can be formulated as follows.

$$\min GC + BC + SC + WC - SI \tag{1}$$

In Equation (1), *GC* is the yearly electricity billing cost from the grid, which includes both electricity consumption charge based on the electricity consumed and power demand charge based on the maximum level of power drawn from the grid throughout the billing cycle, typically, a month. *BC*, *SC*, and *WC* are the depreciation and operational & maintenance costs of BESS, solar PV, and wind turbine, respectively. *SI* is the income when the excess energy generated from the microgrid system is sold back to the grid.

*GC* can be calculated by Equation (2).

$$GC = \sum_{m=1}^{M} \sum_{t_m=1}^{T_m} g_{t_m} \cdot \Delta t \cdot E_{t_m}^{p} + \sum_{m=1}^{M} P_m \cdot \max_{t_m}(g_{t_m}) \tag{2}$$

where $g_{t_m}$ is the power drawn from the grid at interval $t_m$. $E_{t_m}^{p}$ is the electricity purchasing price at interval $t_m$. $P_m$ is the power demand charging rate in month $m$.

BC can be calculated by Equation (3).

$$BC = C_B \cdot e \cdot f + OM_B \tag{3}$$

where $C_B$ is investment per unit capacity of BESS ($/kW). $e$ is the capacity of the BESS (kW). $f$ is the factor that transfers the present value of the BESS investment to the annual values throughout the lifetime of BESS, which can be calculated by

$$f = \frac{i(1+i)^n}{(1+i)^n - 1} \tag{4}$$

where *i* is the yearly discount rate, and *n* is the number of years of the lifetime of the microgrid system. In this research, to simplify the problem formulation, we first assume that the lifetimes of solar PV and wind turbine systems are the same since existing literature shows that their lifetimes are close (Ziegler et al., 2018; Vasel-Be-Hagh and Archer, 2017). Further, we also make the BESS lifetime match the solar and wind turbine system lifetimes via constraining the charging-discharging cycles in each year (see constraint in Equation (20).

$OM_B$ is the yearly operational & maintenance cost of the BESS, which can be calculated by

$$OM_B = r_B \cdot e \cdot C_B \tag{5}$$

where $r_B$ is the percentage of operation & maintenance cost for BESS with respect to the total initial investment.

*SC* can be calculated by Equation (6).

$$SC = C_S \cdot W_S \cdot f + OM_S \tag{6}$$

where $C_S$ is investment per unit capacity of solar PV ($/kW). $W_S$ is the rated capacity (kW) of solar PV system, which can be calculated as follows.

$$W_S = a \cdot I_{ave} \cdot \delta / 1000 \tag{7}$$

where $I_{ave}$ is the average solar irradiance of the given location (W/m$^2$). $\delta$ is the efficiency of the solar PV system. *a* is the area of solar PV (m$^2$).

$OM_S$ is the yearly operation & maintenance cost of the solar PV system, which can be calculated by

$$OM_S = r_s \cdot W_s \tag{8}$$

where $r_s$ is the operation & maintenance cost per unit capacity of the solar PV system.

*WC* can be calculated by Equation (9)

$$WC = C_W \cdot W_W \cdot f + OM_W \tag{9}$$

In Equation (9), $C_W$ is investment per unit capacity of the wind turbine ($/kW). $W_W$ is the rated capacity (kW) of the wind turbine, which can be calculated by

$$W_W = \frac{1}{2} \cdot \rho \cdot \pi \cdot r^2 \cdot v_{avg}^3 \cdot \theta \cdot \eta_t \cdot \eta_g \cdot h / 1000 \tag{10}$$

where $\rho$ is the density of air. $v_{avg}$ is average wind speed. $\theta$ is the power coefficient of the wind turbine. $r$ is the radius of the wind turbine blade. $\eta_t$ is the gearbox transmission efficiency of the wind turbine. $\eta_g$ is the electrical generator efficiency of the wind turbine. $h$ is the number of wind turbines. It is better to mention that the effect of hub height is neglected in this study. It is assumed that the hub height of the wind turbines used to design the microgrid system is set to its optimal hub height (either the maximum or minimum hub height) to maximize the wind generation (Eberhart and Kennedy, 1995).

$OM_W$ is the yearly operation and maintenance cost of the wind turbine, which can be calculated by

$$OM_W = r_W \cdot W_W \tag{11}$$

where $r_W$ is the operation & maintenance cost per unit capacity of the wind turbine system.

*SI* can be calculated by Equation (12)

$$SI = \sum_{m=1}^{M} \sum_{t=1}^{t_m} s_{t_m} \cdot \Delta t \cdot E_{t_m}^s \tag{12}$$

where $s_{t_m}$ is the power (kW) sold back to the grid at interval $t_m$. $E_{tm}^s$ is the electricity sold back price ($/kWh) at interval $t_m$.

The constraints of the problem are introduced as follows. The energy flow balance constraint can be described by

$$g_{t_m} = D_{t_m} - r_{t_m} - w_{t_m} + s_{t_m} + bc_{t_m} - bd_{t_m} \tag{13}$$

where $D_{t_m}$ is the electricity demand of the manufacturing plant at interval $t_m$. It can be generated by the integrated simulation model described in Section 2. $bc_{t_m}$ and $bd_{t_m}$ are the BESS charging and discharging rates (kW) at interval $t_m$, respectively.

In Equation (13), $r_{t_m}$ is the electricity generated by the solar PV, which can be calculated by

$$r_{t_m} = a \cdot I_{t_m} \cdot \delta / 1000 \tag{14}$$

where $I_{t_m}$ is the solar irradiance at interval $t_m$ (W/m$^2$).

In Equation (13), $w_{t_m}$ is the electricity generated by the wind turbine, which can be calculated by

$$w_{t_m} = \frac{1}{2} \cdot \rho \cdot \pi \cdot r^2 \cdot v_{t_m}^3 \cdot \theta \cdot \eta_t \cdot \eta_g \cdot h / 1000 \tag{15}$$

where $v_{t_m}$ is the wind speed at interval $t_m$. The state of charge of BESS has to be bounded within a given range, which can be formulated as

$$SOC_{\min} \le SOC_{t_m} \le SOC_{\max} \tag{16}$$

where $SOC_{max}$ and $SOC_{min}$ are the maximum and minimum states of charge of the BESS (%). $SOC_{t_m}$ can be calculated recursively as follows

$$SOC_{t_m+1} \cdot e = SOC_{t_m} \cdot e + \eta_c \cdot bc_{t_m} \cdot \Delta t - \frac{1}{\eta_d} \cdot bd_{t_m} \cdot \Delta t \tag{17}$$

In addition to maintaining the state of charge, the charging or discharging rate of the BESS should not exceed the maximum limit, which can be formulated as follows

$$bc_{t_m} \le e / X \tag{18}$$

$$bd_{t_m} \le e / X \tag{19}$$

where $X$ is the minimum time required to charge or discharge the BESS.

The lifetime of BESS is mainly determined by the charging-discharging cycles. As mentioned earlier, we make the BESS lifetime match the solar and wind turbine system lifetimes by constraining the yearly charging-discharging cycles as shown in (20).

$$\sum_{m} \sum_{t_m=1}^{T_m} \left( \frac{(bc_{t_m} + bd_{t_m}) \cdot \Delta t}{2e(SOC_{\max} - SOC_{\min})} \right) \le N / n \tag{20}$$

where $N$ is the maximum allowed charging-discharging cycles of BESS.

The overall energy-related cost with microgrid system should be less than or equal to the energy billing cost without microgrid system, which can be formulated as

$$GC + BC + SC + WC - SI \le GC' \tag{21}$$

where $GC'$ is the electricity billing cost without microgrid system. It can be formulated by

$$GC' = \sum_{m=1}^{M} \sum_{t_m=1}^{T_m} D_{t_m} \cdot \Delta t \cdot E_{t_m}^{p} + \sum_{m=1}^{M} P_m \max_{t_m}(D_{t_m}) \tag{22}$$

In addition, Equation (23) is formulated to avoid simultaneous charging and discharging of the BESS at any interval. Similarly, Equation (24) restricts the model from simultaneously purchasing and selling back the electricity from/to the grid.

$$bc_{t_m} \cdot bd_{t_m} = 0 \tag{23}$$

$$g_{t_m} \cdot s_{t_m} = 0 \tag{24}$$

## 3.4. SOLUTION STRATEGY

The solution strategy adopted in this section is described below:

**3.4.1. Linearization.** It can be seen that the problem formulated in Section 3.3 is a MINLP. A linearization strategy is adopted as follows to linearize the formulation so that some existing linear programming solver can be used to solve the problem.

There are three nonlinear terms in the formulated problem, i.e., the demand charge in electricity billing cost shown by the 2nd term on the right hand side of Equation (2), non-simultaneous charging/discharging of BESS constraint shown in Equation (23), and non-simultaneous electricity purchasing and sold back from/to the grid constraint shown in Equation (24).

Equation (2) can be linearized by

$$GC = \sum_{m=1}^{M} \sum_{t_m=1}^{T_m} g_{t_m} \cdot \Delta t \cdot E_{t_m}^{p} + \sum_{m=1}^{M} P_m \cdot K_m \tag{25}$$

where $K_m$ is an auxiliary variable to determine the maximum value of $g_{t_m}$ over the time horizon of month $m$, which can be formulated by (26)

$$K_m \geq g_{t_m} \tag{26}$$

Equation (23) can be linearized by

$$bc_{t_m} \leq u_{t_m} \cdot (e / X) \tag{27}$$

$$bd_{t_m} \leq (1 - u_{t_m}) \cdot (e / X) \tag{28}$$

$$z_{t_m} = u_{t_m} \cdot e \tag{29}$$

$$z_{t_m} \leq M_1 \cdot u_{t_m} \tag{30}$$

$$z_{t_m} \le e \tag{31}$$

$$z_{t_m} \ge e - (1 - u_{t_m}) \cdot M_1 \tag{32}$$

$$z_{t_m} \ge 0 \tag{33}$$

where $u_{t_m}$ is an auxiliary binary variable. $z_{t_m}$ is a continuous variable and $M_1$ is a large real number.

Similarly, Equation (24) is linearized by introducing the following constraints:

$$g_{t_m} \le y_{t_m} \cdot M_2 \tag{34}$$

$$s_{t_m} \le (1 - y_{t_m}) \cdot M_3 \tag{35}$$

where $y_{t_m}$ is an auxiliary binary variable. $M_2$ and $M_3$ are two large real numbers.

After applying the linearization strategy aforementioned, the MINLP problem can be transformed into a Mixed Integer Linear Programming (MILP) problem. The toolbox "intlinprog" in Matlab is used to solve the MILP based on the algorithm of dual simplex. "intlinprog" can work very well to solve the proposed problem for a three-month timescale using 14,805 seconds.

Considering the periodic variation of the availability of the renewable sources in a given area, one year is an appropriate time scale for determining the size of the microgrid system in this model. However, when the time scale is increased from three months to one year as intended by the proposed problem, the toolbox becomes inefficient, and the computational time becomes extremely long. For the planning horizon of three months, 12,966 variables and 23,761 constraints are required to represent the optimization problem. When the planning horizon increases to one year, additional 47,529 variables and 71,280 constraints need to be added to the problem. Therefore, the dimension of the

yearly problem becomes significantly large (60,495 variables and 95,041 constraints). Consequently, almost 490,000,000 new elements are required to be added to the new coefficient matrix for generating each constraint equation of the yearly analysis. Meanwhile, from the perspective of linearization procedure, for a one-year time horizon formulation, additional 25,920 variables and 51,840 constraints need to be added to the original formulation (34,575 variables and 60,481 constraints) for linearizing all the nonlinear terms. Thus, even we use a cluster computer of 64 processors with 256 GB memory, it takes more than 168 hours without obtaining the solution. Therefore, a pure linearization strategy is not very efficient to solve the proposed problem with the desired time scale.

**3.4.2. Particle Swarm Optimization.** Considering the high dimension of the proposed model and the inefficiency of using linear solver toolbox to solve the problem after linearization, we propose to use a widely used meta-heuristic method, Particle Swarm Optimization (PSO), to solve the proposed problem to obtain a set of near-optimal solutions with a reasonable computational cost. PSO is a swarm intelligence and population-based optimization technique inspired and characterized by foraging behaviors of animal swarms (Hakimi et al., 2007).

Due to simplicity and powerful search capability, the PSO algorithm has been widely used for sizing, operation management, and performance analysis of the hybrid renewable energy system for the end use customers in residential sector (Hakimi and Moghaddas-Tafreshi, 2009; Gudi et al., 2011; Upadhyay and Sharma, 2015), commercial & office building sector (Liu et al., 2015; Karaguzel et al., 2014; Karaguzel et al., 2014), industry sector (Stoppato et al., 2014) , agricultural sector (Mushtaha and Krost, 2011),

and critical facility such as hospital (Buonomano et al., 2014). Recently, some researchers have further explored the theoretical connection between such heuristic algorithms and some existing analytical models such as Hamiltonian systems and gradient-based method (Hu and Li, 2017).

In this subsection, we introduce the PSO method to solve the proposed model as follows. The candidate solution is represented as a particle in a swarm when using PSO. The particles can fly in the search space based on the updated velocity towards its best location over time. After each flying step (or iteration), the velocity and location of each particle are updated according to Equation (36).

$$\begin{aligned} V(s+1) &= \alpha V(s) + c_1 w_1 (L_{PB} - L(s)) + c_2 w_2 (L_{GB} - L(s)) \\ L(s+1) &= L(s) + V(s+1) \end{aligned} \tag{36}$$

where $V(s+1)$ and $V(s)$ are the velocity matrix of the individual particle at iteration $s$ and $s+1$, respectively. $L(s)$ and $L(s+1)$ are the location matrix of the individual particle at iteration $s$ and $s+1$, respectively. $c_1$ and $c_2$ are the learning factors and $w_1$ and $w_2$ are the random real numbers between zero and one. $\alpha$ is the inertia weight. $L_{PB}$ is the particle's best solution that has been identified up to the $s$th iteration. $L_{GB}$ is the global best solution of the entire swarm.

The inertia weight is adaptively tuned with the iteration number as shown in Equation (37).

$$\alpha(s) = \alpha_{\max} - \frac{[(\alpha_{\max} - \alpha_{\min}) \cdot s]}{S} \tag{37}$$

where $\alpha_{max}$ and $\alpha_{min}$ are the maximum and minimum inertia weights, respectively. $S$ is the maximum iteration number. At the beginning, the inertia weight is large to explore complete solution space and move quickly towards the global minimum. With the

increase of iterations, the weight becomes smaller. Consequently, the particles can finely tune the solutions to converge to the near optimality.

The fitness function of an individual particle can be formulated as shown in (38) where all the constraints are integrated as penalty terms.

$$\begin{aligned} & GC + BC + SC + WC - SI + A \cdot \{ \sum_{m} \sum_{t_m=1}^{T_m} \left| g_{t_m} - D_{t_m} + r_{t_m} + w_{t_m} - s_{t_m} - bc_{t_m} + bd_{t_m} \right| \\ & + \sum_{m} \sum_{t_m=1}^{T_m} \max(0, SOC_{t_m} - SOC_{\max}) + \sum_{m} \sum_{t_m=1}^{T_m} \max(0, SOC_{\min} - SOC_{t_m}) \\ & + \sum_{m} \sum_{t_m=1}^{T_m} \max(0, bc_{t_m} - e / X) + \sum_{m} \sum_{t_m=1}^{T_m} \max(0, bd_{t_m} - e / X) \\ & + \sum_{m} \sum_{t_m=1}^{T_m} \max(0, (((bc_{t_m} + bd_{t_m}) \cdot \Delta t) - \frac{N}{n} \cdot 2 \cdot e \cdot (SOC_{\max} - SOC_{\min})) \\ & + \max(0, GC + BC + SC + WC - GC') + (bc_{t_m} \cdot bd_{t_m}) + (g_{t_m} \cdot s_{t_m}) \} \end{aligned} \tag{38}$$

where $A$ is a large real number.

### 3.5. CASE STUDY

A case study is conducted below to illustrate the effectiveness of the model.

**3.5.1. Input Parameters.** A real auto component manufacturing plant is used to build the case study for the proposed model. Considering the seasonal variation of the manufacturing demand and weather parameters (solar irradiance, wind speed), the temporal horizon selected in this case study is one year. Moreover, the time horizon is discretized into a set of one-hour intervals since hourly discretization of the time horizon for analyzing the energy behavior of the different systems (manufacturing, office building etc.) considering the thermal and energy dynamics is a reasonable practice in this field (Dhar et al., 1999; Solar Energy Local: Solar Energy Data and Resources in the US, 2018).

The manufacturing facility of this auto component plant is a one-story and one-thermal zone building as shown in Figure 3.2. The floor area of the facility is 100m by 50m and the height is 10m. Different materials are used for the construction of the facility. The walls and the roof are made of wood fiberglass and plasterboard. The floor consists of heavy concrete. The location is in Chicago, Illinois. The layout of the auto component manufacturing system is shown in Figure 3.3.

Figure 3.2 Manufacturing plant with the onsite microgrid system.

The manufacturing system consists of two major processes, i.e., machining and assembly. The machining process includes three stages of RM, SM, and HM that are used to fulfill the initial surface cutting, deeper surface cutting and drilling, and final finishing, respectively. Three parallel processing stations, i.e., Station A, Station B, and Station C are deployed to conduct RM process (they will also be denoted as RMA, RMB, and RMC in the rest of the parts of this section). Two parallel processing stations, i.e., Station D

and Station E are deployed to conduct SM process (denoted as SMD and SME). Two parallel processing stations, i.e., Station F and Station G are deployed to conduct HM process (denoted as HMF and HMG). One assembly station, i.e., Station H is deployed to conduct assembly process (denoted as ASS). Each processing station consists of several different machines with different functionalities like turning, grinding, and milling. In addition, other auxiliary machines such as demagnetization machine, washing machine, and balance machine are also included in certain stations. The assembly station includes several workplaces where the operators can fulfill the assembly tasks using the parts after machining and other part materials.

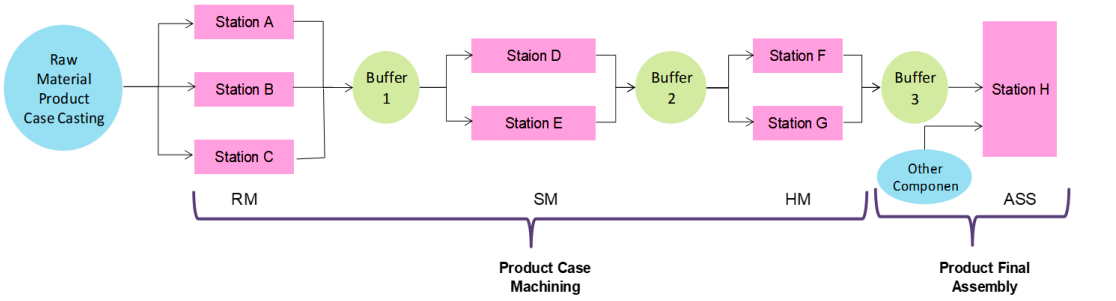


Figure 3.3 Layout of the auto component manufacturing plant.

The plant is assumed to be operated with a schedule of three eight-hour shifts per day, seven days per week, and all the weeks per year. The productivity related parameters and the part of energy-related parameters are shown in Tables 3.1- 3.3 for illustration. The relevant energy-related data of other machines are not given due to the confidentiality requirement.

Using such real productivity-related and energy-related data, a simulation model of this auto component manufacturing system is built on Plant Simulation. Snapshot of simulating the manufacturing system on Plant Simulation platform is shown in Figure 3.4.

Table 3.1 Cycle time of stations

| | RMA | RMB | RMC | SMD | SME | HMF | HMG | ASS |
|---|---|---|---|---|---|---|---|---|
| Cycle time (s) | 135 | 135 | 135 | 80 | 80 | 80 | 80 | 40 |

Table 3.2 Buffer capacity and initial content

| | Capacity | Initial Content |
|---|---|---|
| Buffer 1 | 1800 | 400 |
| Buffer 2 | 1800 | 400 |
| Buffer 3 | 1800 | 400 |

Table 3.3 Rated power of the manufacturing machines in RMA

| Machine Name | Rated Power (kW) |
|---|---|
| OP10 Turn-1 | 105 |
| OP20 Turn-2 | 105 |
| OP30 Turn-3 | 105 |
| OP40 Window milling | 155 |
| OP50 Turn-4 | 120 |

The model is run for the entire year with 30 replications and the power consumption profile of the manufacturing system is obtained. The power consumption profile of the manufacturing system from a certain replication is shown in Figure 3.5.

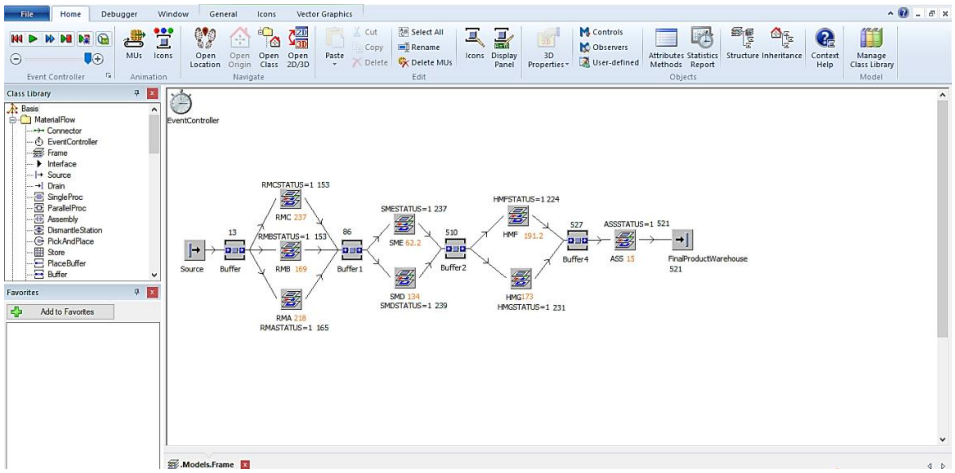


Figure 3.4. Snapshot of simulating the manufacturing system on Plant Simulation platform.

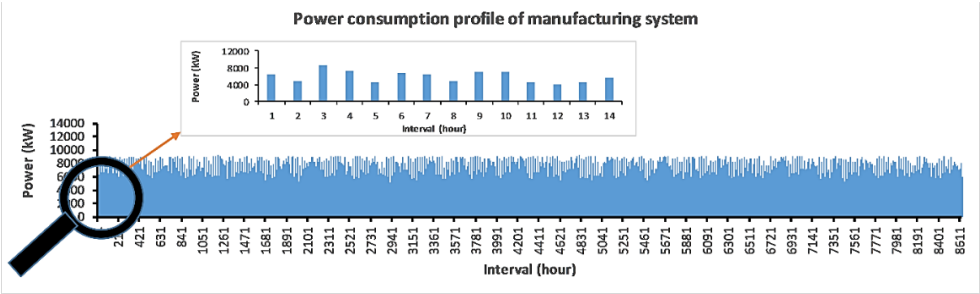


Figure 3.5 Yearly power consumption profile of the manufacturing system.

The resultant output of energy consumption profiles of the manufacturing system obtained from Plant Simulation is then used as the input in the EnergyPlus model along with the other specified parameters of the manufacturing facility. The target indoor temperature for the facility is set from 20 to 24 (degrees Celsius) for summer and 16 to

18 (degrees Celsius) for winter. The fraction radiant of the electric equipment of the manufacturing system is set as 0.3 and the convection coefficient is 0.7 (Wang et al., 2010). By specifying the weather condition of the year 2016 and using different inputs of the energy demand of manufacturing system, the thermal behavior of the construction material, and the variation of outdoor temperature, the HVAC power consumption profile can be obtained. Figure 3.6 demonstrates the snapshot of configuring the parameters in EnergyPlus.

The total power consumption profile of the manufacturing plant is computed by aggregating the power consumption profiles of the manufacturing system and the HVAC system. Thus, one critical input of the optimization model can be obtained. Figure 3.7 illustrates the total power consumption profile of the manufacturing plant including both manufacturing system and HVAC system at each interval of the year. The consumption and demand charge rates of the electricity purchased from the grid as well as sold back price are shown in Table 3.4. Here, the summer is from July 1st to September 31st, while the winter is from October 1st to June 30th.The data of solar irradiance and wind speed are collected from Solar Energy Local and State Climatologist of Illinois, respectively (State climatologist office for Illinois, 2018; Wikipedia, 2018). The efficiency of the solar PV is 21.5% (Clean Energy Reviews, 2018).

The parameters used to calculate the wind turbine power generation are shown in Table 3.5. The charging/discharging efficiency for the BESS is 90% (Rohani and Nour, 2014). Allowable maximum and minimum state of charge for the BESS is 90% and 10%, respectively. The parameters used to calculate the investment cost and operation & maintenance cost for the solar PV, wind turbine, and BESS are presented in Table 3.6.

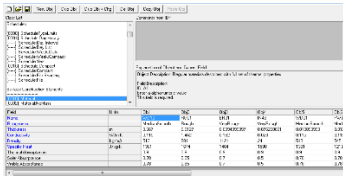

Figure 3.6 (a) Material selection

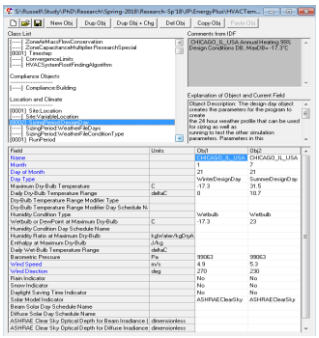

Figure 3.6 (b) Designing a day

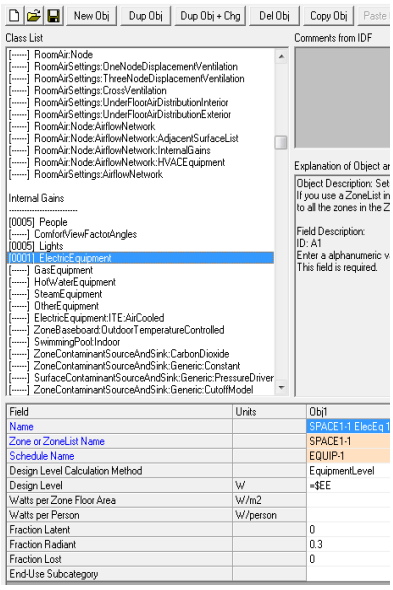

Figure 3.6 (e) Designing a day

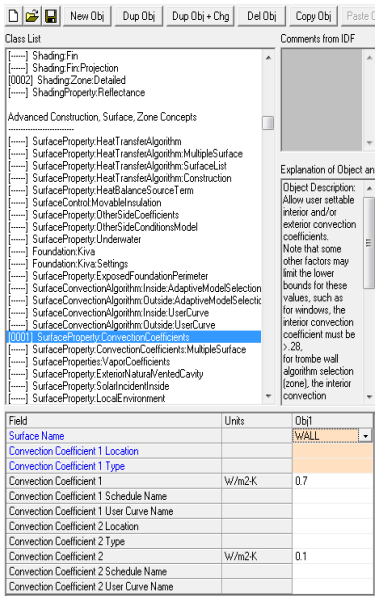

Figure 3.6 (g) Surface configuration

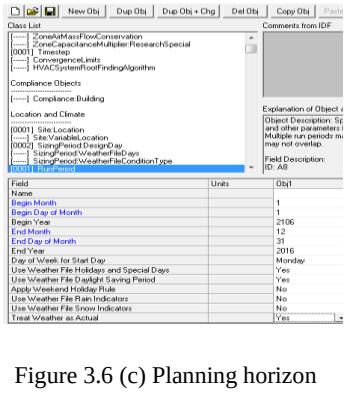

Figure 3.6 (c) Planning horizon

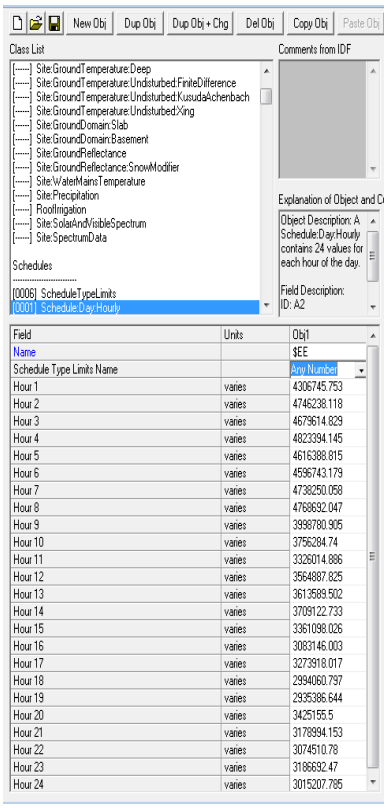

Figure 3.6 (f) Scheduling hourly consumption

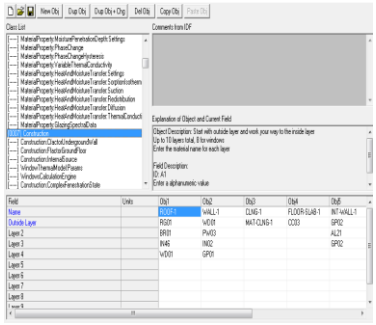

Figure 3.6 (h) Construction of the zone

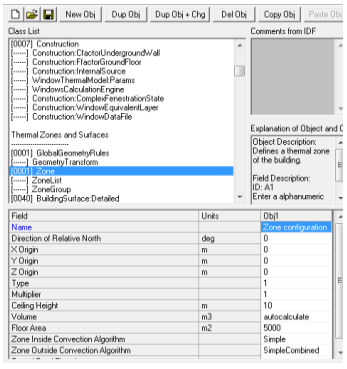

Figure 3.6 (d) Zone configuration

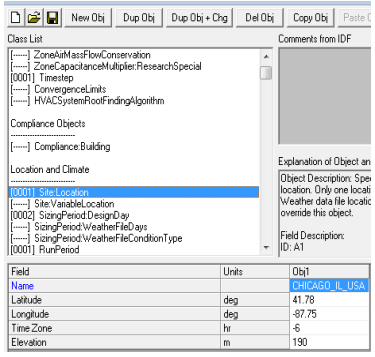

Figure 3.6 (i) Site selection

Figure 3.6 Snapshot of parameter configuration in EnergyPlus.

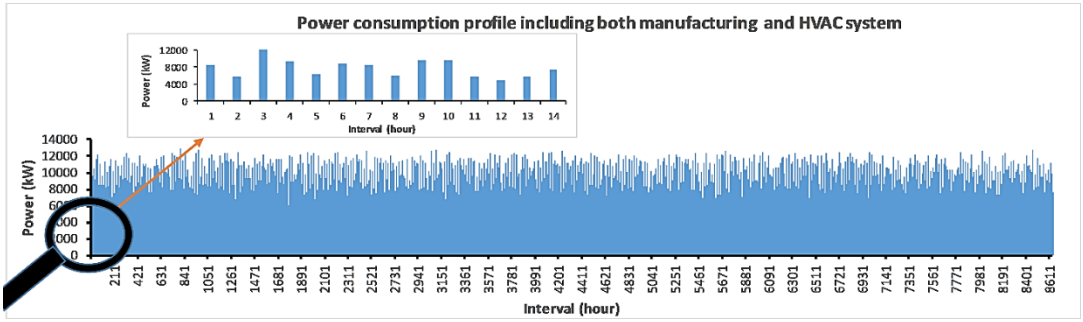


Figure 3.7 Yearly power consumption profile including HVAC system.

Table 3.4 Electricity purchase rate and sold back price

| Season | Period | Time | Consumption charge[1] ($/kWh) | Demand charge[1] ($/kW) | Sold back price[2] ($/kWh) |
|---|---|---|---|---|---|
| Summer | On-Peak | 1:00 pm-6:00 pm | 0.35 | 8.65 | 0.17 |
| | Mid-Peak | 10:00 am-1:00 pm<br>6:00 pm-9:00 pm | 0.19 | | 0.07 |
| | Off-Peak | 9:00 pm-10 am | 0.06 | | 0.00 |
| Winter | On-Peak | 5:00 pm-9:00 pm | 0.09 | 6.04 | 0.07 |
| | Off-Peak | 9:00 pm-5:00 pm | 0.06 | | 0.00 |

1. Time of Use Rate, NV Energy 2. Solar Quotes, 2018.

Table 3.5 Parameters used for wind turbine power generation[1]

| Parameters | Value |
|---|---|
| density of air ($\rho$) | 1.225 (kg/m3) |
| Power coefficient of the wind turbine ($\theta$) | 0.593 |
| Gearbox transmission efficiency of the wind turbine ($\eta_t$) | 90% |
| Electrical generator efficiency of the wind turbine ($\eta_g$) | 90% |

1. Wind Turbine Power Calculations, The Royal Academy of Engineering.

Table 3.6 Investment and operation & maintenance cost for the hybrid microgrid system with BESS

| System | Investment cost ($/kW) | Operation & maintenance cost ($/kW) |
|---|---|---|
| Solar PV[1] | 1770 | 7.5 |
| Wind Turbine[2] | 1590 | 28 |
| BESS[3] | 110 | 1% of investment |

1. U.S. Photovoltaic prices and cost breakdown, 2015. 2. Wind Technologies Market Report, 2016

3. Battery Energy Storage Market, 2016

PSO is encoded in Matlab. After tuning different PSO parameters, we use 500 as population size, 2000 as total number of iterations, and 1.7 as the learning factors. The maximum ($\alpha max$) and minimum ($\alpha min$) inertia weights are 0.09 and 0.01, respectively. The hardware used to implement the PSO in Matlab is a desktop with an Intel(R) Xeon(R) CPU W3505@ 2.53 GHZ processor and a 4 GB memory.

**3.5.2. Result Analysis.** Based on the aforementioned conditions and parameters, we first compare the solution quality and computational time between linearization strategy and PSO based on a three-month time horizon as shown in Table 3.7.

Table 3.7 Solution and computational time comparison between MILP after linearization and MINLP using PSO

| Model | MILP after Linearization | MINLP as Proposed |
|---|---|---|
| Tools | | PSO |
| Cost ($) | 603,489 | 616,162 |
| Performance Gap of Cost | +2.08% | |
| Computation Time (seconds) | 14,805 | 11,575 |
| Computing Time Difference | -27.90% | |

From Table 3.7, it is observed that PSO can obtain a very close solution while with a much-lowered computational time compared to the linearization strategy, which illustrates that PSO can be a good alternative for solving proposed MINLP problem considering the balance of computational cost and solution quality. The upper and lower bound with mean electricity purchased from the grid using 95% confidence intervals are illustrated in Figure 3.8. Note that there is no variation with respect to the number of wind turbines. This is because the incremental cost by adding a wind turbine is much higher than the incremental cost by increasing one $m^2$ of solar PV or one kW for BESS.

The PSO with such parameters is used to solve the proposed MINLP problem with 30 different scenarios of energy demand of the manufacturing plant obtained by the integrated simulation model. The 95% confidence intervals of the design parameters (area of the solar PV, number of wind turbines, and capacity of BESS) and the overall energy-related cost are identified as shown in Table 3.8.

Table 3.8 Statistical results of the design parameters and corresponding cost of the system

| Parameter | Mean value | Upper limit (95% confidence interval) | Lower limit (95% confidence interval) |
|---|---|---|---|
| Area of Solar PV ($m^2$) | 97,721 | 98,098 | 97,345 |
| Number of wind turbine | 3 | 3 | 3 |
| BESS Capacity (kW) | 33,257 | 33,854 | 32,659 |
| Cost ($) | 2,743,929.36 | 2,792,367.22 | 2,695,491.51 |

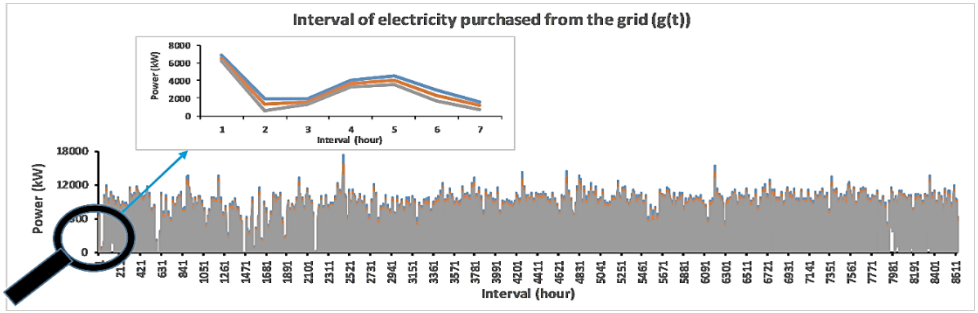


Figure 3.8 Interval of the electricity purchased from the grid.

The mean power generation profiles from the proposed onsite solar PV system and wind turbine system are presented in Figure 3.9 and Figure 3.10, respectively.

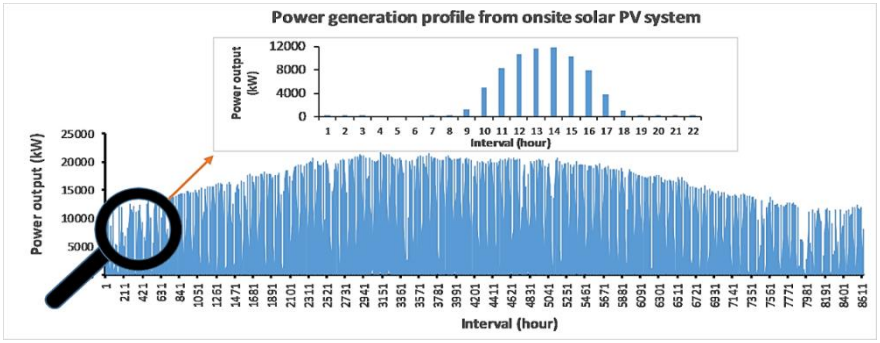


Figure 3.9 Power generation profile from onsite solar PV system.

From Figure 3.9, it is observed that the solar power generation increases during the summer season. It happens because the generation from solar panel depends on solar irradiance and the solar irradiance reaches its peak at summer. Moreover, the days are long in summer. However, the scenario is opposite in winter. Due to lower irradiance, the generation is less in winter. The generation from the wind turbine depends on the wind speed. In the winter of 2016, especially from January to April, the wind speed was

relatively higher than any other months. Therefore, Figure 3.10 shows several peaks of wind power during these months.

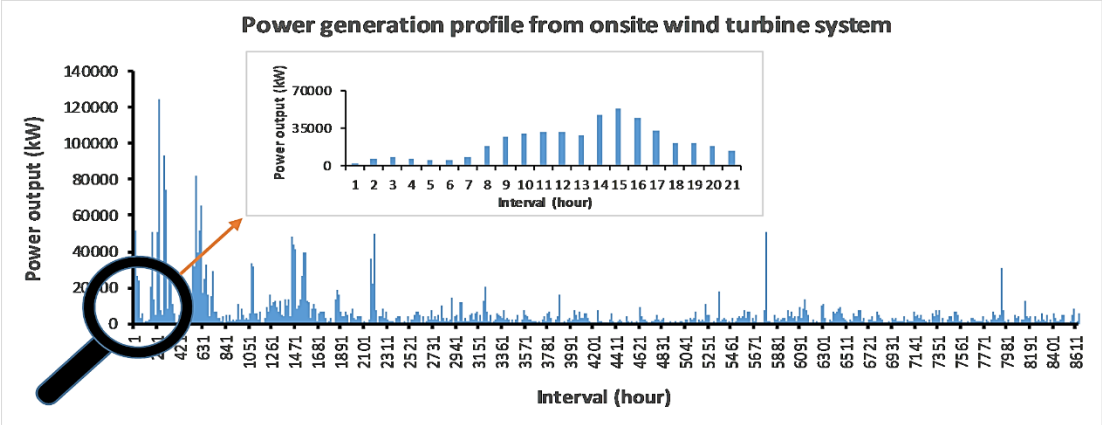


Figure 3.10 Power generation profile from onsite wind turbine system.

The mean power demanded and supplied at each interval of 12 months are illustrated in Figure 3.11. The supply and demand curves of each month depicted in Figure 3.11 represent that the supplied power meets the quantity demanded by the manufacturing plant throughout the year. Several peaks are observed at some intervals. The reason behind it is the high generation of wind energy as shown in Figure 3.10.

To meet the excess supply at those intervals, the amount of sold back energy to the grid and the resultant charging rate to the BESS are relatively higher than other intervals. The amount of electricity purchased from the grid and discharging rate from the BESS are higher when the generation from the onsite renewable sources are less. Due to the variation of the charging-discharging, the state of charge of the BESS fluctuates throughout the year as illustrated in Figure 3.12.

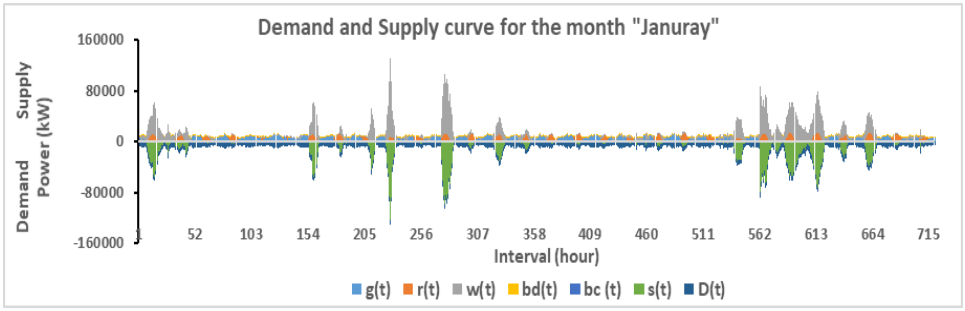


(a)

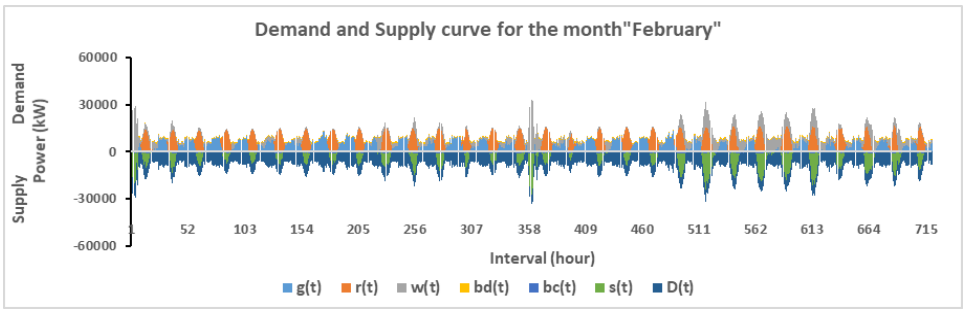


(b)

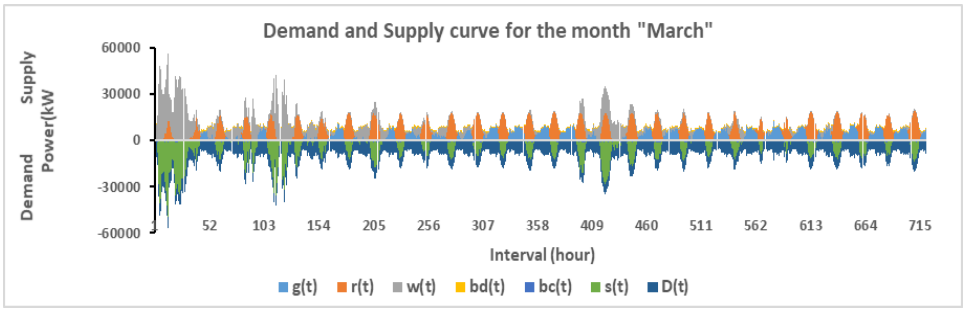


(c)

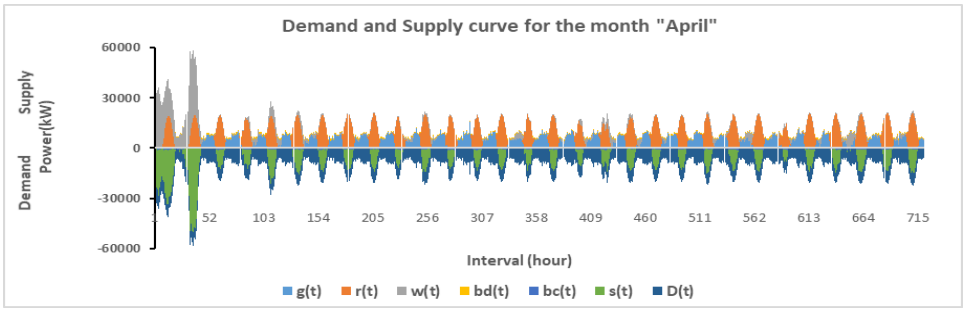


(d)

Figure 3.11 Supply and demand curve for the planning horizon

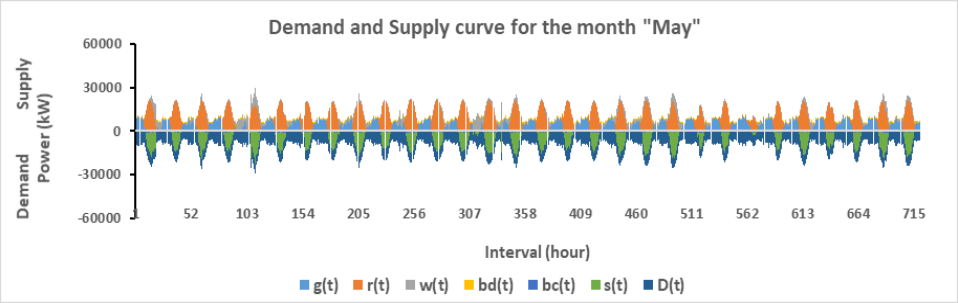


(e)

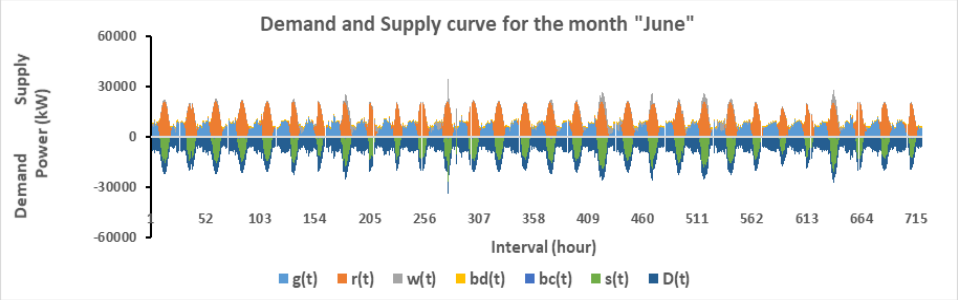


(f)

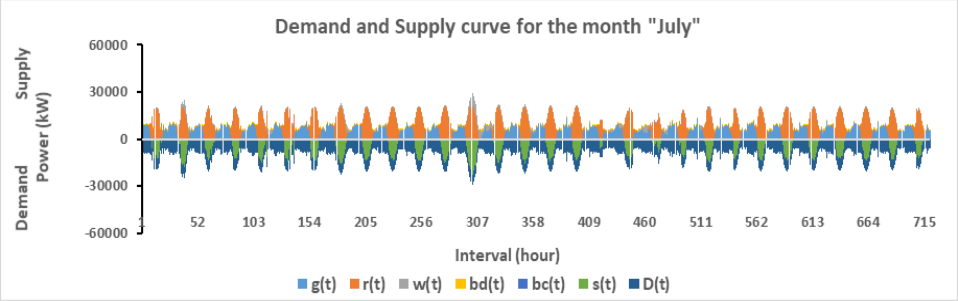


(g)

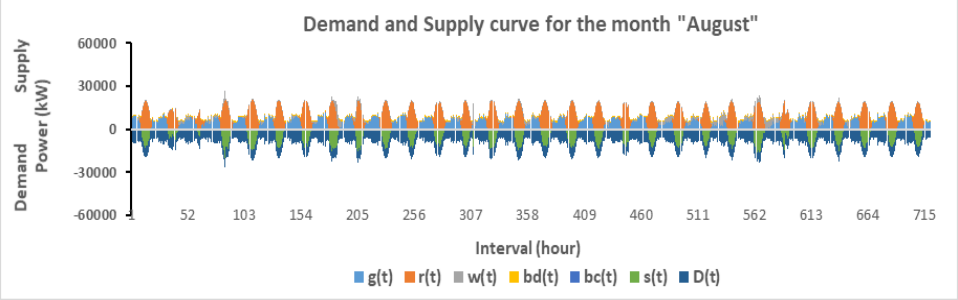


(h)

Figure 3.11 Supply and demand curve for the planning horizon (cont.)

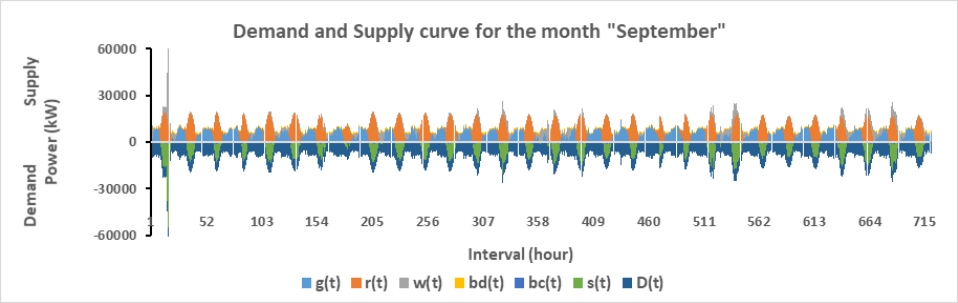


(i)

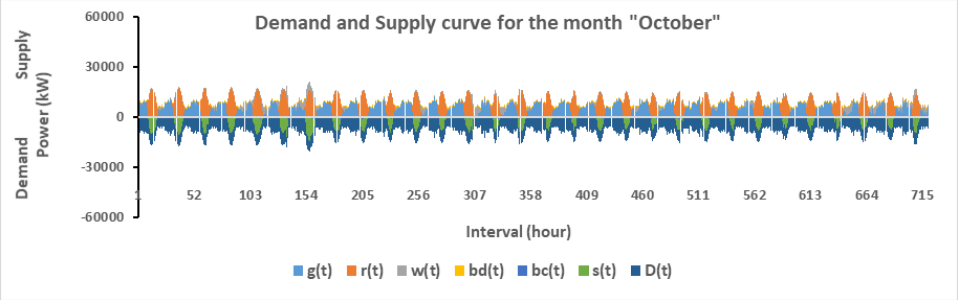


(j)

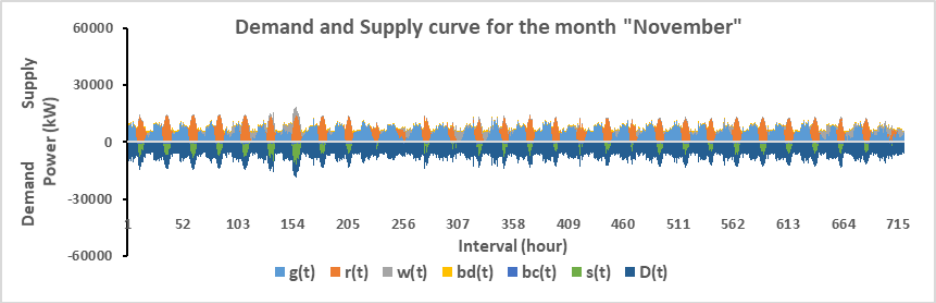


(k)

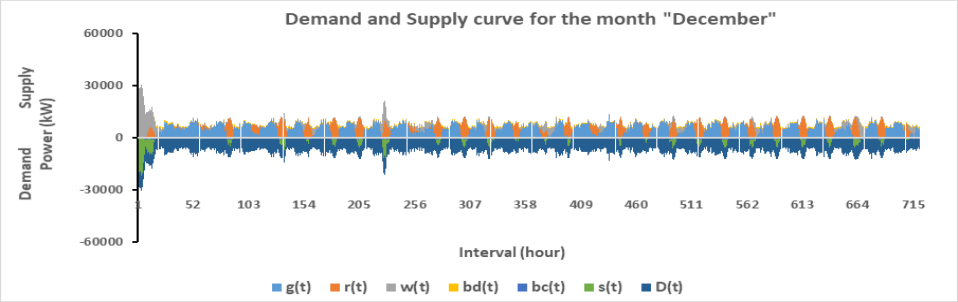


(l)

Figure 3.11 Supply and demand curve for the planning horizon (cont.)

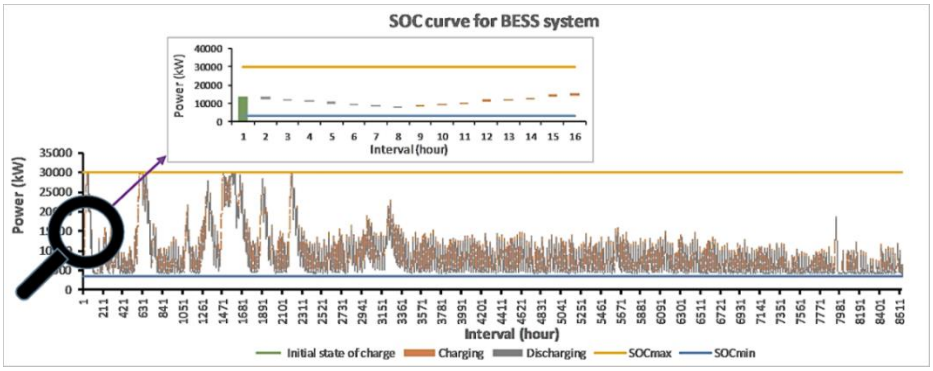


Figure 3.12 SOC curve for the BESS.

Furthermore, payback period analysis is conducted to determine the time to recover the investment for building the onsite microgrid system. It is assumed that the yearly benefit due to operating the onsite microgrid system will be approximately same throughout the lifetime (15 years in this study). The payback period based on the worst-case scenario is calculated and shown in Table 3.9.

Table 3.9 Payback period analysis

| Cost/benefit | Amount |
|---|---|
| Yearly electricity cost without microgrid system | $5,384,754.51 |
| Yearly electricity cost with microgrid system | $2,411,781.95 |
| Yearly electricity cost reduction | $2,972,973.56 |
| Yearly benefit from sold back energy to the grid | $1,313,387.97 |
| Total benefit from microgrid system | $4,288,393.55 |
| Total cost for hybrid renewable sources (Initial investment + O&M cost) | $24,683,031.69 |
| Simple Payback period | 5.76 years (95% CI: 5.69 to 5.82) |
| Discounted Payback period (2.75% discount rate) | 6.35 years (95% CI: 6.27 to 6.44) |

**3.5.3. Sensitivity Analysis.** The sensitivity analysis is conducted to determine the impact of the variations from some critical input parameters on the resultant decision variables with respect to system design. The critical parameters considered in the analysis are the amount of renewable sources available in the planning horizon (yearly solar irradiance and wind speed) and the price of sold back energy. Yearly average (derived from the monthly average mentioned in the references (Solar Energy Local, 2018) is used to measure the available level of the renewable sources. Average solar irradiance and wind speed from 2012 to 2016 are shown in Table 3.10.

Table 3.10 Average solar irradiance and wind speed from 2012 to 2016

| Year | 2012 | 2013 | 2014 | 2015 | 2016 |
|---|---|---|---|---|---|
| Average solar irradiance ($W/m^2$) | 221.41 | 219.26 | 216.10 | 225.05 | 238.75 |
| Average wind speed (m/s) | 4.00 | 3.94 | 3.87 | 4.36 | 3.97 |

The Scenario-I and Scenario-II are built to illustrate the sensitivity of the resultant design parameters on the amount of available renewable sources using the average energy demand of the manufacturing system. The Scenario-I represents a lower renewable source scenario (minimum solar irradiance and wind speed) while Scenario-II represents a higher renewable source scenario (maximum solar irradiance and wind speed). The year 2014 is selected for the lower renewable source scenario since both average solar irradiance and average wind speed of the year is the lowest among the years from 2012 to 2016. However, there is no single year in Table 3.10 with both higher solar and higher wind sources. Therefore, the Scenario-II is formulated based on the combination of the

years of 2015 (highest wind speed) and 2016 (highest solar irradiance). As the scenario is the combination, the average temperature of the two years is used for identifying the HVAC demand of the manufacturing plant in the integrated simulation model. Table 3.11 shows the comparison of design parameters and corresponding costs between Scenario-I and Scenario-II.

Table 3.11 Comparison of the design parameters and corresponding costs between Scenario-I and Scenario-II

| Scenario | Description of Scenario | Area of Solar PV ($m^2$) | Number of Wind Turbine | Size of the BESS (kW) | Cost ($) |
|---|---|---|---|---|---|
| I | Low renewable source and average demand | 117,948 | 3 | 32,359 | 2,782,324.48 |
| II | High renewable source and average demand | 97,499 | 3 | 33,073 | 2,368,636.87 |

In Scenario-I with the decreased of renewable sources (solar irradiance and wind speed), the size of the solar PV is increased while the number of the wind turbine keeps constant to meet the demand of the manufacturing plant. The total cost is slightly increased. It implies that compared to purchasing electricity from the grid, it is more profitable to increase the size of the microgrid system depending on the energy consumption profile of the system. If the variation of energy demand is significant, as well as occurs more frequently, and mostly during the peak period, it would be more profitable to change the size of the microgrid system rather than changing the amount of

electricity purchased from the grid. Otherwise, compensating the variation of energy demand by changing the electricity purchased from the grid would be an optimal strategy to minimize the total cost.

In Scenario-II with the increased of renewable sources, the size of the solar PV is decreased while the number the wind turbine still keeps constant. The cost is significantly reduced due to the fact that the excess generation after meeting the demand of the manufacturing plant is sold back to the grid. It is also observed that the installation of the wind turbine is not sensitive to the variation of the available renewable sources like the solar PV. This is mainly due to a higher incremental investment cost by adding one-unit wind turbine compared to solar PV and BESS.

In addition, we also examine the sizing results with the highest energy demand and the lowest renewable source for a worst-case analysis based on the Scenarios I and II. The design parameters and corresponding cost obtained are illustrated in Table 3.12.

Table 3.12 Design parameters of microgrid system and corresponding cost for maximum demand and minimum renewable sources

| Parameters | Area of Solar PV ($m^2$) | Number of Wind Turbine | Size of the BESS (kW) |
|---|---|---|---|
| Value | 129,073 | 3 | 31,925 |
| Cost ($) | | 3,119,277.35 | |

The sizes of the solar PV and BESS are sensitive to the variations of the demand, while the number of the wind turbine is still insensitive. Compared to Scenario I, the solar PV area is increased to provide more energy to meet a higher demand, however, the

size of the BESS is reduced because the electricity generated from the extended system is consumed by largely to meet the excess demand of the manufacturing plant and consequently, less amount of charging/discharging through the BESS is required.

Furthermore, Scenario-III and Scenario-IV are examined to illustrate the impact of sold back price on the design parameters. In Scenario-III, a higher sold back price is set as \$0.27/kWh during the peak periods in summer and \$0.09 during the mid-peak periods in summer as well as the peak periods in winter (Lee and Chen, 2009). No sold back is examined in Scenario-IV. In this scenario, the excess energy generated from the onsite sources will go for curtailment. Table 3.13 shows the comparison of the design parameters and corresponding costs between Scenario-III and Scenario-IV.

Table 3.13 Comparison of the design parameters and corresponding costs between Scenario-III and Scenario-IV

| Scenario | Description of Scenario | Area of Solar PV ($m^2$) | Number of Wind Turbine | Size of the BESS (kW) | Cost (\$) |
|---|---|---|---|---|---|
| III | High sold back price and average demand | 128,236 | 4 | 34,312 | 2,263,198.86 |
| IV | No sold back and average demand | 56,883 | 2 | 30,358 | 3,634,355.59 |

From Table 3.13, it can be inferred that the design parameters of the microgrid system (both solar PV and wind turbine) are sensitive to the variations of the electricity sold back price. The higher the sold back rate, the larger the size of all the components in

the microgrid system will be. The total cost can also be reduced because of purchasing less amount of electricity from the grid and selling more energy back to the grid. On the contrary, it is recommended to reduce the size of the microgrid system when there is no sold back advantage.

**3.5.4. Model Validation.** In this section, the proposed model is compared with two benchmark models using other methods based on the state of the art. In the first benchmark model (Model-I), only the demand of manufacturing system is considered as the input when designing the size of the microgrid system, while the HVAC is ignored, as many existing literatures do (Hakimi et al., 2011; Hung et al., 2017; bin Othman and Musirin, 2010). The resultant design parameters of the microgrid system by Model-I are shown in Table 3.14 (note that, for convenience in comparison, the resultant parameters using proposed model are also illustrated in the same table). It can be seen that there is no statistical difference with respect to the size of BESS and wind turbine, while the size of solar PV is statistically lower than the proposed model since the overall demand is underestimated in Model-I.

The comparison of the payback period between Model-I and the proposed model is shown in Table 3.15. It shows that the payback period of the proposed model is statistically shorter than Model-I although a higher initial investment of the proposed model can be expected since a higher demand is used for design. This is mainly due to a higher electricity billing cost saving when using the microgrid system with an accurate size that is designed by the proposed model considering both manufacturing load and HVAC load.

Table 3.14 Resultant design parameters of Model-I and proposed model

| | Parameter | Mean value | Upper limit (95% confidence interval) | Lower limit (95% confidence interval) |
|---|---|---|---|---|
| Proposed Model | Area of Solar PV ($m^2$) | 97,721 | 98,098 | 97,345 |
| | Number of wind turbine | 3 | 3 | 3 |
| | BESS Capacity (kW) | 33,257 | 33,854 | 32,659 |
| Model-I | Area of Solar PV ($m^2$) | 96,182 | 96,553 | 95,810 |
| | Number of wind turbine | 3 | 3 | 3 |
| | BESS Capacity (kW) | 32,554 | 33,512 | 31,596 |

Table 3.15 Comparison of the payback period analysis between Proposed model and Model-I

| | Parameter | Mean value | Upper limit (95% confidence interval) | Lower limit (95% confidence interval) |
|---|---|---|---|---|
| Proposed Model | Simple Payback period | 5.76 years | 5.82 years | 5.69 years |
| | Discounted Payback period (2.75% discount rate) | 6.35 years | 6.44 years | 6.27 years |
| Model-I | Simple Payback period | 6.10 years | 6.14 years | 5.99 years |
| | Discounted Payback period (2.75% discount rate) | 6.73 years | 6.82 years | 6.63 years |

In the *second* benchmark model (Model-II), the mean of the demand (including both manufacturing system and HVAC system) is used as the input for the design model as many existing literatures do (Chen, 2012; Kazem et al., 2013; Khatib et al., 2012), which largely ignores the variation of the demand and underestimates the uncertainty of the overall system. The resultant design parameters of the microgrid system by Model-II as well as the proposed model are shown in Table 3.16. It can be seen that the resultant sizes of the solar PV and wind turbine by Model-II are not statistically different compared to the proposed model. The solar PV size by Model-II falls in the confidence interval by the proposed model. The wind turbine size by Model-II has same mean as well as same zero width of confidence interval because of the higher incremental cost.

Table 3.16 Resultant design parameters of Model-II and proposed model

| | Parameter | Mean value | Upper limit (95% confidence interval) | Lower limit (95% confidence interval) |
|---|---|---|---|---|
| Proposed Model | Area of Solar PV ($m^2$) | 97,721 | 98,098 | 97,345 |
| | Number of wind turbine | 3 | 3 | 3 |
| | BESS Capacity (kW) | 33,257 | 33,854 | 32,659 |
| Model-II | Area of Solar PV ($m^2$) | 97,581 | 97,581 | 97,581 |
| | Number of wind turbine | 3 | 3 | 3 |
| | BESS Capacity (kW) | 30,211 | 30,211 | 30,211 |

The BESS size by Model-II is statistically lower than the proposed model. Since the BESS is typically used as an energy buffering system to resist the variations and uncertainties from both demand and supply for the microgrid system, less consideration for the variation of the demand in Model-II implies a less requirement the variation resistance capability, i.e., the BESS system size, of the microgrid system.

The payback analysis is implemented for Model-II and the comparison of payback period between Model-II and the proposed model is shown in Table 3.17.

Table 3.17 Comparison of the payback period between the proposed model and Model-II

| | Parameter | Mean value | Upper limit (95% confidence interval) | Lower limit (95% confidence interval) |
|---|---|---|---|---|
| Proposed Model | Simple Payback period | 5.76 years | 5.82 years | 5.69 years |
| | Discounted Payback period (2.75% discount rate) | 6.35 years | 6.44 years | 6.27 years |
| Model-II | Simple Payback period | 6.46 years | 6.55 years | 6.37 years |
| | Discounted Payback period (2.75% discount rate) | 7.21 years | 7.33 years | 7.10 years |

From the Table 3.17, it can be seen that the payback period of the proposed model is statistically shorter than Model-II when the variation from the demand side is appropriately modeled when designing the size of the microgrid system.

## 3.6. SUMMARY OF THE OPTIMIZATION MODEL FOR MICROGRID DESIGN AND CONTROL UNDER TOU DEMAND RESPONSE PROGRAM

A MINLP optimization model is proposed in this section to identify the size of the components in a typical microgrid system consisting of solar PV, wind turbine, and BESS and the corresponding yearly control strategy to minimize the overall energy-related cost for manufacturing plant. An integrated simulation model is used to generate the various energy loads from both manufacturing system and HVAC of a manufacturing plant for the use of the input in the proposed model. A meta-heuristic method, PSO, is used to solve the proposed MINLP problem considering the tradeoff between computational cost and solution quality. A case study employing a real auto component manufacturing plant along with the data series of the renewable sources is implemented. Further, the critical parameters of the model are investigated to analyze the sensitivity of resultant size to the variations of the critical input parameters.

The main advantage of the proposed model is that it extends the literature on sizing the microgrid system with renewable sources from customers from commercial and residential end use sectors and critical facilities to the manufacturing end use customers. It captures the overall electricity demand from a typical manufacturing plant with both manufacturing and HAVC systems and considers the variations of such demands when sizing the microgrid system. The proposed model can lead to a shorter payback period due to the accurate demand input and sufficient variation consideration in the model.

# 4. OPTIMAL SIZING AND PLANNING OF MICROGRID SYSTEM FOR MANUFACTURING IN CRITICAL PEAKING PRICING DEMAND RESPONSE PROGRAM

## 4.1. STRATEGIC OVERVIEW

The objective of this section is to investigate the economic viability of sizing an OGS for manufacturer when considering the participation of CPP program. Mixed Integer Non-Linear Programming (MINLP) is used to build the formulation so that the size and utilization strategy of the OGS for manufacturing as well as the corresponding optimal production plan minimizing the overall energy related cost when participating in CPP program can be optimally identified. The remaining part of this section is organized as follows. The MINLP formulation of the proposed sizing model is given in Section 4.2. Different solution strategies are then discussed and compared in Section 4.3. After that, a case study based on a real manufacturing system and an existing CPP program is carried out in Section 4.4. Finally, the section is concluded, and the future work is discussed in Section 4.5.

## 4.2. SIZING MODEL

The special events that trigger the CPP may usually happen in the summer period of a year, e.g., from June to October, in the north hemisphere. For the manufacturers who participate in the CPP program, the credit of unit consumption charge ($/kWh) will be applied to only on-peak periods, both on-peak and mid-peak periods or all periods depending on the specific programs. An additional unit consumption charge is applied for the energy consumed during the event durations. In addition, the credit of unit demand

charge ($/kW) is also given to the participating manufacturers at different types of the periods.

Consider a typical manufacturing system where $J$ sequential manufacturing tasks are conducted as shown in Figure 4.1. Each task can be conducted by a few parallel manufacturing stations while each station may include multiple manufacturing machines to perform different manufacturing functionalities. The rectangles in Figure 4.1 denote the manufacturing stations, while the circles in Figure 4.1 denote the buffer locations where the work-in-progress parts can be stored. Let $j$ be the indexes of the manufacturing tasks ($j$=1, …, $J$) and buffer locations ($j$=1, …, $J$-1). Let $i$ be the index of the manufacturing stations in the manufacturing system. Let $P_i$ be the rated power of station $i$ in the manufacturing system.

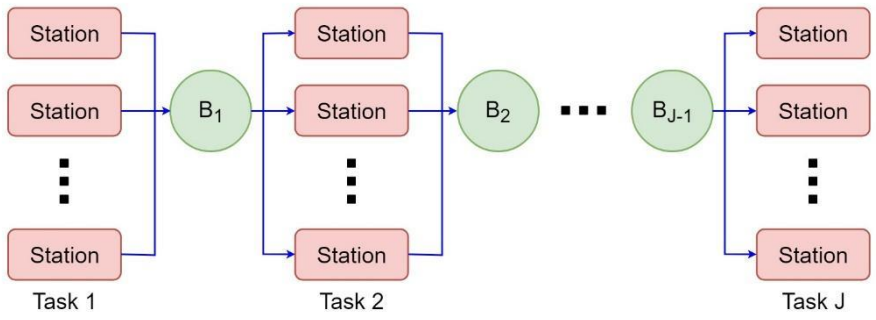


Figure 4.1 A multi-task manufacturing system.

Let $m$ be the index of the months in a calendar year. The time horizon of each month includes a set of discretized intervals indexed by tm ($t_m$=1, …, $T_m$) with constant duration of $\Delta t$. Also, we define $z$ as the size of the OGS to be determined. We define $x_{it_m}$

as the binary decision variable to represent the production plan of the manufacturing system. $x_{it_m}$ is equal to one if the production plan specifies that the station *i* will produce in time interval $t_m$, while taking the value of zero if not. Let $y_{t_m}$ be the decision variable denoting the energy offered by the OGS in time interval $t_m$. The purpose is to minimize the yearly energy relevant cost including both electricity billing cost and the microgrid cost, which can be formulated by Equation(39).

$$\min_{x_{it_m}, y_{t_m}, z} \sum_{m} (E_m + F_m) \tag{39}$$

where $E_m$ and $F_m$ are the electricity billing cost and the microgrid cost in month *m*, respectively. $E_m$ can be calculated by Equation (40).

$$\begin{aligned} E_m = & \sum_{t_m \in \mathbf{T_m} \setminus \mathbf{T_m^D}} [(\sum_i x_{it_m} P_i - y_{t_m}) \cdot \Delta t \cdot c_{t_m}^r] + \sum_{t_m \in \mathbf{T_m^D}} [(\sum_i x_{it_m} P_i - y_{t_m}) \cdot \Delta t \cdot (c_{t_m}^r + c_{t_m}^a)] \\ & + (d_{on} - cr_{on}) \cdot \max_{t_m \in \mathbf{T_m^{ON}}} (\sum_i x_{it_m} P_i - y_{t_m}) + (d_{mid} - cr_{mid}) \cdot \max_{t_m \in \mathbf{T_m^{MID}}} (\sum_i x_{it_m} P_i - y_{t_m}) \\ & + (d_{off} - cr_{off}) \cdot \max_{t_m \in \mathbf{T_m^{OFF}}} (\sum_i x_{it_m} P_i - y_{t_m}) + (d_{base} - cr_{base}) \cdot \max_{t_m \in \mathbf{T_m}} (\sum_i x_{it_m} P_i - y_{t_m}) \end{aligned} \tag{40}$$

where $c_{t_m}^r$ is the electricity consumption charging rate ($/kWh) at interval $t_m$ after the credit is applied due to the participation in CPP demand response program. $c_{t_m}^a$ is the additional charge rate for unit energy consumption during the intervals that belong to CPP demand response duration. $d_{on}$, $d_{mid}$, and $d_{off}$ are the electricity demand charging rate ($/kW) for on-peak, mid-peak, and off-peak periods, respectively. $d_{base}$ is the demand charging rate ($/kW) for all the time intervals throughout the billing cycle. Note that, in addition to the demand charge for peak, mid-peak, and off-peak periods, there also exists a base demand charge depending on the maximum power level drawn from the grid throughout all the time intervals in the month. $cr_{on}$, $cr_{mid}$, $cr_{off}$, and $cr_{base}$ are the credits of

electricity demand charging rates ($/kW) for on-peak, mid-peak, off-peak, and all the time intervals, respectively, when the manufacturer participates in the CPP demand response program. $T_m$ is the set including all the time intervals in month $m$. $\mathbf{T_m}$ is the set including the time intervals when CPP demand response events happen in month $m$. $\mathbf{T_m^{ON}}$, $\mathbf{T_m^{MID}}$, and $\mathbf{T_m^{OFF}}$ are the sets including the time intervals belonging to on-peak, mid-peak, and off-peak periods, respectively, in month $m$.

On the right-hand side of Equation (40), the first two terms mean the electricity consumption charge in month $m$. Depending on the occurrence of CPP demand response events, two different unit consumption charging rates are applied. The remaining four terms are the electricity demand charge throughout the entire month.

$F_m$ can be calculated by Equation (41).

$$F_m = \sum_{t_m \in \mathbf{T_m}} f \cdot y_{t_m} \tag{41}$$

where $f$ is the operation, maintenance, and fuel cost of the OGS for generating unit electricity.

The constraints of the problem are formulated as follows. The customer demand is represented by the purchase order from the customers with specified periodic shipment quantity, thus, the total production at each shipment cycle (i.e., between two required shipment time points), in practice, typically needs to be no less than the shipment quantity specified by the customer purchase order. It is formulated by Equation (42).

$$\sum_{t \in \mathbf{T_k}} \sum_{i \in \mathbf{J}} x_{it} \cdot PR_i \cdot \Delta t \geq A_k \tag{42}$$

where $\mathbf{J}$ is the set of the manufacturing stations executing manufacturing task $J$. $PR_i$ is the production rate of the station $i$. $A_k$ is the required shipment quantity specified by the

customer purchase order at shipment cycle *k*. $\mathbf{T_k}$ is the set including the time intervals belong to the shipment cycle *k*. Note that the subscript *m* is removed from subscript *t* in Equation (42), since the shipment does not have to be organized on a monthly basis. We also assume the shipment occurs at the first discretized time interval belongs to $\mathbf{T_k}$.

The energy output from the OGS needs to be no higher than the energy demand from the manufacturing system and the designed size of the OGS, whichever is smaller. It can be formulated by Equation (43).

$$y_{t_m} \le \min(\sum_i x_{it_m} \cdot P_i, z), \forall t_m \tag{43}$$

The work-in-progress parts stored in the buffer locations should be maintained between the required minimum buffer stock and the capacities of the buffer locations, which can be formulated by Equation (44).

$$C_{j\_\min} \le B_{jt_m} \le C_{j\_\max} \tag{44}$$

where $C_{j\_min}$ is the minimum level of work-in-progress parts need to be maintained at buffer location *j* and $C_{j\_max}$ is the capacity of buffer location *j*. $B_{jt_m}$ is the buffer content in buffer location *j* at the beginning of interval $t_m$, which can be calculated by Equation (45).

$$B_{jt_m} = B_{j(t_m-1)} + \sum_{i\in\mathbf{j}} x_{i(t_m-1)} \cdot PR_i \cdot \Delta t - \sum_{i\in\mathbf{j+1}} x_{i(t_m-1)} \cdot PR_i \cdot \Delta t, \forall t_m, \forall j \tag{45}$$

where **j** is the set of the manufacturing stations executing manufacturing task *j*. The OGS typically has hardware operational constraints such as minimum ON (OFF) time after the system is activated (turned off), which can be described by Equation (46).

$$\begin{cases} y_{t_m} > 0, \text{ if } 1 \le V_{t_m} \le V_{on} \\ y_{t_m} > 0, \text{ if } -1 \ge V_{t_m} \ge -V_{off} \end{cases} \quad t_m = 2,\ldots,T_m \tag{46}$$

In Equation (46), $V_{on}$ is the shortest required ON duration of the OGS after start-up; $V_{off}$ is the shortest required OFF duration of the OGS after shut-down; and $V_{t_m}$ is the consecutive ON or OFF duration of OGS up to the beginning of interval $t_m$. A positive (negative) value is used for the consecutive ON (OFF) time. $V_{t_m}$ can be formulated by Equation (47).

$$V_{t_m} = \begin{cases} \max(V_{t_m-1}, 0) + 1, & \text{if } y_{t_m-1} = 1 \\ \min(V_{t_m-1}, 0) - 1, & \text{if } y_{t_m-1} = 0 \end{cases} \quad t_m = 2, ..., T_m \tag{47}$$

where, the initial condition of $V_{t_m}$ is assumed to be $V_1 = 0$. The inventory of the finished products needs to be maintained within a given range at the end of each interval $t_m$, which can be formulated by Equation (48).

$$L \le Q_{t_m} \le U \tag{48}$$

where $Q_{t_m}$ is the inventory of the finished products at the end of interval $t_m$ after shipping the final products to satisfy the customer demand if required. $L$ is the lower bound, while $U$ is the upper bound of the inventory of finished products. $Q_{t_m}$ can be recursively calculated by Equation (49).

$$Q_{t_m} = Q_{t_m-1} + \sum_{i \in \mathbf{J}} x_{it_m} \cdot PR_i \cdot \Delta t - S_{t_m} \tag{49}$$

where $S_{t_m}$ is the shipment quantity of the final products at the beginning of interval $t_m$. $S_{t_m}$ can be calculated by Equation (50).

$$S_{t_m} = \begin{cases} A_k, & \text{if shipment } A_k \text{ is required at interval } t_m \\ 0, & \text{otherwise} \end{cases} \tag{50}$$

The net present value (*NPV*) of building an OGS with size of *z* over the expected lifetime needs to be positive. It can be represented by Equation (51).

$$NPV = -z \cdot H + \sum_{g=1}^{G} \frac{SA}{(1+r)^g} > 0 \tag{51}$$

where *H* is the setup cost of the OGS per unit size. *r* is the yearly discount rate. *G* is the lifetime of the OGS. *g* is the index of the year. *SA* is the yearly saving due to the use of OGS, which can be calculated by Equation (52).

$$SA = B' - (\sum_{m} E_m + F_m) \tag{52}$$

where *B′* is the yearly electricity billing cost without OGS. It can be obtained through running the revised optimization model by removing OGS related decision variables, parameters, objectives, and constraints, i.e., to identify an optimal production plan that can minimize the yearly electricity billing cost when participating in the CPP program. Here we assume the model parameters across the years within the lifetime are the same and thus the yearly saving is constant.

### 4.3. SOLUTION STRATEGY

It can be seen that the sizing model proposed in Section 4.2 is a Mixed Integer Non-Linear Programming (MINLP). To solve this MINLP model, we can either employ a certain software solver that is typically applicable to the linearity formulation to obtain the optimal solution or use a certain meta-heuristic algorithm to obtain a near optimal solution considering the balance between solution qualities and computing cost. Various linearization strategies have been proposed to linearize the MINLP formulation to Mixed Integer Linear Programming (MILP) formulation (Sirvent et al., 2017; Hamzeei and

Luedtke, 2014; Belotti et al., 2013) so that the existing solver requiring the assumptions of "differentiable", "convexity", and "continuous" can be used. While, the meta-heuristic algorithms can be used directly without such assumptions. For example, the evolutionary-based meta-heuristics, like Genetic Algorithm (Eiben et al., 1994) and Particle Swarm Optimization (Eberhart et al., 2001) have been extensively studied and widely used when solving the high-dimension complex optimization problems (Jerald et al., 2005; Du et al., 2015; McCall, 2005; Liu et al., 2014). Some researchers have recently explored the theoretical connection between such heuristic algorithms and existing analytical models such as Hamiltonian systems and Nesterov's method (Freidlin and Hu, 2011). In this section, we investigate and discuss the solution strategies considering both pathways.

**4.3.1. Linearization.** We first adopt the linearization strategies as follows to linearize the non-linear terms in Equation (40), Equation (43), and Equation (46).

For the "max" operator in Equation (40), it is linearized by Equation (53) where the "max" operator is substituted by the new variables: $h_{ON}$, $h_{MID}$, $h_{OFF}$, and $h_{BASE}$.

$$\begin{aligned} E_m = & \sum_{t_m \in \mathbf{T_m} \setminus \mathbf{T_m^D}} [(\sum_i x_{it_m} P_i - y_{t_m}) \cdot \Delta t \cdot c_{t_m}^r] + \sum_{t_m \in \mathbf{T_m^D}} [(\sum_i x_{it_m} P_i - y_{t_m}) \cdot \Delta t \cdot (c_{t_m}^r + c_{t_m}^a)] \\ & + (d_{on} - cr_{on}) \cdot h_{ON} + (d_{mid} - cr_{mid}) \cdot h_{MID} + (d_{off} - cr_{off}) \cdot h_{OFF} + (d_{base} - cr_{base}) \cdot h_{BASE} \end{aligned} \tag{53}$$

Given the new variables, the following additional constraints need to integrate into the model to achieve the linearized versions of the nonlinear "max"operator.

$$\begin{aligned} & h_{ON} \geq \sum_i x_{it_m} P_i - y_{t_m}, \ \forall t_m \in \mathbf{T_m^{ON}} \\ & h_{MID} \geq \sum_i x_{it_m} P_i - y_{t_m}, \ \forall t_m \in \mathbf{T_m^{MID}} \\ & h_{OFF} \geq \sum_i x_{it_m} P_i - y_{t_m}, \ \forall t_m \in \mathbf{T_m^{OFF}} \\ & h_{BASE} \geq \sum_i x_{it_m} P_i - y_{t_m}, \ \forall t_m \in \mathbf{T_m^{BASE}} \end{aligned} \tag{54}$$

For the purpose of linearizing the Equation (43), we disaggregate it to two linear constraints which are shown below.

$$y_{t_m} \le \sum_i x_{it_m} P_i, \ \forall t_m \tag{55}$$

$$z \ge y_{t_m}, \ \forall t_m \tag{56}$$

For the nonlinearity in Equation (46), the Equation (57) is used for linearization. In Equation (57), two auxiliary binary variables, i.e., $l_{on}^{t_m}$ and $l_{off}^{t_m}$, are defined to denote if the ON/OFF status of the OGS is changed or not at the beginning of interval $t_m$. $l_{on}^{t_m}$ and $l_{off}^{t_m}$ take the value of one if the system starts and shuts off, respectively, at the beginning of interval $t_m$, and zero otherwise.

$$\begin{aligned} l_{on}^{t_m} &\le \sum_i y_{t_m+q}, \ t_m = 2,...,T_m, \ \forall q \in \{1...V_{on}-1\} \\ l_{off}^{t_m} &\le \sum_i 1 - y_{t_m+q}, \ t_m = 2,...,T_m, \ \forall q \in \{1...V_{off}-1\} \end{aligned} \tag{57}$$

After applying the linearization strategy aforementioned, the MINLP problem can be transformed to a Mixed Integer Linear Programming (MILP) problem. The toolbox "OR-Tools" from Google Optimization Tools is used to solve the MILP. The algorithm used in the toolbox implements Coin or Branch and Cut (CBC) as the solver. OR-Tools can work very effectively to solve the proposed problem with a three-month (e.g., June, July, and August, since most CPP events occur in the months of June, July, and August in the United States) time scale using 12,514 seconds.

However, when the time scale is increased from three months to one year as intended by the proposed problem, due to the computational complexity of the problem, the time required by the solution increased dramatically and the toolbox becomes

inefficient. The number of variables is increased from 6,261,197 to 98,710,310. Further, the amount of memory required for linear optimization also increases by a magnitude. Thus, the toolbox becomes impractical due to extremely long computational time. Although we tried to use a high-performance cluster computer of dual 16 core Haswell CPUs with 256 GB DDR4 RAM for the computation, which took over 168 hours without obtaining the solution.

**4.3.2. Implementing the Genetic Algorithm.** Due to the high dimension of the proposed model and the inefficiency of using linear solver toolbox to solve the problem after linearization, we propose to use a widely used meta-heuristic method, Genetic Algorithm (GA), to solve the proposed problem to obtain a near optimal solution with a reasonable computational cost. GA is inspired by the process of natural selection that belongs to the larger class of evolutionary algorithms, which has been widely used in high dimension scheduling problem involving binary decision variables.

We discretize the optimization horizon, i.e., one year, into $\sum_m T_m$ same duration intervals during which the production plan of the manufacturing system with $D$ manufacturing stations and the utilization strategy of the OGS need to be encoded. Thus, here we represent the production plan of each station and the utilization strategy of OGS as one chromosome with $\sum_m T_m$ genes. Together, they form a genotype of $(D+1)\sum_m T_m$ genes. The genes in the D chromosomes for production plan are encoded as binary variables (0, 1) and the genes in the chromosome for the OGS are encoded as double values within the range between zero and the maximum demand of the manufacturing system.

Considering that the search space of this problem is fairly large, we initially generate a population with a certain number of genotypes randomly. Then, we use tournament selection method to select the fitter parent genotypes while keeping the diversity of the population. For evolution process, uniform crossover and mutation are introduced for a broader exploration of the search space. The evolution is allowed to continue for a given number of generations. The fitness of each genotype can be calculated by Equation (58) where all the constraints are integrated as penalty terms. After the last round of evolution, the genotype that shows the best fitness is returned as the result.

$$\begin{aligned}
&\sum_{m}(E_m + F_m) + W([\sum_{k}\min(\sum_{t\in \mathrm{T}_k}\sum_{i\in \mathrm{J}} x_{it}\cdot PR_i\cdot \Delta t - A_k, 0)]^2 \\
&+\sum_{t_m}\max(y_{t_m} - \min(\sum_{i} x_{it_m}\cdot P_i, z), 0) + \sum_{j}\sum_{t_m}[\min(B_{jt_m} - C_{j_\min}, 0)]^2 \\
&+\sum_{j}\sum_{t_m}\max(B_{jt_m} - C_{j_\max}, 0) + \sum_{t_m}\max(Q_{t_m} - U, 0) \\
&+\sum_{t_m}[\min(Q_{t_m} - L, 0)]^2 + [\min(NPV, 0)]^2 \\
&+\sum_{t_m=2}^{T_m}[\min(\left|y_{t_m} - y_{t_m-1}\right|.\left|V_{t_m-1}\right| - y_{t_m-1}\cdot V_{on} - (1-y_{t_m-1})\cdot V_{off}, 0)]^2)
\end{aligned} \tag{58}$$

In Equation (58), $W$ is a large positive real number to scale up the penalty due to the violations to the constraints.

## 4.4. CASE STUDY

The manufacturing system we use in this case study is an auto component manufacturing system with the layout as shown in Figure 4.2.

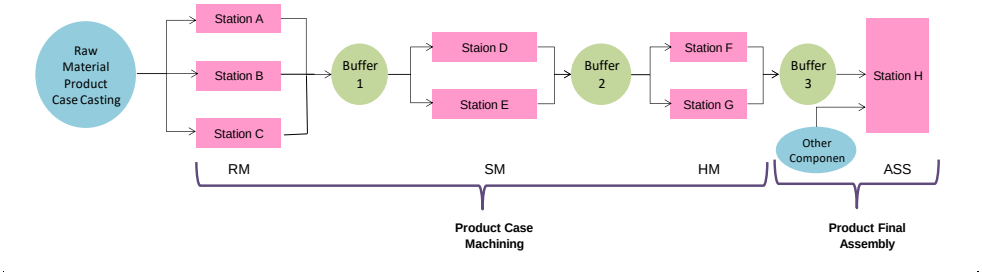


Figure 4.2 Layout of an auto component manufacturing system.

Two major processes, i.e., machining and assembly are included in this auto component manufacturing system. The machining process can be further disaggregated to three sequential sub-processes (i.e., RM, SM, and HM). First, the initial surface processing on the raw materials of castings is fulfilled by RM. Next, the casting surface cutting, and drilling are fulfilled by SM. Finally, the final finishing of the castings is completed by HM. In RM, Stations A/B/C are deployed in parallel, while in SM and HM, two machining stations, i.e. Station D/E, and Station F/G are deployed in parallel, respectively. Various computer numerical controlled (CNC) machines with respective purposes, e.g., grinding, drilling, turning, milling, etc., as well as several special machines with auxiliary purposes like balancing, demagnetization, and cleaning, are included in specific machining stations. An illustrative demonstration of Station A is show in Figure 4.3.

The assembly process consists of a single assembly station denoted Station H to conduct assembly tasks. The assembly team conducts the required tasks in several workplaces deployed in assembly station to assemble the parts after machining along with the other components to finally complete the entire production process. The

productivity related data (cycle time of each station, buffer capacity, buffer initial contents) is given in Table 4.1 and Table 4.2.


Figure 4.3 An illustrative demonstration of the stations.

Table 4.1 Cycle time of stations

| Station | A | B | C | D | E | F | G | H |
|---|---|---|---|---|---|---|---|---|
| Cycle time (s) | 135 | 135 | 135 | 80 | 80 | 80 | 80 | 40 |

Table 4.2 Buffer size and the content at the beginning

| | Capacity | Initial Content |
|---|---|---|
| Buffer 1 | 1800 | 400 |
| Buffer 2 | 1800 | 400 |
| Buffer 3 | 1800 | 400 |

The rated power of the manufacturing machines in Station A is shown in Table 4.3 for illustration (the relevant data of other machines is not given due to confidentiality requirement). The customer demand that needs to be satisfied on a weekly basis is 4800 units per week. The safety stock of the finished products requested by the customer needs to be maintained at the level that can cover one- or two-weeks' demand, i.e., between 4800 and 9600. The manufacturing system runs a five-day per week and two eight-hour

shifts per day working schedule. The production schedule and OGS planning are generated on an hourly basis. The minimum ON/OFF time of the OGS is two hours. The lifetime of the OGS is 20 years. The yearly discount rate is set to be 3%.

Table 4.3 Rated power of the manufacturing machines in RMA

| Machine Name | Rated Power (kW) |
|---|---|
| OP10 Turn-1 | 21 |
| OP20 Turn-2 | 21 |
| OP30 Turn-3 | 21 |
| OP40 Window milling | 31 |
| OP50 Turn-4 | 24 |

Since the total rated power of the manufacturing system described in Figure 4.2 is 720.5 kW, we select tariff “SCE TOU-8” (Southern California Edison, 2015), which is applicable for the customers with peak demand ranging from 500kW to infinity, as the CPP demand response program in the case study. In “SCE TOU-8”, there exists a fixed amount of 12 event days in one year and each event lasts four hours. The charging rates at different periods and the credits for the participating customers are illustrated in Tables 4.4 and 4.5, respectively. We also retrieve the historical demand response events data of CPP in 2017 from SCE. Note that, due to the fact that CPP is relatively new, the existing historical dataset does not have enough size so that the proposed model cannot be run with stochastic inputs in term of various occurrence times of the CPP to obtain statistical results. Thus, we select the data from the most recent year in this case.

Table 4.4 Charging rates of SCE TOU-8

| Months | Energy Charge ($/kWh) | | | Demand Charge ($/kW) | | | Monthly Charge ($) |
|---|---|---|---|---|---|---|---|
| | On-peak | Mid-peak | Off-peak | On-peak | Mid-peak | Base (Any time) | |
| Jun-Sep | 0.15267 | 0.09289 | 0.06592 | 25.16 | 7.11 | 14.99 | 596.11 |
| Oct-May | | 0.09454 | 0.07165 | | | | |

Table 4.5 Credits in SCE TOU-8 for participating customers

| Discount Months | Demand Charge Credits ($/kW) | Adder During CPP Events ($/kWh) | Event Time Period |
|---|---|---|---|
| Jun - Sep | On-Peak: 11.9 | 1.37 | 14:00-18:00 |

For comparison, we first run a baseline model without the OGS to examine the total energy billing cost under the same CPP demand response program. Then, we compare the optimization results and computing time between MILP after linearization and GA for a three-month case (June, July, and August) in Table 4.6 and Table 4.7.

As we can see, although the cost reduction achieved by MILP is 7% better than GA as shown in Table 4.6, the computational time of MILP is much higher than GA. It implies that the proposed GA algorithm can obtain a near optimal solution by striking a balance between optimization quality and computational time. Thus, we use GA to solve our proposed problem over one-year time scale. We generate an initial population of 50,000 genotypes and run the evolution algorithm for 500 generations. The GA convergence of the fitness is demonstrated in Figure 4.4.

Table 4.6 Optimization results ($) comparison between GA and MILP

| | GA | MILP |
|---|---|---|
| Baseline | 83,627.32 | 75,150.40 |
| Proposed Method | 48,411.6 | 37,964 |
| Reduction (%) | 42% | 49% |

Table 4.7 Computational time (s) comparison between GA and MILP solver

| | Baseline | Proposed Method |
|---|---|---|
| GA | 29,600 | 35,016 |
| MILP | 125,140 | 200,920 |
| Difference (%) | -76.3 | -82.6 |

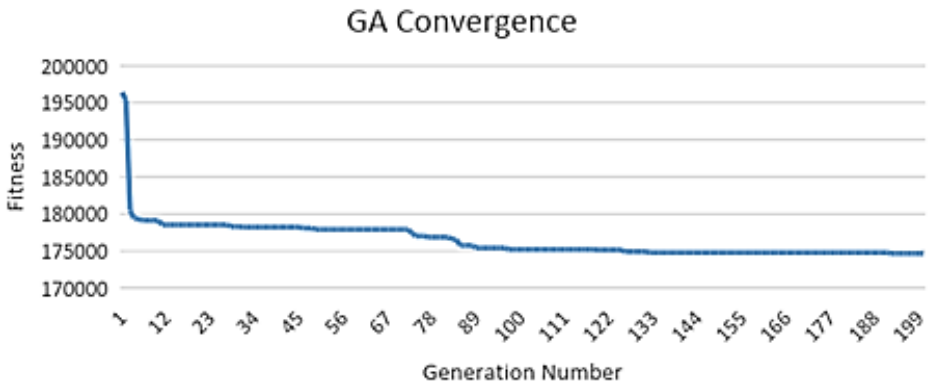


Figure 4.4 GA convergence of the proposed model.

The size of the OGS is optimized to be 700 kW. The comparison of the yearly energy related costs between the proposed model with the OGS and the baseline model without the OGS is illustrated in Table 4.8. It shows that with an appropriately sized

OGS, the electricity billing cost can be further significantly reduced under the CPP demand response program.

Table 4.8 Cost reduction between the proposed model and baseline model

| Yearly Energy Cost ($) | | Reduction (%) |
|---|---|---|
| Baseline | Proposed Method | |
| 288,994.24 | 174,652.5 | 39.6 |

Further, sensitivity analysis is also implemented to examine the variations of the yearly energy cost reduction led by the change of modeling parameters including yearly discount rate, system lifetime, demand charge credit, and consumption charge adder during CPP as shown in Table 4.9.

Table 4.9 Sensitivity analysis

| Parameters | Discount Rate (%) | | | Lifetime (years) | | |
|---|---|---|---|---|---|---|
| Level | 1 | 3 | 5 | 15 | 20 | 25 |
| Cost Reduction (%) | 39.60 | 39.56 | 39.76 | 39.70 | 39.56 | 39.78 |
| Parameters | Demand charge credit ($/kW) | | | Adder during CPP ($/kWh) | | |
| Level | 10.9 | 11.9 | 12.9 | 1.07 | 1.37 | 1.67 |
| Cost Reduction (%) | 39.50 | 39.56 | 39.30 | 38.74 | 39.56 | 40.87 |

From the Table 4.9, it can be seen that the cost reduction is fairly constant due to the variations of discount rate, lifetime, and demand charge credit. However, there is a slight increase of the saving percentage due to the increase of the additional consumption charge ($/kWh) during CPP event duration. It indicates that the higher the penalty imposed on the energy consumption during CPP period by the program, the more cost reduction can be expected using the microgrid system.

## 4.5. SUMMARY OF THE OPTIMIZATION MODEL FOR MICROGRID DESIGN AND CONTROL UNDER CPP DEMAND RESPONSE PROGRAM

In this section, we investigate the economic sizing problem for the OGS used by manufacturers, especially for the participation in CPP demand response program. An MINLP model is proposed to identify the optimal OGS size and utilization strategy as well as the optimal production plan for the manufacturing system that can minimize the total energy related cost when manufacturing end use customers enroll in CPP program. A real auto component manufacturing system and an existing CPP program are used in the numerical case study to examine and analyze the model effects. The case study shows that the installation and use of the OGS can further facilitate and promote the CPP program participation from manufacturer end use customers.

# 5. OPTIMAL SCHEDULING OF MANUFACTURING AND MICROGRID SYSTEMS IN OVER-GENERATION MITIGATION ORIENTED ELECTRICITY DEMAND RESPONSE PROGRAM (DRP)

## 5.1. STRATEGIC OVERVIEW

An analytical decision-making model for manufacturing industrial end use customers with microgrid system is proposed to identify an optimal strategy to handle the overgeneration mitigation-oriented electricity demand response programs (DRP). The optimal decisions regarding participating or not, corresponding production schedule, and microgrid utilization schedule will be identified to minimize the overall cost including utility incentive or penalty due to achieving or not achieving the committed consumption level, microgrid cost, electricity billing cost, and production loss penalty cost. The decision making is formulated as a mixed nonlinear integer programming problem. Particle swarm optimization (PSO) is used to find the near optimal solution. A numerical case study is used to illustrate the effectiveness of the proposed model. The rest of the section is organized as follows. Section 5.2 introduces the proposed decision-making model including both problem formulation and solution technique. Section 5.3 implements the case study. Section 5.4 draws the conclusion of the section and discusses the future work.

## 5.2. PROPOSED MODEL

In the previous sections, the onsite microgrid system was designed optimally based on different energy tariffs introduced by the electricity grid. After designing the microgrid system, it is required to optimally control the microgrid and manufacturing

system. Considering the demand response program named over-generation mitigation-oriented electricity demand response program, a mathematical model is proposed in this section. The notations used in this section are listed as follows.

*Sets*

| | |
|---|---|
| **NP** | set of non-peak intervals |
| **OP** | set of peak intervals |
| **SP** | set of the intervals that belong to over-generation period |

*Upper Case*

| | |
|---|---|
| $A_1$, $A_2$, $A_3$, $A_4$ | large real numbers |
| $B_{ij}$ | number of the parts in buffer $i$ at the beginning of interval $j$ |
| $C$ | total cost |
| $E_{t_m}^{p}$ | electricity consumption charging rate ($/kWh) at interval $t_m$ |
| $C_E$ | total billing cost |
| $C_F$ | cost for running the microgrid system |
| $C_p$ | total production loss cost |
| $CB_i$ | capacity of buffer $i$ |
| $D_j$ | total desired electricity load that needs to be achieved at interval $j$ |
| $H$ | duration of each interval |
| $L$ | location matrix of individual particle |
| $L_{PB}$ | particle's best location |
| $I$ | total incentive |
| $P$ | total penalty |

| | |
|---|---|
| $PR_i$ | production rate of machine *i* |
| $S$ | total number of iterations |
| $T$ | total number of intervals |
| $TA$ | target production |
| $TP$ | planned production |
| $V$ | velocity matrix of individual particle |
| $Z$ | capacity of microgrid system |

*Lower Case*

| | |
|---|---|
| $b_j$ | incentive rate at interval *j* |
| $c_1$, $c_2$ | learning factors |
| $c_j$ | charge rate of electricity consumption ($/kWh) at interval *j* |
| $d_{\mathbf{NP}}$ | charge rates of power demand ($/kW) for non-peak intervals |
| $d_{\mathbf{OP}}$ | charge rates of power demand ($/kW) for peak intervals |
| $e_i$ | efficiency of machine *i* |
| $f$ | cost per unit electricity generation from the microgrid system ($/kWh) |
| $i$ | index of the machines |
| $j$ | index of each interval |
| $p_j$ | penalty rate at interval *j* |
| $p_{pl}$ | unit production loss cost |
| $rp_i$ | rated power of machine *i* |
| $s$ | iteration number |
| $w_1$, $w_2$ | random real numbers between zero and one |

$x_{ij}$ decision variable to denote the production schedule of machine $i$ at interval $j$ (1 if scheduled otherwise 0)

$y_j$ decision variable denoting the customer's participation decision at interval $j$ (1 if participating otherwise 0)

$z_j$ power supplied from the microgrid system for the manufacturing at interval $j$

*Greek*

$\alpha_{max}$ maximum inertia weight

$\alpha_{min}$ minimum inertia weight

$\alpha(s)$ inertia weight at iteration $s$

$\varphi$ maximum allowed unsatisfied production

**5.2.1. Problem Formulation.** For an industrial manufacturing end use customer, the energy consumption of their manufacturing system dominates their total energy consumption. Thus, in this section, we assume all the load adjustment of industrial customers is from manufacturing system. A typical serial manufacturing system with $n$ machines and $n$-1 buffers is shown in Figure 5.1, where the rectangle denotes the machine and the circle denotes the buffer. Let $i$ be the indexes of the machines ($i$=1, 2, …, $n$) and the buffers ($i$=1, 2, …, $n$-1). Also, we consider an onsite microgrid system that can provide electricity to support the production of manufacturing system.


Figure 5.1 A typical serial manufacturing system

The time horizon is discretized into a set of intervals with constant duration of $H$. Let $j$=1, …, $T$ be the index of such intervals. Let **SP** be the set of the intervals that belong to over-generation period. For interval $j$ belonging to **SP**, the utility company will publish the desired electricity load $D_j$ (kW) that needs to be achieved by participating manufacturers. Let $y_j$ be the decision variable denoting in interval $j$, whether the industrial customer will participate in the demand response program via making a commitment of load adjustment based on the request from the utilities or not. It takes the value of one if they will participate and make such a commitment, and zero otherwise. Let $x_{ij}$ be the decision variable to denote the production schedule of machine $i$ at interval $j$, which takes the value of one if machine $i$ is scheduled for production in interval $j$, and zero otherwise. Let $z_j$ denote the power supplied from the microgrid system for the manufacturing at interval $j$. Moreover, let $b_j$ be the incentive that manufacturers can obtain if they can achieve the required $D_j$ at interval $j$. Let $p_j$ be the penalty that manufacturers need to pay if they fail to do so in interval $j$. Let $e_i$ be the production efficiency of machine $i$; and $rp_i$ be the rated power of machine $i$.

The total incentive $I$ that manufacturer may receive can be formulated by

$$I = \sum_{j \in \mathbf{SP}} y_j \cdot b_j \cdot \delta_{D_j}\left(\sum_{i=1}^{n}(x_{ij} \cdot rp_i \cdot e_i), z_j\right) \tag{59}$$

where $\delta_{D_j}\left(\sum_{i=1}^{n}(x_{ij} \cdot rp_i \cdot e_i), z_j\right)$ is defined as follows:

$$\delta_{D_j}\left(\sum_{i=1}^{n}(x_{ij} \cdot rp_i \cdot e_i), z_j\right) = \begin{cases} 1, \textit{if } \sum_{i=1}^{n}(x_{ij} \cdot rp_i \cdot e_i) - z_j \geq D_j,\ j \in \mathbf{SP} \\ 0, \textit{otherwise} \end{cases} \tag{60}$$

Here, we use production efficiency $e_i$ to model the possible random failure of machine $i$. It takes the value between zero and one to denote probability of breakdown of machine $i$. We also assume that breakdown machine consumes zero energy. The total penalty $P$ due to the non-achievement of the desired load level $D_j$ can be formulated by Equation (61)

$$P = \sum_{j \in \mathbf{SP}} y_j \cdot p_j \cdot \varsigma_{D_j}(\sum_{i=1}^{n}(x_{ij} \cdot rp_i \cdot e_i), z_j) \tag{61}$$

where $\varsigma_{D_j}(\sum_{i=1}^{n}(x_{ij} \cdot rp_i \cdot e_i), z_j)$ is defined as follows:

$$\varsigma_{D_j}(\sum_{i=1}^{n}(x_{ij} \cdot rp_i \cdot e_i), z_j) = \begin{cases} 1, \textit{if } \sum_{i=1}^{n}(x_{ij} \cdot rp_i \cdot e_i) - z_j < D_j,\ j \in \mathbf{SP} \\ 0, \textit{otherwise} \end{cases} \tag{62}$$

The energy billing cost, $C_E$, can be formulated by Equation (63).

$$C_E = \sum_{j=1}^{T} c_j[\sum_{i=1}^{n}(x_{ij} rp_i e_i H) - z_j H] + d_{\mathbf{OP}} \max_{j \in \mathbf{OP}}(\sum_{i=1}^{n}(x_{ij} rp_i e_i) - z_j) + d_{\mathbf{NP}} \max_{j \in \mathbf{NP}}(\sum_{i=1}^{n}(x_{ij} rp_i e_i) - z_j) \tag{63}$$

where $c_j$ is the charge rate of electricity consumption ($/kWh) at interval $j$. **OP** and **NP** are the set of peak and non-peak intervals, respectively. $d_{\mathbf{OP}}$ and $d_{\mathbf{NP}}$ are the charge rates of power demand ($/kW) for peak and non-peak intervals, respectively. Note that we assume the over-generation period belongs to non-peak intervals. The production loss cost, $C_P$, is can be calculated by Equation (64).

$$C_P = p_{pl} \cdot \max(TA - TP, 0) \tag{64}$$

where $p_{pl}$ be the cost per unit production loss. $TA$ is the target production, and $TP$ is the planned production throughput in the planning horizon with the given production schedule.

*TP* can be formulated by Equation (65).

$$TP = \sum_{j=1}^{T} (x_{nj} \cdot PR_n \cdot e_n) \tag{65}$$

where $PR_i$ is the production rate (units per interval) of machine *i*.

The cost for running the microgrid system to provide electricity to support the manufacturing system, $C_F$, can be formulated by Equation (66).

$$C_F = \sum_{j=1}^{T} z_j \cdot H \cdot f \tag{66}$$

where *f* is the cost per unit electricity generation from the microgrid system ($/kWh).

Hence, the total cost, *C*, can be formulated by Equation (67).

$$C = P - I + C_E + C_P + C_F \tag{67}$$

The objective function can thus be formulated by (68).

$$\min_{x_{ij}, y_j, z_j} C \tag{68}$$

The constraints can be formulated as follows:

1. Production throughput loss constraint

$$TA - TP \le \varphi \tag{69}$$

where $\varphi$ is the maximum allowed unsatisfied production.

2. The buffer contents constraint

$$0 \le B_{ij} \le CB_i \tag{70}$$

where $CB_i$ is the capacity of buffer *i*. $B_{ij}$ is the number of the parts in buffer *i* at the beginning of interval *j*, which can be calculated by

$$B_{ij} = B_{i(j-1)} + x_{i(j-1)} e_i PR_i - x_{(i+1)(j-1)} e_{i+1} PR_{i+1} \tag{71}$$

Here we assume that the machine will take the required amount of buffer contents in one batch from the upstream buffer location at the beginning of each interval for the production of the entire interval. Meanwhile, it will also deliver the completed parts in one batch to the downstream buffer location at the end of the interval when the production of the entire interval is complete.

3. The power provided by the microgrid system cannot exceed the capacity of the microgrid system or the demand of the manufacturing system, whichever is smaller.

$$z_j \le \min(Z, \sum_{i=1}^{n} x_{ij} \cdot rp_i \cdot e_i) \tag{72}$$

where $Z$ is the capacity of the microgrid system. Here we do not consider the option that the energy generated by the microgrid system can be sold back to the grid.

4. All $x_{ij}$ and $y_j$ variables are restricted to be binary, which can be formulated by Equation (73) and Equation (74)

$$x_{ij} \in \{0,1\}, i = 1, ..., n;\ j = 1, ..., T \tag{73}$$

$$y_j \in \{0,1\},\ j = 1, ..., T \tag{74}$$

5. The value of $z_j$ is discretized into a set of discrete possible values, which can be formulated by Equation (75)

$$z_j \in \{0, 0.1Z, 0.2Z, ...., 0.8Z, 0.9Z, Z\},\ j = 1, ..., T \tag{75}$$

**5.2.2. Solution Technique.** It is a huge challenge to solve the problem formulated in Section 5.2.1 due to the involvement of highly non-linear calculations and binary/discrete variables. Although, there exist different calculus-based algorithms for solving mixed nonlinear integer programming in literature and commercial software packages with the assumption of convexity so that the convergence to the global

optimum can be guaranteed, they cannot be used to address the problem with non-convex and non-differentiable search space.

Therefore, in this section, we employ particle swarm optimization (PSO), a typical population-based meta-heuristic algorithm inspired and characterized by foraging behaviors of animal swarms (Kennedy and Eberhart, 1995) to solve this high-dimension optimization problem. PSO does not requires continuity and differentiability on the search space of the optimization problem, and thus, it has been widely used in solving many different manufacturing scheduling problems for finding near-optimal solutions of complex combinatorial problems (Chou, 2013; Jerald et al., 2005; Moslehi & Mahnam, 2011; Pongchairerks, 2009).

In PSO, the candidate solution is represented as a particle in a swarm. It is encoded into an $(n+2) \times T$ matrix. The first $n$ rows of the matrix are used to store the decision variable $x_{ij}$. The $(n+1)^{th}$ row of the matrix is used to store the decision variable $z_j$. The last row of the matrix is used to store the decision variable $y_j$. $x_{ij}$ is initialized by the values of one. $z_j$ is initialized by the values randomly selected from the set $\{0, 0.1Z, 0.2Z, \ldots, 0.9Z, Z\}$. $y_j$ is initialized by randomly selecting the values from the set $\{0, 1\}$.

The particles can move in the search space based on the updated velocity towards its best location over time. After each moving step (or iteration), the velocity and location of each particle are updated according to Equation (76).

$$\begin{aligned} V(s+1) &= \alpha(s)V(s) + c_1 w_1(L_{PB} - L(s)) + c_2 w_2(L_{GB} - L(s)) \\ L(s+1) &= L(s) + V(s+1) \end{aligned} \tag{76}$$

where $V(s+1)$ and $V(s)$ are the velocity matrix of individual particle at iteration $s$ and $s+1$, respectively. $L(s)$ and $L(s+1)$ are the location matrix of individual particle at iteration $s$

and $s$+1, respectively. $c_1$ and $c_2$ are the learning factors. $w_1$ and $w_2$ are the random real numbers between zero and one. $L_{PB}$ is the particle's best solution that has been identified up to the $s^{th}$ iteration. $L_{GB}$ is the global best solution of the entire swarm. $\alpha(s)$ is the inertia weight at iteration s, it can be calculated by Equation (77).

$$\alpha(s) = \alpha_{\max} - \frac{[(\alpha_{\max} - \alpha_{\min})s]}{S} \tag{77}$$

where $\alpha_{\max}$ and $\alpha_{\min}$ are the maximum and minimum inertia weights, respectively. $S$ is the maximum iteration number. With this dynamic inertia weight in PSO, particles can move with larger step towards the global minimum more quickly at the earlier iterations. For the later iterations, the particle can move with smaller step to find the global minimum and coverage to the near optimality.

The initial velocity $V$ for each particle is also an ($n$+2) $T$ matrix. For the first $n$ rows of the matrix $V$, the elements are randomly selected from the set {-1, 0, 1}. For the ($n$+1)$^{th}$ row of the matrix $V$, the elements are randomly selected from the set {-0.1$Z$, 0, 0.1$Z$}. For the last row of the matrix $V$, the elements are randomly selected from the set {-1, 0, 1}.

Since both $V$ and $L$ are updated using real numbers in Equation (76), Equation (78) and Equation (79) below are defined in a manner such that the elements of the first $n$ rows and the last row of the updated $V$ and $L$ can be in the sets {-1, 0, 1} and {0, 1}, respectively (Wang and Li, 2014).

$$V_{x_{ij}, y_j}(s+1) = \begin{cases} -1, & \text{if } V_{x_{ij}, y_j}(s+1) < -0.05 \\ 0, & \text{if } -0.05 \le V_{x_{ij}, y_j}(s+1) \le 0.05 \\ 1, & \text{if } V_{x_{ij}, y_j}(s+1) > 0.05 \end{cases} \tag{78}$$

$$L_{x_{ij},y_j}(s+1)=\begin{cases}0, & \text{if } L_{x_{ij},y_j}(s)+V_{x_{ij},y_j}(s+1)\le 0\\ 1, & \text{if } L_{x_{ij},y_j}(s)+V_{x_{ij},y_j}(s+1)\ge 1\end{cases} \tag{79}$$

The subscripts $x_{ij}$ and $y_j$ in Equation (78) and Equation (79) are used to denote the part of the matrices $V$ and $L$ where $x_{ij}$ and $y_j$ are stored. Similarly, Equation (80) and Equation (81) are also defined to make the elements of the $(n+1)^{th}$ row of the updated $V$ and $L$ be in the sets $\{-0.1Z,0,0.1Z\}$ and $\{Z,0.9Z,0.8Z,\ldots,.0.1Z,0\}$, respectively. That is,

$$V_{z_j}(s+1)=\begin{cases}-0.1Z, & \text{if } V_{z_j}(s+1)<-0.05Z\\ 0, & \text{if } -0.05Z\le V_{z_j}(s+1)\le 0.05Z\\ 0.1Z, & \text{if } V_{z_j}(s+1)>0.05Z\end{cases} \tag{80}$$

$$L_{z_j}(s+1)=\begin{cases}Z, & \text{if } L_{z_j}(s)+V_{z_j}(s+1)>Z\\ L_{z_j}(s)+V_{z_j}(s+1), & \text{if } 0\le L_{z_j}(s)+V_{z_j}(s+1)\le Z\\ 0, & \text{if } L_{z_j}(s)+V_{z_j}(s+1)<0\end{cases} \tag{81}$$

The subscript $z_j$ in Equation (80) and Equation (81) is used to denote the part of the matrices $V$ and $L$ where $z_j$ is stored. The fitness function of an individual particle can be formulated as shown in Equation (82) where the constraints Equation (69)- Equation (72) are integrated as penalty terms.

$$\begin{aligned}&C+A_1\cdot\max(TA-TP-\varphi,0)^2+A_2\cdot\sum_{i=1}^{n-1}\sum_j\min(CB_i-B_{ij},0)^2\\ &+A_3\cdot\sum_{i=1}^{n-1}\sum_j\min(B_{ij},0)^2+A_4\cdot\sum_j\min[\min(Z,\sum_{i=1}^{n}x_{ij}\cdot rp_i\cdot e_i)-z_j,0]^2\end{aligned} \tag{82}$$

where $A_1$, $A_2$, $A_3$, and $A_4$ are four large real numbers.

When implementing PSO, a swarm of particles will be first generated, and the velocity will be initialized. The fitness of each particle is evaluated using Equation (82). $L_{PB}$ will be identified based on the particle location with the best fitness so far. The global

best of the entire swarm $L_{GB}$ will also be updated if necessary. Equations (76)-(81) will be used to update the velocity and location of each particle at each iteration. These steps will be repeated until the maximum iteration number $S$ is reached.

## 5.3. CASE STUDY

Consider a five machine and four buffer manufacturing system with a microgrid system as shown in Figure 5.2.

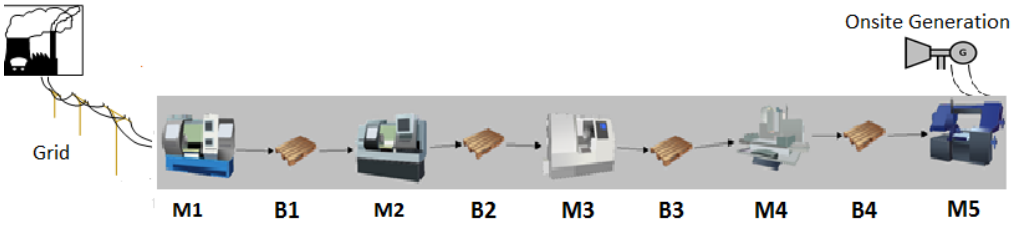


Figure 5.2 A five machine and four buffer manufacturing system with a microgrid system.

The parameters of each machine including rated power, production efficiency, and production rate are illustrated in Table 5.1. The parameters of each buffer including initial contents and respective buffer capacities are illustrated in Table 5.2.

The capacity of the microgrid system ($Z$) is set as 40 kW. An eight-hour shift from 7:00 AM to 3:00 PM is examined. The fixed duration of each period ($H$) is set as 15 minutes. The target production ($TA$) is set as 250. Unit production loss cost ($p_{pl}$) is set as \$50. Unit generation cost of the microgrid system ($f$) is set to be \$0.2/kWh. The maximum allowed unmet production ($\varphi$) is set to be 20. The overgeneration period is set to be between 10:00AM to 12:00PM.

Table 5.1 Machine parameters

| Machine | Power (kW) | Production rate ($PR_i$) (units/period) | Production efficiency ($r_i$) |
|---|---|---|---|
| 1 | 20 | 10.25 | 0.95 |
| 2 | 15 | 10.5 | 0.92 |
| 3 | 21 | 9.5 | 0.94 |
| 4 | 16 | 10.5 | 0.90 |
| 5 | 13 | 9.25 | 0.94 |

Table 5.2 Buffer parameters

| Buffer | Initial contents | Capacity |
|---|---|---|
| 1 | 90 | 180 |
| 2 | 80 | 160 |
| 3 | 75 | 150 |
| 4 | 80 | 180 |

The electricity consumption rate ($/kW) and demand rate ($/kW) for off-peak, overgeneration, and peak period are shown in Table 5.3. The required load level for each period during overgeneration periods ($D_j$) is given in Table 5.4. The penalty $g_j$ and bonus $b_j$ are set to be $12 and $8, respectively, for each overgeneration period.

In this case, we consider three different scenarios as follows. Scenario-I represents the situation that the manufacturer does not participate in such over-generation mitigation-oriented demand response programs, which is considered the baseline scenario. The production schedule and microgrid system utilization schedule of scenario I is obtained by minimizing the total cost including the energy billing cost, potential production loss penalty cost, and microgrid cost. The formulation for scenario I can be easily obtained by removing non necessary variables and parameters from the model proposed in Section 2. Scenario II describes a simple heuristic participation strategy. Based on results obtained from scenario I, the production schedule and onsite microgrid

utilization schedule will be revised so that all the machines will be kept on and the microgrid system will be kept off during the overgeneration period. Scenario III employs the strategy obtained by solving the proposed model.

Table 5.3 Electricity consumption and power demand rates

| | Peak Period | Over-generation Period | Non-Peak Period |
|---|---|---|---|
| Time Periods | 12:00PM-3:00PM | 10:00AM-12:00PM | 7:00AM-10:00PM |
| Consumption Rate ($/kWh) | 0.17 | 0.05 | 0.1 |
| Demand Rate ($/kW) | 18.80 | 8.00 | |

Table 5.4 Required load for periods *j* belong to **SP**

| Time | 10:00-10:15 | 10:15-10:30 | 10:30-10:45 | 10:45-11:00 | 11:00-11:15 | 11:15-11:30 | 11:30-11:45 | 11:45-12:00 |
|---|---|---|---|---|---|---|---|---|
| Required Power (KW) | 93 | 97 | 65 | 94 | 85 | 63 | 61 | 82 |

PSO is encoded in MATLAB to deal with the three scenarios aforementioned. The learning factors, $c_1$ and $c_2$, are both set as 1.7. The maximum and minimum values of inertia weight are set as 0.09 and 0.01, respectively. PSO is implemented for different swarm size and iteration number. The computational time and quality of the solution are recorded. Based on the records, we find that (8000, 100) is a reasonable parameter combination regarding the swarm size and iteration number that can be used to balance

the solution quality and computational cost. The computational time to solve this case is 460 s. The computer used is a desktop with an Intel(R) Xeon(R) CPU W3505@ 2.53 GHZ processor, and a 4 GB memory.

After running the PSO with the specified parameters, the obtained resultant profiles of the power consumption of manufacturing system supplied by both external grid and microgrid system of the three scenarios are illustrated in Figure 5.3– Figure 5.5, respectively. The obtained system throughput for all the scenarios is 250. The comparisons of the total cost between Scenario III (the proposed model) and Scenarios I and II are illustrated in Table 5.5.

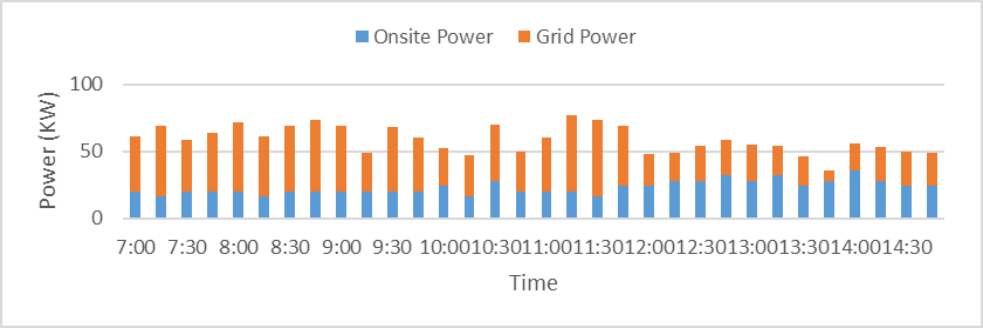


Figure 5.3 Power consumption profile of scenario I (baseline model).

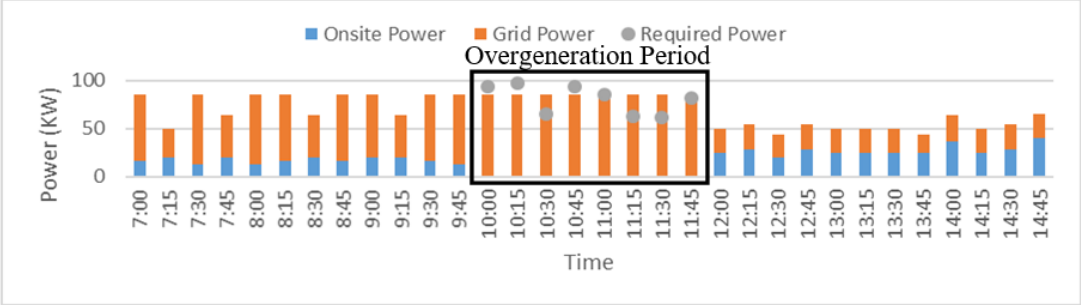


Figure 5.4 Power consumption profile of scenario II (heuristic strategy).

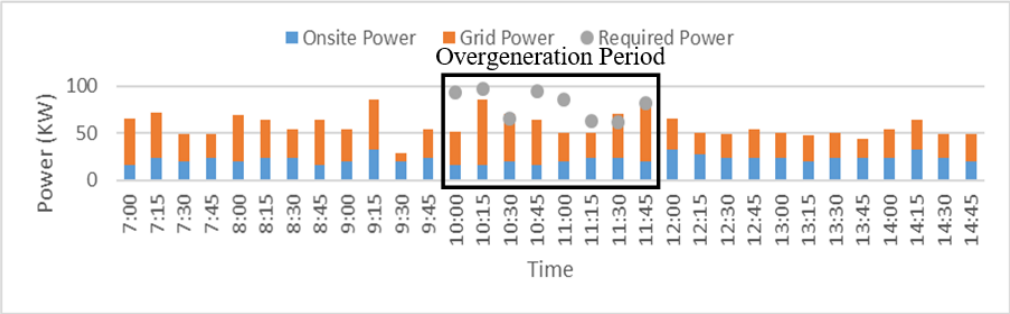


Figure 5.5 Power consumption profile of Scenario III (proposed model).

Table 5.5 Cost comparisons between Scenario III (the proposed model) and two other scenarios

| Proposed model | Scenario-I (Baseline) | Cost reduction |
|---|---|---|
| $1255.8 | $ 1393.9 | **9.9%** |
| Proposed model | Scenario II | Cost reduction |
| $1255.8 | $1313.8 | **4.46%** |

From Table 5.5, it can be seen that the proposed decision-making model can significantly reduce the overall cost compared to the Scenario I (baseline). It also outperforms the simple heuristic method (Scenario II) regarding overall cost reduction. The convergence of the solution shown in Figure 5.6 illustrates that after 30 iterations, the solution converges. In addition, the robustness of the proposed model is tested with different values of the input parameters, such as the initial buffer, incentive/penalty ratio, production rate, production efficiency, unit production loss penalty, microgrid cost etc. The cost reductions of three scenarios considering such variations are illustrated in Table 5.6. From Table 5.6, it is noted that for the variation with a lowered production efficiency, the cost reduction seems to be less than the ones from the other variations.

This can be explained by the fact that a lowered production efficiency may lead to a reduced production throughput and a higher production loss cost.

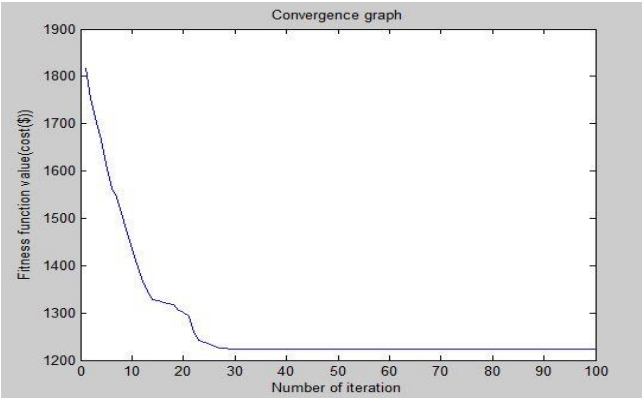


Figure 5.6 Convergence graph.

Table 5.6 Cost reductions for different input parameters

| Parameters | Production efficiency (%) | | Production rate (Units/hr.) | | Incentive/ penalty ratio | | Unit production loss penalty | | Onsite microgrid cost | |
|---|---|---|---|---|---|---|---|---|---|---|
| Variation | 95% | 105% | 95% | 105% | 90% | 110% | 90% | 110% | 90% | 110% |
| Scenario I | 1514.4 | 1316.1 | 1468.5 | 1316.1 | 1393.9 | 1393.9 | 1393.9 | 1393.9 | 1325.1 | 1408.5 |
| Scenario II | 471.8 | 240.1 | 391.8 | 239.6 | 308.8 | 308.8 | 313.8 | 1313.8 | 1305.4 | 286.8 |
| Scenario III | 1445.57 | 1217.6 | 1361.3 | 1217.6 | 1258.8 | 1255.8 | 1255.8 | 1255.8 | 1241.4 | 1270.2 |
| Scenario II Saving | 2.8% | 5.78% | 2.19% | 6.17% | 3.8% | 3.8% | 4.46% | 4.46% | 1.5% | 8.69% |
| Scenario III Saving | 4.54% | 7.5% | 7.28% | 7.53% | 9.69% | 10% | 9.9% | 9.9% | 6.3% | 9.7% |
| Parameters | Peak demand charge rate | | Off-peak demand charge rate | | Consumption charge rate | | Required load | | Initial buffer | |
| Variation | 90% | 110% | 90% | 110% | 90% | 110% | 90% | 110% | 90% | 110% |
| Scenario I | 1316.9 | 1463.4 | 1341.9 | 1445.9 | 1362.1 | 1395.3 | 1393.9 | 1393.9 | 1517.8 | 1319.8 |
| Scenario II | 1210.7 | 1368.9 | 1325.8 | 1381.8 | 1348.2 | 1359 | 1312.7 | 1331.9 | 1390.6 | 1256.3 |
| Scenario III | 1187.8 | 1317.9 | 1213.4 | 1298.2 | 1254.5 | 1257.2 | 1255.8 | 1267.8 | 1280.2 | 1210.1 |
| Scenario II Saving | 8% | 6.45% | 1.2% | 4.43% | 1.02% | 2.60% | 5.82% | 4.4% | 7.9% | 4.8% |
| Scenario III Saving | 9.8% | 9.91% | 9.5% | 10.10% | 7.89% | 9.89% | 9.9% | 9% | 15.5% | 8.3% |

It can also be observed from the Table 5.6 that for the variations regarding other major parameters, the cost reduction by adopting the proposed model for the case of participating in over-generation mitigation-oriented demand response program is quite consistent compared to the baseline and heuristic models.

Further, a finer discretization of the output of microgrid system is tested such that the decision variable $z_j$ can be extracted from a finer set $\{0, 0.05Z, 0.1Z\ldots 0.95Z, Z\}$. Table 5.7 shows the comparison of the cost between the finer discretization and the previous one. It can be seen that the fine discretization can further reduce the total cost.

Table 5.7 Cost reductions for discretization of microgrid system

| | Coarse discretization of the output of microgrid system $z_j \in \{0,0.1Z,0.2Z,\ldots,0.9Z, Z\}$ | Fine discretization of the output of microgrid system $z_j \in \{0, 0.05Z,0.1\ Z,\ldots,0.95Z, Z\}$ | Reduction |
|---|---|---|---|
| Proposed Model | 1255.8 | 1223.45 | 2.54% |

## 5.4. SUMMARY OF THE OPTIMIZATION MODEL FOR OPTIMALLY PLANNING THE MANUFACTURING AND MICROGRID SYSTEMS UNDER THE OVERGENRATION ORIENTED DRP

In this section, a mathematical model is proposed to identify the optimal participation strategy for the manufacturing end use customers with onsite energy generation system in the demand response program designed for mitigating the electricity over-generation from renewable sources in electricity grid. The particle swarm optimization is used to solve the formulated problem to obtain a near optimal strategy for

the manufacturers. The optimal decisions on participating or not, and corresponding production schedule as well as onsite generation utilization schedule can be identified from the model to minimize the overall costs, including benefits due to participation (i.e., the incentive or penalty due to achieving or not achieving the committed consumption level), onsite generation cost, electricity billing cost, and production loss penalty. A numerical case study with sensitivity analysis is conducted to illustrate the effectiveness and robustness of the proposed model.

# 6. BATTERY LIFE ESTIMATION FOR PERFORMANCE EVALUATION OF THE ONSITE MICROGRID SYSTEM IN A PROSUMER-BASED COMMUNITY NETWORK

## 6.1. STRATEGIC OVERVIEW

Onsite generation system (OGS) with renewable sources for modern manufacturing plant is considered as a critical alternative energy source for the manufacturers. Prosumer community can be formed by aggregating such manufacturers to achieve a mutual goal of sustainable and resilient power system. As the sustainability of the network depends on the reliable operations of each component in the network, it is required to estimate the lifetime of the components existed in the network to monitor the performance of the OGS. One of the critical as well as costly components used to enhance the reliability and performance of the network is the battery energy storage system (BESS). The section proposes a model to estimate the lifetime of the battery energy storage system (BESS) for performance evaluation of the OGS using an integrated approach of cellular automata and system dynamic (SD). The cellular automata model investigates the complex dynamic of energy sharing capability (offer excess energy or demand the shortage of generation) of the neighboring manufacturers while participating as a member in such a community. Considering the energy sharing capability of the neighbors along with the generation from onsite generation system (OGS), demand of the manufacturer, and the price of grid electricity at any interval, the manufacturer can take the decision of charging/discharging of the battery and corresponding depth of discharge. The degradation due to the decision of charging/discharging is analyzed through a simulation model based on the principles of the system dynamics methodology. Based on

the results, the prosumers can optimally plan for the maintenance/replacement schedule as well as control the charging/discharging scheme to prolong the battery lifetime and thus, ensure a reliable energy management infrastructure for the community.

The major contributions of the section can be summarized as follows:

1. The dynamics of the energy sharing capability of the neighbors in such a manufacturer-based prosumer community is investigated through the cellular automata model.

2. Later, the lifetime of the BESS is estimated using SD model to evaluate the performance of the OGS considering the effect of irregular charging/discharging under a stochastic operating condition.

The rest of the section is organized as follows. Section 6.2 demonstrates the integrative modeling approach. Section 6.3 implements the proposed model through a hypothetical case study to illustrate the effectiveness of the model. Section 6.4 analyzes the results and sensitivity analysis. Section 6.5 concludes the section and discusses the future work.

## 6.2. MODEL DESCRIPTION

The model developed to estimate the remaining lifetime of the BESS is discussed into two subsections: (a) Identifying the energy sharing capability of the neighbors using cellular automata model, and (b) Estimating the remaining lifetime of BESS using SD Simulation. The subsections are described below:

### 6.2.1. Identifying the Energy Sharing Capability of the Neighbors Using Cellular Automata Model.

To build a self-sufficient, cost-effective, and sustainable

community, the prosumers develop a network through sharing their surplus electricity to the neighbors during the period of excess generation. The sharing capability of each prosumer depends on the energy demand of its manufacturing plant, generation from the OGS, charging state of the BESS etc. Besides, the prosumer can also share energy (purchase the shortage of electricity or sell back the excess generation) with the grid based on its energy state, electricity demand of the neighbors, price of electricity etc. Such a community with a representative manufacturer is shown in Figure 6.1

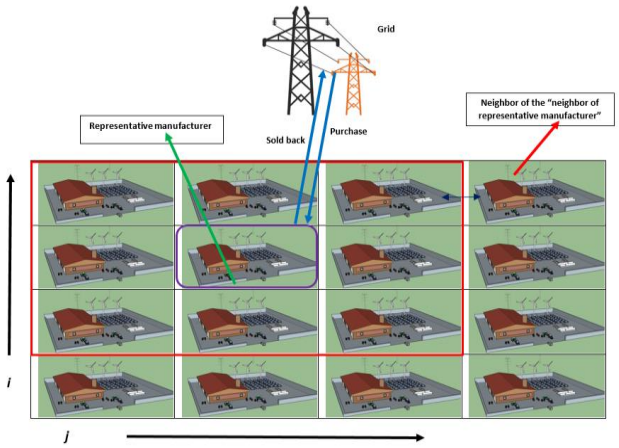


Figure 6.1 Grid connected prosumer community of manufacturers with OGS.

Like other components in this network, the energy dynamics of the BESS will be influenced by not only the states (excess/shortage of generation, corresponding amount, state of charge of BESS) of the individual but also the states of its immediate neighbors. Therefore, to determine the energy sharing capability of each prosumer through investigating the interaction and temporal dynamics of the neighbors, cellular automata model is implemented.

In cellular automata model, the state of the BESS control scheme for the representative prosumer is a function of the state of energy status of the prosumer and its neighborhood in accordance with a set of transition rules which can be represented by:

$$CB_{ij}^{t} = f(ES_{ij}^{t}, \Omega_{ij}^{t}, C, NP) \tag{83}$$

where $CB_{ij}^{t}$, $ES_{ij}^{t}$, and $\Omega_{ij}^{t}$ are the control schemes (charging/discharging and depth of discharge) of the battery, energy state, neighborhood evaluation function for the manufacturer at cell *ij* at decision epoch *t*, respectively. *f* is the transition function. *C* and *NP* are constraints for feasible power flow and number of participants in the community, respectively.

**6.2.1.1. Cell and its state definitions.** The square-lattice represents the prosumer community while the 2D-regular square grid illustrates each manufacturer in the cellular automata framework. The possible states of each manufacturer (prosumer) can be characterized by:

State 1: The cell representing manufacturer are able to share.

State 2: The cell representing manufacturer are not able to share

State 3: The cell representing manufacturer are not participating.

**6.2.1.2. Transition rules.** In this model, the state of each cell (each manufacturer) evolves in discrete time steps based on the transition rules defined as follows:

Rule 1. If the representative manufacturer (RM) has excess generation, RM can share electricity with any number of the neighbors if the neighbors have shortage of electricity.

Rule 2. If everyone meets their demand in the community, no sharing will happen among themselves.

Rule 3. If the neighbors have excess generation and RM has less generation than demand, RM will first choose the manufacturer who has maximum excess generation among all the neighbors.

**6.2.2. Estimating the Battery Lifetime using SD Simulation.** The SD simulation model is developed to determine the health state of BESS and corresponding degradation periodically to estimate the remaining lifetime considering the actual operating conditions mentioned earlier.

**6.2.2.1. Model variables.** The structure of a SD model contains stock and flow variables. In this model, stock variables represent the energy states within the system. The flow variables represent the flows in the system (i.e. power), which result from the decision-making process. The model variables (stock and flow) and parameters are illustrated below with their explanation and corresponding units:

*Model Variables*

| | |
|---|---|
| current_gen | current generation from the solar and wind (kW) |
| available_gen | available generation considering both current generation and amount of energy shared by the neighbors (kW) |
| gen_stat | generation status which defines the excess or shortage of the generation compared to the demand (kW) |
| grid | available grid power (kW) |
| sold_back | sold back amount (kW) |
| battery_state | status of the charge of the BESS (kW) |

| | |
|---|---|
| charging | amount of energy available for charging in BESS (kW) |
| discharging | amount of energy available for discharging in BESS (kW) |
| battery_health | status of the battery health (%) |
| total_degradation | amount of battery health degraded (%) |
| *Model Parameters* | |
| solar_gen | amount of solar generation (kW) |
| wind_gen | amount of wind generation (kW) |
| ca_decision | decisions from cellular automata model whether the neighbors have the capability to share energy or not (binary decision; 0: not capable to share, 1: capable to share) |
| neigh_share | amount that can be shared by the neighbors (kW) |
| demand_manf | demand of the manufacturing system (kW) |
| cost_chack | grid electricity cost ($/kW) |
| capacity_grid | capacity of the grid (kW) |
| initial_charge | initial state of charge in BESS at the beginning of the simulation (kW) |
| battery capacity | capacity of the BESS (kW) |

**6.2.2.2. System Dynamics (SD) diagram.** The first step of building a SD model is to construct a SD diagram based on the interrelationships among the system operations. Figure 6.2 illustrates the SD simulation model for the system developed in Anylogic platform. The diagram is constructed using three building blocks: stocks, flows, and parameters. The stock variables (symbolized by rectangles) represent the state over time, flow variables (symbolized by arrow with valves) represent the rates of change in stock variables used to fill in or drain the stock variables.

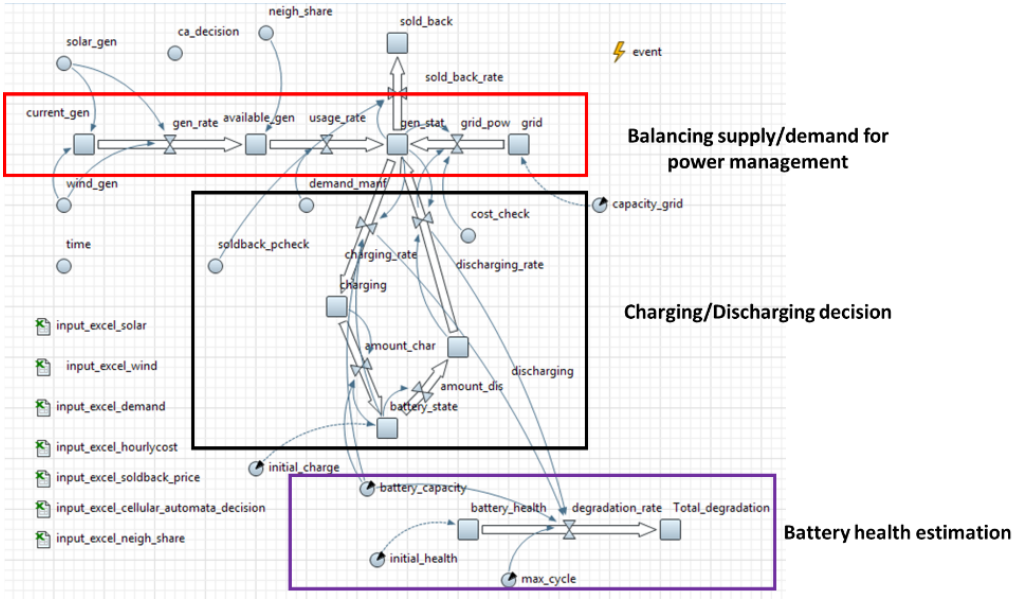


Figure 6.2 SD model diagram.

**6.2.2.3. Physical constraints for the SD model.** The next step of SD methodology includes the physical constraints which are required to develop the feasible model based on the interrelationships existed among the variables. The stock-flow diagram can be easily translated to a system of differential equations. The state of the stock variables can be defined by

$$Stock(t) = \int_{t_0}^{t'} [Inflow(t) - Outflow(t)] \cdot dt + Stock(t_0) \tag{84}$$

where $Inflow(t)$ and $Outflow(t)$ represent the value of the inflow and outflow at any time $t$ between the initial time $t_0$ and current time $t$.

The energy flow constraints in the model are determined as follows:

$$\frac{d(current\_gen)}{dt} = solar\_gen + wind\_gen - gen\_rate \tag{85}$$

$$\frac{d(available\_gen)}{dt} = gen\_rate + neigh\_share \tag{86}$$

$$\frac{d(gen\_stat)}{dt} = grid\_pow + usage\_rate \tag{87}$$

The power generation from different sources, battery degradation estimation, and important model assumptions are presented below:

The power generated by the solar PV, $r_{t_m}$, can be calculated by

$$r_{t_m} = a \cdot I_{t_m} \cdot \delta / 1000 \tag{88}$$

where $I_{t_m}$ is the solar irradiance at interval $t_m$ (W/m$^2$) and *m* represents the month.

The power generated by the wind turbine, $w_{t_m}$, can be calculated by

$$w_{t_m} = \frac{1}{2} \cdot \rho \cdot \pi \cdot r^2 \cdot v_{t_m}^3 \cdot \theta \cdot \eta_t \cdot \eta_g \cdot h / 1000 \tag{89}$$

where $v_{t_m}$ is the wind speed at interval $t_m$.

The state of charge in BESS must be bounded within a given range, which can be formulated as

$$SOC_{\min} \le SOC_{t_m} \le SOC_{\max} \tag{90}$$

where $SOC_{max}$ and $SOC_{min}$ are the maximum and minimum states of charge of the BESS (%). $SOC_{t_m+1}$ can be calculated recursively as follows

$$SOC_{t_m+1} \cdot e = SOC_{t_m} \cdot e + \eta_c \cdot bc_{t_m} \cdot \Delta t - \frac{1}{\eta_d} \cdot bd_{t_m} \cdot \Delta t \tag{91}$$

where $\eta_c$ and $\eta_d$ are the charging and discharging efficiencies, respectively. *e* is the battery capacity. $bc_{t_m}$ and $bd_{t_m}$ are the charging and discharging rate at decision epoch $t_m$.

The degradation of the BESS can be calculated by

$$degradation_{t_m} = \sum_{m} \sum_{t_m=1}^{T_m} \left( \frac{(bc_{t_m} + bd_{t_m}) \cdot \Delta t}{2Ne(SOC_{\max} - SOC_{\min})} \right) \quad (92)$$

where $N$ is the maximum number of recommended charging/discharging cycle for BESS.

## 6.3. IMPLEMENTATION OF THE PROPOSED MODEL

A hypothetical manufacturing prosumer community is used to build the case study. Total number of prosumers participated in the study is 100. The temporal horizon selected for the study is 50 months based on the cyclic performance of the battery for 50% depth of discharge mentioned in reference (Sandia Report, 2016). The location used for the weather data is Chicago, Illinois. The manufacturing plant is assumed to be operated with twenty-four hours per day, seven days per week, and all the weeks per year. The energy-related parameters are shown in Table 6.1 for illustration.

Table 6.1 Rated power of the manufacturing machines in RMA

| Machine Name | Rated Power (kW) |
|---|---|
| OP10 Turn-1 | 105 |
| OP20 Turn-2 | 105 |
| OP30 Turn-3 | 105 |
| OP40 Window milling | 155 |
| OP50 Turn-4 | 120 |

For simplicity, it is assumed that every prosumer has similar size of OGS; area of the solar PV: 2000 m2, number of wind turbine: 2, and capacity of BESS: 1000 kW.

Initially, the BESS is charged by 10%. The maximum number of cycles the battery can go for full depth of discharge is considered as 5000 cycles. The power generation profile from the solar and wind turbine as well as the energy demand of the manufacturing system used for the SD simulation model are shown in Figure 6.3.

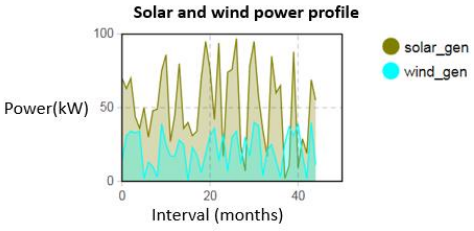


Figure. 6.3a. Power generation profile from the OGS


Figure 6.3b. Power demand profile for manufacturing

Figure 6.3 Power generation and demand profile for the simulation.

Based on the simulated demand and generation from the OGS, the energy status (excess generation, or shortage of generation, or equal to the demand) of each prosumer is determined and used as the input for the cellular automata model. It is considered that each prosumer has eight neighbors and each of the neighbors has also eight neighbors. Therefore, in cellular automata, while the energy sharing capability of the representative prosumer is determined, not only the energy status of the representative prosumer but also the energy sharing capability of their neighbors are also considered.

## 6.4. RESULT AND SENSITIVITY ANALYSIS

The following section discusses the result and investigates the sensitivity of the parameters based on a case study.

**6.4.1. Result Analysis.** As the energy sharing capability of each prosumer changes over time based on the parameters (energy demand of manufacturing, generation from OGS, price of the grid electricity, and state of BESS), the state of the prosumer in square-lattice (energy sharing capability of the capability) will be changed accordingly. Based on the result obtained from the cellular automata model, the state of the representative manufacturer (blue dot: able to share; white cell: not able to share) at two different intervals are shown in Figure 6.4.

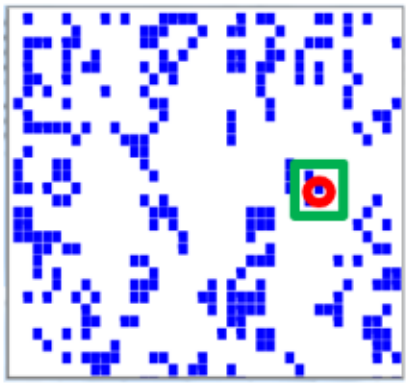

Figure 6.4a. Neigboring state of the RM at decision epoch *t*

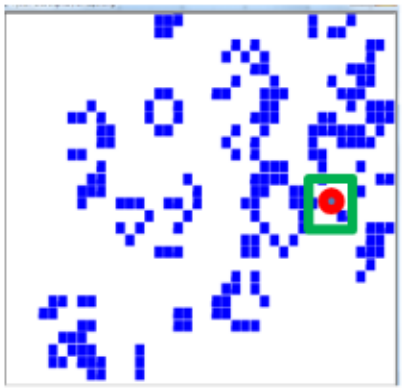

Figure 6.4b. Neigboring state of the RM at decision epoch *t*+1

Figure 6.4 Sharing capability of the neighbors at decision epoch *t* and *t*+1.

The dynamics of the energy sharing capability of each prosumer obtained from the cellular automata is used as the input of the SD model. Considering the energy sharing capability of the neighbors of representative manufacturer along with other factors (demand of the representative manufacturer, generation from his OGS, price of the grid electricity, and state of BESS), the SD model is simulated to estimate the

degradation over time. The degradation or battery health profile obtained from the model is shown in Figure 6.5.

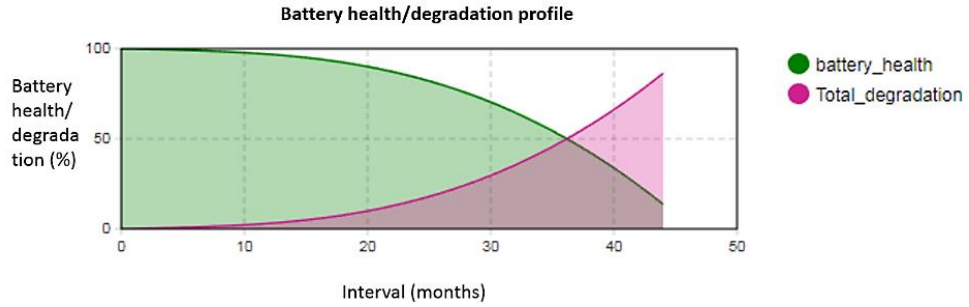


Figure 6.5 Battery health and degradation profile.

From Figure 6.5, it can be seen that the estimated life of BESS is 43 months based on the stopping criteria (10 percent of the battery life) while the expected battery life is 50 months. This is happening due to actual operating condition (irregular charging/discharging cycle and depth of discharge) which is quite different from the standard ones. Again, the actual conditions are influenced by the stochastic parameters such as the generation from the OGS, energy demand of manufacturer, sharing capability of the neighbors etc.

**6.4.2. Sensitivity Analysis.** To determine the impact of the variations of the critical parameters on battery degradation and further, extend the lifetime of the BESS through controlling those parameters, the sensitivity analysis is conducted in this study. The critical parameters considered for the analysis are the available renewable sources and sold back price of the electricity. The results obtained based from the sensitivity analysis are shown in Table 6.2 and Table 6.3. The Table 6.2 follows the intuition. Due to

high generation from the renewable sources, the number of charging and discharging is increased. Therefore, the degradation rate is higher which leads to a reduced lifetime of the BESS.

Table 6.2 Comparison of the battery health and degradation profile based on the available renewable sources

| Scenarios | Description of the scenario | Percentage | Lifetime (months) | Battery health and degradation profile |
|---|---|---|---|---|
| I | Low renewable sources | 90% | 49 | 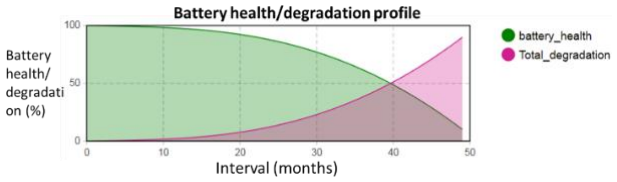 |
| II | Baseline renewable sources | 100% | 43 | 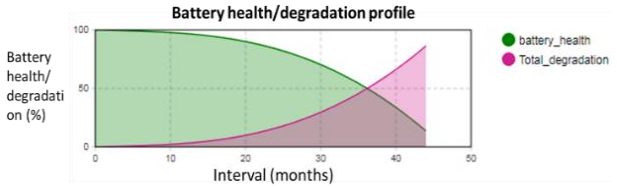 |
| III | High renewable sources | 110% | 41 | 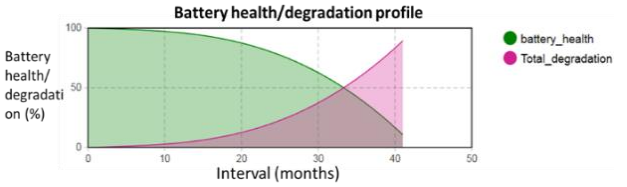 |



From Table 6.3, it is noted that the battery degradation is sensitive with the sold back price. When the sold back price is high, it is more cost-effective to sell the excess energy rather than storing for future. Therefore, the number of charging/discharging cycles is reduced, and the lifetime of the BESS is increased.

Table 6.3 Comparison of the battery health and degradation profile based on different sold back price of electricity

| Scenarios | Description of the scenario | Percentage | Lifetime (months) | Battery health and degradation profile |
|---|---|---|---|---|
| I | High sold back cost | 110% | 48 | 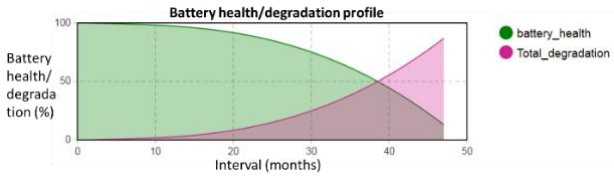 |
| II | Baseline sold back cost | 100% | 43 | 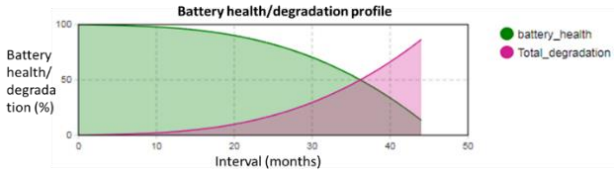 |
| III | Low sold back cost | 90% | 42 | 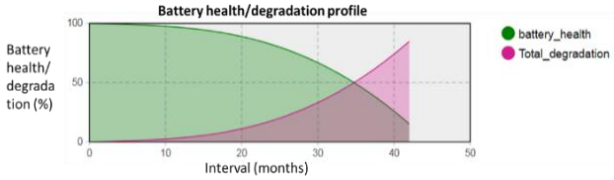 |



## 6.5. SUMMARY OF THE MICROGRID PERFORMANCE EVALUATION MODEL

The proposed model will help the prosumers to evaluate the performance of the BESS through estimating the lifetime of the BESS accurately considering the actual operating conditions. The health state of BESS and corresponding degradation can be determined periodically. Therefore, based on the estimation, the prosumer can control the battery management plan (charging/discharging scheme) to ensure reliable energy management for the community.

# 7. CONCLUSION AND OPPORTUNITIES FOR FUTURE WORK

## 7.1. CONCLUSION

The proposed mathematical models have the following advantages over the existing literature: 1. The research has developed a mathematical model to optimally design and control a microgrid system considering the detailed variations of the energy demand of a manufacturing plant including both manufacturing system and HVAC system for the lifetime of the microgrid. 2. Based on the configuration of the microgrid, the optimal energy management plan for both manufacturing and microgrid has been developed considering the demand response programs: TOU, CPP, and overgeneration mitigation-based demand response program. 3. The performance of the OGS is evaluated through the estimation of the lifetime of BESS to ensure reliable operation and therefore, develop a sustainable infrastructure for the prosumer community. 4. The results obtained from the case study and its sensitivity analysis will help the manufacturers to understand the framework of designing the microgrid, developing the operational strategies for both microgrid and manufacturing system under different demand response programs, integrating the uncertainty of the parameters into the model, evaluating the performance of the critical parameters, and realizing the sensitivity of the parameters.

This research is expected to fill the research gap of a systematic framework of microgrid design and operational strategies considering the total energy demand of the manufacturing plant considering both manufacturing and HVAC system and different demand response programs. The research extends the framework through evaluating the performance of the critical parameters of the OGS considering the stochasticity of the

demand, environmental uncertainty, and dynamic energy sharing capability of the prosumers (manufacturers) while establishing a community-based energy sharing network. Therefore, the framework can be considered as a tool to investigate the complex system of systems architecture, their interdependency, the process of designing and controlling, performance evaluation of the system, and challenges as well as opportunities for future microgrid technology for manufacturing customers. In addition, it is expected to serve the readers (including manufacturers, academic peers, industrial users etc.) who are interested in further enhancing the future microgrid technology for the manufacturing and other similar industrial sectors.

## 7.2. OPPORTUNITIES FOR FUTURE WORK

Both manufacturing and microgrid systems consist of several systems and the systems are highly interrelated, interconnected, and interwoven entities. To develop the optimal and intelligent control strategy for such a complex system, it is required to investigate the structure of the control policy that jointly can control the components of the system. In addition, the manufacturers need to understand the manufacturing loads completely and determine the number of controllable loads that can be shifted from high price-low generation to the low price-high generation hours to minimize the energy cost as well as improve the microgrid reliability. These two significant considerations can make the future microgrid control more intelligent, reliable, and resilient. It will also open a new horizon for the researchers to investigate further in developing a sustainable microgrid architecture and optimal energy management plan for the microgrid and manufacturing.

**7.2.1. Joint Dynamic Decision-Making Model for the Optimal Control of the Systems.** The manufacturing industry is considered as a complex system where the demand is quite uncertain and energy management is crucial to meet the target demand. The architecture of the microgrid is also complex and the generation from the sources is intermittent. In addition to the stochasticity and architectural complexity, both systems are highly interconnected and interdependent. Therefore, the control strategy for the components of each system will impact on the state of another system. Significant number of studies on microgrids have been conducted from the perspectives of the optimal design and sizing of the microgrid for manufacturing plant (Zhong et al., 2017; Zhang et al., 2018; Islam et al., 2019), as well as the optimal energy control from the manufacturing side (Levron et al., 2013; Li et al., 2012; Guerrero et al., 2010) towards sustainability. However, the joint energy control strategy for both onsite microgrid system and manufacturing plant has not been investigated yet. Therefore, considering the interrelationship and uncertainty involved in the systems, it is required to develop a mathematical framework to control both systems simultaneously to enhance the sustainability, resiliency, and cost-effectiveness for the energy management system.

To achieve the goal, a joint control problem can be formulated considering the inherent stochasticity and time dependency of energy demand, renewable power supply, and cost for grid power. The problem is a discrete time stochastic control problem where the decision of connecting the components of the microgrids (solar PV, wind turbine, BESS, generator) to the manufacturing unit and the operational decision for the machines (on/off) will be primarily determined by the decision of the actor (decision maker). However, the final state of the system will be determined based on the decision of the

actor and the impact of the stochastic environment (solar irradiance, wind speed, machine failure etc.). The final state of the system will be determined based on the integrated decision of the actor and the impact of the stochastic environment (solar irradiance, wind speed, machine failure etc.). Therefore, the decision making in such a problem can be considered as partly random and partly under the control of a decision maker. Considering the characteristics of the system dynamics, a joint optimal control problem to coordinate the energy supply of the microgrid and the load of the manufacturing plant can be formulated using Markov Decision Process.

The state of the entire system at any decision epoch includes the states of manufacturing system, microgrid system, and environmental system. The manufacturing system can be modeled as typical serial production line with machines and buffers where the machine states include operational, idle, off, and breakdown. At each machine state, there is a corresponding power consumption level. The microgrid state (i.e., connected or not to the load) will be determined based on the joint outcome of the working status of the actor (i.e., connecting or disconnecting) and the environmental response (solar irradiance, wind speed, machine failure etc.). The action adopted by the actor is known as the policy and therefore, the objective is to determine the optimal policy that can maximize the use of the onsite generation and minimize the cost of grid electricity without sacrificing the target production in manufacturing.

The environment dynamics for the problem are quite complex to describe explicitly for the problem and in such a multi-component system, the system state and action spaces scale up exponentially with the number of components. Therefore, it becomes intractable to solve the problem using any conventional solution scheme or

advanced Markov Decision Processes (MDPs) or Partially Observable MDPs algorithm. To solve such large-scale multi-component domain problem, it is required to implement the state and action space reduction technique to alleviate the curse of dimensionality of the state space. Therefore, an off-policy actor-critic deep reinforcement learning algorithm can be a good candidate to operate in high-dimensional spaces, directly generalize the state/belief space of the underlying MDP and provide efficient control policies.

**7.2.2. Flexible Load Identification for Demand Response Program.** Among all the industrial sectors, the manufacturing itself is responsible for at least 65% of the energy usage in 2012, and this share is expected to increase until 2040 (Beck et al., 2018). The loads existed in this sector are not all critical. There are some loads which can be manipulated as there is a slackness in its consumption time without affecting the outcomes of the system and can be used for participating in the demand response program to minimize the energy cost and improve reliability of smart microgrid. However, it is quite challenging to identify the flexible load and the degree of flexibility for the manufacturing end use customers considering its complex architecture consisting of various manufacturing processes that are mutually interconnected and interdependent. While the literature on scheduling the machines in the manufacturing system to minimize the cost drivers such as energy (Shrouf et al., 2014; Moon et al., 2013), set up times (Johnson, 1954; Kim et al., 2002; Rocha et al., 2008), maintenance (Ji et al., 2007; Cassady et al., 2003; Yulan et al., 2008) without sacrificing the production target is extensive, very few attempts to determine the flexibility in terms of energy consumption of the manufacturing system under the constraints of production throughput have been

made. Therefore, an analytical model is required for the manufacturers to identify the load characteristic such as non-flexible load (base load) and flexible load, corresponding profile of each type of load, and the latest start time as a measure of flexibility. Further, the model can be extended to identify the production schedule of each machine of the flexible line to reduce the power consumption level considering the demand response programs so that the overall electricity cost can be minimized and the reliability of future microgrid can be enhanced.

# BIBLIOGRAPHY

Agarwal, V., Uthaichana, K., DeCarlo, R. A., & Tsoukalas, L. H. (2010). Development and validation of a battery model useful for discharging and charging power control and lifetime estimation. *IEEE Transactions on Energy Conversion*, 25(3), 821-835.

Ahourai, F., & Al Faruque, M. A. (2013). Grid impact analysis of a residential microgrid under various EV penetration rates in GridLAB-D. *Center for Embedded Computer Systems*, Irvine, CA.

Alramlawi, M., & Li, P. (2020). Design Optimization of a Residential PV-Battery Microgrid with a Detailed Battery Lifetime Estimation Model. *IEEE Transactions on Industry Applications*.

Al Busaidi, A. S., Kazem, H. A., Al-Badi, A. H., & Khan, M. F. (2016). A review of optimum sizing of hybrid PV–Wind renewable energy systems in oman. *Renewable and Sustainable Energy Reviews*, *53*, 185-193.

Al-Saedi, W., Lachowicz, S. W., Habibi, D., & Bass, O. (2013). Power flow control in grid-connected microgrid operation using Particle Swarm Optimization under variable load conditions. *International Journal of Electrical Power & Energy Systems*, *49*, 76-85.

Amrollahi, M. H., & Bathaee, S. M. T. (2017). Techno-economic optimization of hybrid photovoltaic/wind generation together with energy storage system in a stand-alone micro-grid subjected to demand response. *Applied energy*, 202, 66-77.

Arcuri, P., Florio, G., & Fragiacomo, P. (2007). A mixed integer programming model for optimal design of trigeneration in a hospital complex. *Energy*, *32*(8), 1430-1447.

Bahmani-Firouzi, B., & Azizipanah-Abarghooee, R. (2014). Optimal sizing of battery energy storage for micro-grid operation management using a new improved bat algorithm. *International Journal of Electrical Power & Energy Systems*, *56*, 42-54.

Bahramirad, S., Reder, W., & Khodaei, A. (2012). Reliability-constrained optimal sizing of energy storage system in a microgrid. *IEEE Transactions on Smart Grid*, 3(4), 2056-2062.

Beck, F. G., Biel, K., & Glock, C. H. (2019). Integration of energy aspects into the economic lot scheduling problem. *International Journal of Production Economics*, *209*, 399-410.

Belotti, P., Kirches, C., Leyffer, S., Linderoth, J., Luedtke, J., & Mahajan, A. (2013). Mixed-integer nonlinear optimization. *Acta Numerica*, *22*, 1-131.

bin Othman, M. M., & Musirin, I. (2010). Optimal sizing and operational strategy of hybrid renewable energy system using homer. In *2010 4th International Power Engineering and Optimization Conference (PEOCO)* (pp. 495-501). IEEE.

Boyle G. Renewable energy. Oxford University Press; 2004. p. 456. ISBN-10: 0199261784. ISBN-13: 9780199261789, 456.

Buonomano, A., Calise, F., Ferruzzi, G., & Vanoli, L. (2014). A novel renewable polygeneration system for hospital buildings: Design, simulation and thermo-economic optimization. *Applied Thermal Engineering*, *67*(1-2), 43-60.

California Energy Commission. A guide to photovoltaic (PV) system design and installation. Energy technology development division. 2001. p. 1516.

California Public Utilities Commission (2014). Demand Response. Retrieved from <http://www.cpuc.ca.gov/PUC/energy/Demand+Response/>.

Carroquino, J., Dufo-López, R., & Bernal-Agustín, J. L. (2015). Sizing of off-grid renewable energy systems for drip irrigation in Mediterranean crops. *Renewable energy*, *76*, 566-574.

Cassady, C. R., & Kutanoglu, E. (2003). Minimizing job tardiness using integrated preventive maintenance planning and production scheduling. *IIE transactions*, *35*(6), 503-513.

Chen, S. G. (2012). An efficient sizing method for a stand-alone PV system in terms of the observed block extremes. *Applied energy*, *91*(1), 375-384.

Chino Valley Unified School D. (2012). Energy Management Success Story: Chino Valley Unified School District. Retrieved from <https://www.sce.com/wps/wcm/connect/f6e4ba65-f019-4f9b-849c-4495112d4b9d/CSChinoValley_AA.pdf?MOD=AJPERES>.

Chong, W. T., Naghavi, M. S., Poh, S. C., Mahlia, T. M. I., & Pan, K. C. (2011). Techno-economic analysis of a wind–solar hybrid renewable energy system with rainwater collection feature for urban high-rise application. *Applied Energy*, *88*(11), 4067-4077.

Chou, F. D. (2013). Particle swarm optimization with cocktail decoding method for hybrid flow shop scheduling problems with multiprocessor tasks. *International Journal of Production Economics*, *141*(1), 137-145.

Clean Energy Reviews (2018). Complete Solar Battery Review.

Connolly, D., Lund, H., Mathiesen, B. V., Pican, E., & Leahy, M. (2012). The technical and economic implications of integrating fluctuating renewable energy using energy storage. *Renewable energy*, *43*, 47-60.

Crawley, D. B., Lawrie, L. K., Pedersen, C. O., & Winkelmann, F. C. (2000). Energy plus: energy simulation program. *ASHRAE journal*, *42*(4), 49-56.

Deshmukh, M. K., & Deshmukh, S. S. (2008). Modeling of hybrid renewable energy systems. *Renewable and sustainable energy reviews*, *12*(1), 235-249.

Dhar, A., Reddy, T. A., & Claridge, D. E. (1999). A Fourier series model to predict hourly heating and cooling energy use in commercial buildings with outdoor temperature as the only weather variable. *Journal of solar energy engineering*, *121*(1), 47-53.

Dohn, R. L. (2011). The business case for microgrids. *white paper Siemens*.

dos Anjos, P. S., da Silva, A. S. A., Stošić, B., & Stošić, T. (2015). Long-term correlations and cross-correlations in wind speed and solar radiation temporal series from Fernando de Noronha Island, Brazil. *Physica A: Statistical Mechanics and its Applications*, 424, 90-96.

Drouilhet, S., Johnson, B., Drouilhet, S., & Johnson, B. (1997). A battery life prediction method for hybrid power applications. In *35th Aerospace Sciences Meeting and Exhibit* (p. 948).

Du, S. C., Huang, D. L., & Wang, H. (2015). An adaptive support vector machine-based workpiece surface classification system using high-definition metrology. *IEEE Transactions on Instrumentation and Measurement*, *64*(10), 2590-2604.

Eberhart, R., & Kennedy, J. (1995). A new optimizer using particle swarm theory. In *MHS'95. Proceedings of the Sixth International Symposium on Micro Machine and Human Science* (pp. 39-43). IEEE.

Eberhart, R. C., Shi, Y., & Kennedy, J. (2001). *Swarm Intelligence (Morgan Kaufmann series in evolutionary computation)*. Morgan Kaufmann Publishers.

Ecker, M., Gerschler, J. B., Vogel, J., Käbitz, S., Hust, F., Dechent, P., & Sauer, D. U. (2012). Development of a lifetime prediction model for lithium-ion batteries based on extended accelerated aging test data. *Journal of Power Sources*, 215, 248-257.

Eiben, A. E., Raue, P. E., & Ruttkay, Z. (1994). Genetic algorithms with multi-parent recombination. In *International Conference on Parallel Problem Solving from Nature* (pp. 78-87). Springer, Berlin, Heidelberg.

Eichholtz, P., Kok, N., & Quigley, J. M. (2010). Doing well by doing good? Green office buildings. *American Economic Review*, *100*(5), 2492-2509.

Elhadidy, M. A., & Shaahid, S. M. (2000). Parametric study of hybrid (wind+ solar+ diesel) power generating systems. *Renewable energy*, *21*(2), 129-139.

EnergySage National grid net (2018). Metering rates.

Fadaee, M., & Radzi, M. A. M. (2012). Multi-objective optimization of a stand-alone hybrid renewable energy system by using evolutionary algorithms: A review. *Renewable and sustainable energy reviews*, *16*(5), 3364-3369.

Farinet, D., Maurer, M., Vacca, L., Spataru, S. V., & Stroe, D. I. (2019). Battery Lifetime Analysis for Residential PV-Battery System used to Optimize the Self Consumption-A Danish Scenario. In 2019 *IEEE Energy Conversion Congress and Exposition (ECCE)* (pp. 6693-6698). IEEE.

Farret, F. A., & Simoes, M. G. (2006). *Integration of alternative sources of energy*. John Wiley & Sons.

Fazli Khalaf, A., & Wang, Y. (2018). Energy-cost-aware flow shop scheduling considering intermittent renewables, energy storage, and real-time electricity pricing. *International Journal of Energy Research*, *42*(12), 3928-3942.

Federal Energy Regulatory Commission. (2008). Assessment of demand response and advanced metering.

Federal Energy Regulatory Commission. (2009). A national assessment of demand response potential. Prepared by *The Brattle Group, Freeman Sullivan, & Co, and Global Energy Partners*.

Federal Energy Regulatory Commission (2012). Reports on Demand Response & Advanced Metering, Washington D.C., U.S. Retrieved from: https://www.ferc.gov/legal/staff-reports/2018/DR-AM-Report2018.pdf

Freidlin, M., & Hu, W. (2011). On perturbations of generalized Landau-Lifshitz dynamics. *Journal of Statistical Physics*, *144*(5), 978.

Georges, E., Braun, J. E., & Lemort, V. (2017). A general methodology for optimal load management with distributed renewable energy generation and storage in residential housing. *Journal of Building Performance Simulation*, *10*(2), 224-241.

Goldman, C., Reid, M., Levy, R., & Silverstein, A. (2010). National Action Plan for Energy Efficiency, Coordination of Energy Efficiency and Demand Response. *United States Environmental Protection Agency, Washington DC. http://www. epa. gov/cleanenergy/documents/suca/ee_and_dr. pd f*.

Gudi, N., Wang, L., Devabhaktuni, V., & Depuru, S. S. S. R. (2011). A demand-side management simulation platform incorporating optimal management of distributed renewable resources. In *2011 IEEE/PES Power Systems Conference and Exposition* (pp. 1-7). IEEE.

Guerrero, J. M., Vasquez, J. C., Matas, J., Castilla, M., & de Vicuña, L. G. (2008). Control strategy for flexible microgrid based on parallel line-interactive UPS systems. *IEEE Transactions on industrial Electronics*, *56*(3), 726-736.

Guerrero, J. M., Vasquez, J. C., Matas, J., De Vicuña, L. G., & Castilla, M. (2010). Hierarchical control of droop-controlled AC and DC microgrids—A general approach toward standardization. *IEEE Transactions on industrial electronics*, 58(1), 158-172.

Hakimi, S. M., Tafreshi, S. M., & Kashefi, A. (2007). Unit sizing of a stand-alone hybrid power system using particle swarm optimization (PSO). In *2007 IEEE international conference on automation and logistics* (pp. 3107-3112). IEEE.

Hakimi, S. M., & Moghaddas-Tafreshi, S. M. (2009). Optimal sizing of a stand-alone hybrid power system via particle swarm optimization for Kahnouj area in south-east of Iran. *Renewable energy*, *34*(7), 1855-1862.

Hakimi, S. M., Moghaddas-Tafreshi, S. M., & HassanzadehFard, H. (2011). Optimal sizing of reliable hybrid renewable energy system considered various load types. *Journal of renewable and sustainable energy*, *3*(6), 062701.

Hamzeei, M., & Luedtke, J. (2014). Linearization-based algorithms for mixed-integer nonlinear programs with convex continuous relaxation. *Journal of Global Optimization*, *59*(2-3), 343-365.

Hatziargyriou, N. D., Jenkins, N., Strbac, G., Lopes, J. A. P., Ruela, J., Engler, A., ... & Amorim, A. (2006). Microgrids-large scale integration of microgeneration to low voltage grids.

Hawkes, A. D., & Leach, M. A. (2007). Cost-effective operating strategy for residential micro-combined heat and power. *Energy*, *32*(5), 711-723.

Herrando, M., & Markides, C. N. (2016). Hybrid PV and solar-thermal systems for domestic heat and power provision in the UK: Techno-economic considerations. *Applied Energy*, *161*, 512-532.

He, Y. Q., & David, A. K. (1997). Time-of-use electricity pricing based on global optimization for generation expansion planning.

Hill, C., & Chen, D. (2011). Development of a real-time testing environment for battery energy storage systems in renewable energy applications. In *2011 IEEE Power and Energy Society General Meeting* (pp. 1-8). IEEE.

Hill, C. A., Such, M. C., Chen, D., Gonzalez, J., & Grady, W. M. (2012). Battery energy storage for enabling integration of distributed solar power generation. *IEEE Transactions on smart grid*, *3*(2), 850-857.

Hu, W., & Li, C. J. (2017). On the fast convergence of random perturbations of the gradient flow. Available at: *arXiv preprint arXiv:1706.00837*.

Hung, D. Q., Mithulananthan, N., & Lee, K. Y. (2014). Determining PV penetration for distribution systems with time-varying load models. *IEEE Transactions on Power Systems*, *29*(6), 3048-3057.

Islam, M., Sun, Z., & Dagli, C. (2017a). Reward/penalty design in demand response for mitigating overgeneration considering the benefits from both manufacturers and utility company. Accepted by 2017 Complex Adaptive Systems Conference, Chicago, IL.

Islam, M., Sun, Z., & Dagli, C. (2017b). Simulation-based investigations on electricity demand response for manufacturing systems to mitigate overgeneration due to high penetration of renewable sources. *DEStech Transactions on Engineering and Technology Research*, (icpr).

Deshmukh, M. K., and S. S. Deshmukh. (2008). Modeling of hybrid renewable energy systems. Renewable and sustainable energy reviews 12.1: 235-249.

Islam, M.M., and Sun Z. (2019). Onsite generation system sizing for manufacturing plant considering renewable sources towards sustainability. *Sustainable Energy Technologies and Assessments* 32: 1-18.

Jerald, J., Asokan, P., Prabaharan, G., & Saravanan, R. (2005). Scheduling optimisation of flexible manufacturing systems using particle swarm optimisation algorithm. *The International Journal of Advanced Manufacturing Technology*, *25*(9-10), 964-971.

Ji, M., He, Y., & Cheng, T. E. (2007). Single-machine scheduling with periodic maintenance to minimize makespan. *Computers & operations research*, *34*(6), 1764-1770.

Johnson, S. M. (1954). Optimal two-and three-stage production schedules with setup times included. *Naval research logistics quarterly*, *1*(1), 61-68.

Johnstone, N., Haščič, I., & Popp, D. (2010). Renewable energy policies and technological innovation: evidence based on patent counts. *Environmental and resource economics*, *45*(1), 133-155.

Joo, J. Y., Raghavan, S., & Sun, Z. (2016). Integration of sustainable manufacturing systems into smart grids with high penetration of renewable energy resources. In *2016 IEEE Green Technologies Conference (GreenTech)* (pp. 12-17). IEEE.

Jung, J., & Villaran, M. (2017). Optimal planning and design of hybrid renewable energy systems for microgrids. *Renewable and Sustainable Energy Reviews*, *75*, 180-191.

Kaiser, R. (2007). Optimized battery-management system to improve storage lifetime in renewable energy systems. *Journal of Power Sources*, 168(1), 58-65.

Kamyab, F., & Bahrami, S. (2016). Efficient operation of energy hubs in time-of-use and dynamic pricing electricity markets. *Energy*, *106*, 343-355.

Kanase-Patil, A. B., Saini, R. P., & Sharma, M. P. (2011). Sizing of integrated renewable energy system based on load profiles and reliability index for the state of Uttarakhand in India. *Renewable Energy*, *36*(11), 2809-2821.

Karaguzel, O. T., Zhang, R., & Lam, K. P. (2014). Coupling of whole-building energy simulation and multi-dimensional numerical optimization for minimizing the life cycle costs of office buildings. In *Building simulation* (Vol. 7, No. 2, pp. 111-121). Tsinghua University Press.

Kazem, H. A., Khatib, T., & Sopian, K. (2013). Sizing of a standalone photovoltaic/battery system at minimum cost for remote housing electrification in Sohar, Oman. *Energy and Buildings*, *61*, 108-115.

Khatib, T., Mohamed, A., Sopian, K., & Mahmoud, M. (2012). A new approach for optimal sizing of standalone photovoltaic systems. *International Journal of Photoenergy*, 2012.

Koohi-Kamali, S., Tyagi, V. V., Rahim, N. A., Panwar, N. L., & Mokhlis, H. (2013). Emergence of energy storage technologies as the solution for reliable operation of smart power systems: A review. Renewable and Sustainable Energy Reviews, 25, 135-165.

Kim, D. W., Kim, K. H., Jang, W., & Chen, F. F. (2002). Unrelated parallel machine scheduling with setup times using simulated annealing. *Robotics and Computer-Integrated Manufacturing*, *18*(3-4), 223-231.

Lawrence Berkeley National Laboratory. Microgrid Definitions (2016). Available at: https://building-microgrid.lbl.gov/microgrid-definitions

Lasseter, B. (2001). Microgrids [distributed power generation]. In *2001 IEEE power engineering society winter meeting. Conference proceedings (Cat. No. 01CH37194)* (Vol. 1, pp. 146-149). IEEE.

Lasseter, R. H., & Piagi, P. (2004). Microgrid: A conceptual solution. In *IEEE Power Electronics Specialists Conference* (Vol. 6, pp. 4285-4291).

Lasseter, R. H. (2007). Microgrids and distributed generation. *Journal of Energy Engineering*, *133*(3), 144-149.

Layadi, T. M., Champenois, G., Mostefai, M., & Abbes, D. (2015). Lifetime estimation tool of lead–acid batteries for hybrid power sources design. *Simulation Modelling Practice and Theory*, 54, 36-48.

Lee, T. Y., & Chen, C. L. (2009). Wind-photovoltaic capacity coordination for a time-of-use rate industrial user. *IET Renewable Power Generation*, *3*(2), 152-167.

Levron, Y., Guerrero, J. M., & Beck, Y. (2013). Optimal power flow in microgrids with energy storage. *IEEE Transactions on Power Systems*, 28(3), 3226-3234.

Li, S., Proano, J., & Zhang, D. (2012). Microgrid power flow study in grid-connected and islanding modes under different converter control strategies. In *2012 IEEE Power and Energy Society General Meeting* (pp. 1-8). IEEE.

Li, Y., Vilathgamuwa, D. M., & Loh, P. C. (2004). Design, analysis, and real-time testing of a controller for multibus microgrid system. *IEEE Transactions on power electronics*, *19*(5), 1195-1204.

Liu, N., Chen, Q., Liu, J., Lu, X., Li, P., Lei, J., & Zhang, J. (2014). A heuristic operation strategy for commercial building microgrids containing EVs and PV system. *IEEE Transactions on Industrial Electronics*, *62*(4), 2560-2570.

Liu, C. Y., Zou, C. M., & Wu, P. (2014). A task scheduling algorithm based on genetic algorithm and ant colony optimization in cloud computing. In *2014 13th International Symposium on Distributed Computing and Applications to Business, Engineering and Science* (pp. 68-72). IEEE.

Logesh, R. (2017). Resources, configurations, and soft computing techniques for power management and control of PV/wind hybrid system. *Renewable and Sustainable Energy Reviews*, *69*, 129-143.

Luickx, P. J., & D'haeseleer, W. D. (2007). Backup of electricity from wind power: operational backup methods analysed. In *World Wind Energy Conference* (pp. 2-4).

Ma, T., Yang, H., & Lu, L. (2014). A feasibility study of a stand-alone hybrid solar–wind–battery system for a remote island. *Applied Energy*, *121*, 149-158.

Mahieux C, Oudalov A. Microgrids Enter the Mainstream (2015). Available at: http://www.renewableenergyfocus.com/view/43345/microgrids-enter-the-mainstream/

Manoj, S., & Srinivasaiah, P. P. (2012). Estimation and cost effective analysis of hybrid-wind/pv generation for rural/remote electrification. *Int. J. Emerg. Technol. Adv. Eng*, *2*, 740-745.

Marnay, C., Venkataramanan, G., Stadler, M., Siddiqui, A. S., Firestone, R., & Chandran, B. (2008). Optimal technology selection and operation of commercial-building microgrids. *IEEE Transactions on Power Systems*, *23*(3), 975-982.

McCall, J. (2005). Genetic algorithms for modelling and optimisation. *Journal of Computational and Applied Mathematics*, *184*(1), 205-222.

Mizani, S., & Yazdani, A. (2009). Optimal design and operation of a grid-connected microgrid. In *2009 IEEE Electrical Power & Energy Conference (EPEC)* (pp. 1-6). IEEE.

Moon, J. Y., Shin, K., & Park, J. (2013). Optimization of production scheduling with time-dependent and machine-dependent electricity cost for industrial energy efficiency. *The International Journal of Advanced Manufacturing Technology*, *68*(1-4), 523-535.

Moslehi, G., & Mahnam, M. (2011). A Pareto approach to multi-objective flexible job-shop scheduling problem using particle swarm optimization and local search. *International Journal of Production Economics*, *129*(1), 14-22.

Mushtaha, M., & Krost, G. (2011). Sizing a self-sustaining wind-Diesel power supply by Particle Swarm Optimization. In *2011 IEEE Symposium on Computational Intelligence Applications In Smart Grid (CIASG)* (pp. 1-7). IEEE.

Nazaripouya, H., Chu, C. C., Pota, H. R., & Gadh, R. (2017). Battery energy storage system control for intermittency smoothing using an optimized two-stage filter. *IEEE Transactions on Sustainable Energy*, 9(2), 664-675.

Newnham, R. H., & Baldsing, W. G. A. (2004). Advanced management strategies for remote-area power-supply systems. *Journal of Power Sources*, *133*(1), 141-146.

Nikmehr, N., Najafi-Ravadanegh, S., & Khodaei, A. (2017). Probabilistic optimal scheduling of networked microgrids considering time-based demand response programs under uncertainty. *Applied energy*, *198*, 267-279.

Nizami, M. S. H., Hossain, M. J., Amin, B. R., Kashif, M., Fernandez, E., & Mahmud, K. (2019). Transactive Energy Trading of Residential Prosumers Using Battery Energy Storage Systems. In *2019 IEEE Milan PowerTech* (pp. 1-6). IEEE.

NYDHSES (2014). New York State Division of Homeland Security and Emergency Services. Microgrids for Critical Facility Resiliency in New York State. Available at: https://www.nyserda.ny.gov/-/media/Microgrids-Report-Summary.pdf.

Olivares, D. E., Mehrizi-Sani, A., Etemadi, A. H., Cañizares, C. A., Iravani, R., Kazerani, M., ... & Jiménez-Estévez, G. A. (2014). Trends in microgrid control. *IEEE Transactions on smart grid*, *5*(4), 1905-1919.

Pamparana, G., Kracht, W., Haas, J., Díaz-Ferrán, G., Palma-Behnke, R., & Román, R. (2017). Integrating photovoltaic solar energy and a battery energy storage system to operate a semi-autogenous grinding mill. *Journal of cleaner production*, 165, 273-280.

Parker, C. D., & Garche, J. (2004). Battery energy-storage systems for power-supply networks. In *Valve-regulated lead-acid batteries* (pp. 295-326). Elsevier.

Pascual, J., Sanchis, P., & Marroyo, L. (2014). Implementation and control of a residential electrothermal microgrid based on renewable energies, a hybrid storage system and demand side management. *Energies*, *7*(1), 210-237.

Prasad, A. A., Taylor, R. A., & Kay, M. (2017). Assessment of solar and wind resource synergy in Australia. *Applied Energy*, *190*, 354-367.

Pongchairerks, P. (2009). Particle swarm optimization algorithm applied to scheduling problems. *ScienceAsia*, *35*(1), 89-94.

Pourmousavi, S. A., Nehrir, M. H., Colson, C. M., & Wang, C. (2010). Real-time energy management of a stand-alone hybrid wind-microturbine energy system using particle swarm optimization. *IEEE Transactions on Sustainable Energy*, *1*(3), 193-201.

Qdr, Q. J. U. D. E. (2006). Benefits of demand response in electricity markets and recommendations for achieving them. *US Dept. Energy, Washington, DC, USA, Tech. Rep*.

Rathnayaka, A. D., Potdar, V. M., Dillon, T. S., Hussain, O. K., & Chang, E. (2013). A methodology to find influential prosumers in prosumer community groups. *IEEE Transactions on Industrial Informatics*, 10(1), 706-713.

Rehman, S., & Al-Hadhrami, L. M. (2010). Study of a solar PV–diesel–battery hybrid power system for a remotely located population near Rafha, Saudi Arabia. *Energy*, *35*(12), 4986-4995.

Rohani, G., & Nour, M. (2014). Techno-economical analysis of stand-alone hybrid renewable power system for Ras Musherib in United Arab Emirates. *Energy*, *64*, 828-841.

Rocha, P. L., Ravetti, M. G., Mateus, G. R., & Pardalos, P. M. (2008). Exact algorithms for a scheduling problem with unrelated parallel machines and sequence and machine-dependent setup times. *Computers & Operations Research*, *35*(4), 1250-1264.

Roggia, L., Rech, C., Schuch, L., Baggio, J. E., Hey, H. L., & Pinheiro, J. R. (2011). Design of a sustainable residential microgrid system including PHEV and energy storage device. In *Proceedings of the 2011 14th European Conference on Power Electronics and Applications* (pp. 1-9). IEEE.

Ruangpattana, S., Klabjan, D., Arinez, J., & Biller, S. (2011). Optimization of on-site renewable energy generation for industrial sites. In *2011 IEEE/PES Power Systems Conference and Exposition* (pp. 1-8). IEEE.

SANDIA REPORT. (2016). Energy Storage Procurement Guidance Documents for Municipalities. Available at: https://www.cesa.org/assets/2016-Files/Energy-Storage-Procurement-Guidance-Document.pdf

SEIA (2017). Solar industry data. The Solar Energy Industries Association.

Shahidehpour, M., & Clair, J. F. (2012). A functional microgrid for enhancing reliability, sustainability, and energy efficiency. *The Electricity Journal*, *25*(8), 21-28.

Shen, J., Jiang, C., Liu, Y., & Qian, J. (2016). A microgrid energy management system with demand response for providing grid peak shaving. *Electric Power Components and Systems*, *44*(8), 843-852.

Shrouf, F., Ordieres-Meré, J., García-Sánchez, A., & Ortega-Mier, M. (2014). Optimizing the production scheduling of a single machine to minimize total energy consumption costs. *Journal of Cleaner Production*, *67*, 197-207.

Siddaiah, R., & Saini, R. P. (2016). A review on planning, configurations, modeling and optimization techniques of hybrid renewable energy systems for off grid applications. *Renewable and Sustainable Energy Reviews*, *58*, 376-396.

Siddiqui, O., Hurtado, P., & Parmenter, K. (2008). *The Green Grid Energy Savings and Carbon Emissions Reductions Enabled by a Smart Grid*.

Sinha, S., & Chandel, S. S. (2015). Review of recent trends in optimization techniques for solar photovoltaic–wind based hybrid energy systems. *Renewable and Sustainable Energy Reviews*, *50*, 755-769.

Singh, S., Singh, M., & Kaushik, S. C. (2016). Feasibility study of an islanded microgrid in rural area consisting of PV, wind, biomass and battery energy storage system. *Energy Conversion and Management*, *128*, 178-190.

Sirvent, M., Kanelakis, N., GEIßLER, B., & Biskas, P. (2017). Linearized model for optimization of coupled electricity and natural gas systems. *Journal of Modern Power Systems and Clean Energy*, *5*(3), 364-374.

Solar Energy Local (2018). Solar Energy Data and Resources in the US. https://solarenergylocal.com/.

Soto, A., Berrueta, A., Sanchis, P., & Ursúa, A. (2019, June). Influence of renewable power fluctuations on the lifetime prediction of lithium-ion batteries in a microgrid environment. In *2019 IEEE International Conference on Environment and Electrical Engineering and 2019 IEEE Industrial and Commercial Power Systems Europe (EEEIC/I&CPS Europe)* (pp. 1-6). IEEE

Southern California Edison (2015). Rates & Pricing Choices. Available at: https://www.sce.com/regulatory/tariff-books/rates-pricing-choices

Stadler M. (2014). Microgrid Planning and Operations for Critical Facilities Considering Outages due to Natural Disasters. Available at: https://building-microgrid.lbl.gov/sites/all/files/DER-CAM%20-%20microgrid%20resilience_V7.pdf.

State climatologist office for Illinois (2018). Available at: http://www.isws.illinois.edu/atmos/statecli/wind/wind.htm.

Stoppato, A., Cavazzini, G., Ardizzon, G., & Rossetti, A. (2014). A PSO (particle swarm optimization)-based model for the optimal management of a small PV (Photovoltaic)-pump hydro energy storage in a rural dry area. *Energy*, *76*, 168-174.

Stroe, D. I., & Schaltz, E. (2019). Lifetime Evaluation of a Battery Storage System used for Residential Electricity Supply in East Africa. In 13th International Renewable Energy Storage Conference (IRES 2019).

Su, W., Yuan, Z., & Chow, M. Y. (2010). Microgrid planning and operation: Solar energy and wind energy. In *IEEE PES General Meeting* (pp. 1-7). IEEE.

Suazo-Martínez, C., Pereira-Bonvallet, E., & Palma-Behnke, R. (2014). A simulation framework for optimal energy storage sizing. *Energies*, *7*(5), 3033-3055.

Suberu, M. Y., Mustafa, M. W., & Bashir, N. (2014). Energy storage systems for renewable energy power sector integration and mitigation of intermittency. *Renewable and Sustainable Energy Reviews*, 35, 499-514.

Thompson, C. C., Oikonomou, P. K., Etemadi, A. H., & Sorger, V. J. (2016). Optimization of data center battery storage investments for microgrid cost savings, emissions reduction, and reliability enhancement. *IEEE Transactions on Industry Applications*, *52*(3), 2053-2060.

Thornton, A., Kim, S. J., & Kara, S. (2018). Sizing a hybrid renewable energy system to reduce energy costs at various levels of robustness for an industrial site. *Procedia CIRP*, *69*, 371-376.

Truong, C., Naumann, M., Karl, R., Müller, M., Jossen, A., & Hesse, H. (2016). Economics of residential photovoltaic battery systems in Germany: The case of Tesla's Powerwall. *Batteries*, *2*(2), 14.

Upadhyay, S., & Sharma, M. P. (2015). Development of hybrid energy system with cycle charging strategy using particle swarm optimization for a remote area in India. *Renewable Energy*, *77*, 586-598.

Usman, M., Khan, M. T., Rana, A. S., & Ali, S. (2018). Techno-economic analysis of hybrid solar-diesel-grid connected power generation system. *Journal of Electrical Systems and Information Technology*, *5*(3), 653-662. ms without battery storage for off-grid areas. *Renewable energy*, *36*(6), 1780-1787.

U.S. DOE. How Microgrids Work (2014). Available at: https://www.energy.gov/articles/how-microgrids-work

U.S. Energy Information Administration. Manufacturing Energy Consumption Survey (MECS), Washington DC., U.S. (2002). Available at: https://www.eia.gov/consumption/

Vasel-Be-Hagh, A., & Archer, C. L. (2017). Wind farm hub height optimization. *Applied energy*, *195*, 905-921.

Wang, L., Mathew, P., & Pang, X. (2012). Uncertainties in energy consumption introduced by building operations and weather for a medium-size office building. *Energy and Buildings*, *53*, 152-158.

Wang, Y., & Li, L. (2016). Critical peak electricity pricing for sustainable manufacturing: Modeling and case studies. *Applied energy*, *175*, 40-53.

Wichert, B. (1997). PV-diesel hybrid energy systems for remote area power generation—a review of current practice and future developments. *Renewable and Sustainable Energy Reviews*1.3: 209-228.

Wikipedia (2018). Photovoltaics.

Wu, Z., Tazvinga, H., & Xia, X. (2015). Demand side management of photovoltaic-battery hybrid system. *Applied Energy*, *148*, 294-304.

Yamegueu, D., Azoumah, Y., Py, X., & Zongo, N. (2011). Experimental study of electricity generation by Solar PV/diesel hybrid systems without battery storage for off-grid areas. *Renewable energy*, *36*(6), 1780-1787.

Yulan, J., Zuhua, J., & Wenrui, H. (2008). Multi-objective integrated optimization research on preventive maintenance planning and production scheduling for a single machine. *The International Journal of Advanced Manufacturing Technology*, *39*(9-10), 954-964.

Ziegler, L., Gonzalez, E., Rubert, T., Smolka, U., & Melero, J. J. (2018). Lifetime extension of onshore wind turbines: A review covering Germany, Spain, Denmark, and the UK. *Renewable and Sustainable Energy Reviews*, *82*, 1261-1271.

Zhao, B., Zhang, X., Chen, J., Wang, C., & Guo, L. (2013). Operation optimization of standalone microgrids considering lifetime characteristics of battery energy storage system. *IEEE transactions on sustainable energy*, *4*(4), 934-943.

Zhang, D., Shah, N., & Papageorgiou, L. G. (2013). Efficient energy consumption and operation management in a smart building with microgrid. *Energy Conversion and Management*, *74*, 209-222.

Zhang, Y., Islam, M. M., Sun, Z., Yang, S., Dagli, C., & Xiong, H. (2018). Optimal sizing and planning of onsite generation system for manufacturing in Critical Peaking Pricing demand response program. *International Journal of Production Economics*, *206*, 261-267.

Zhang, Z., Shi, J., Gao, Y., & Yu, N. (2019). Degradation-aware Valuation and Sizing of Behind-the-Meter Battery Energy Storage Systems for Commercial Customers. In *2019 IEEE PES GTD Grand International Conference and Exposition Asia (GTD Asia)* (pp. 895-900). IEEE.

Zhong, X., Md, M. I., Xiong, H., & Sun, Z. (2017). Design the capacity of onsite generation system with renewable sources for manufacturing plant. *Procedia computer science*, *114*, 433-440.

# VITA

Md. Monirul Islam was born in Gaibandha, Bangladesh. He received his BS degree in Industrial and Production Engineering from Bangladesh University of Engineering and Technology in July 2014. He worked as a lecturer in BGMEA University of Fashion and Technology from 2014 to 2016. He started his PhD program in the department of Engineering Management and Systems Engineering at Missouri University of Science and Technology (Missouri S&T), Rolla, MO, USA in August 2016. In May 2020, he received his Doctor of Philosophy Degree in Systems Engineering from Missouri S&T with an emphasis in microgrid design, control, and performance evaluation for sustainable energy management in manufacturing.

Md. Monirul Islam has been a member of the International Council on Systems Engineering (INCOSE), American Society of Mechanical Engineers (ASME), Institute of Industrial, Systems Engineers (IISE), and American Society for Engineering Management (ASEM). His research interests included microgrid design and control, real-time energy management in manufacturing, stochastic optimization, artificial intelligence, machine learning, modeling complex systems, and systems simulation.